Aus der Medizinischen Klinik und Poliklinik II

Klinik der Ludwig-Maximilians-Universität München

Direktorin: Prof. Dr. med. Julia Mayerle

Identification of distinct histological signatures associated with different causes of chronic pancreatitis using multiplex staining

Dissertation

zum Erwerb des Doktorgrades Medizin

an der Medizinische Fakultät

der Ludwig-Maximilians-Universität zu München

vorgelegt von

Yonggan Xue

aus

Henan, China

2021

Mit Genehmigung der Medizinischen Fakultät

der Universität München

Berichterstatter:	Prof. Dr. med. Julia Mayerle
Mitberichterstatter:	PD Dr. med. Steffen Ormanns PD Dr. med. Christian Thieke
Mitbetreuung durch den promovierten Mitarbeiter:	Dr. med. Georg Beyer
Dekan:	Prof. Dr. med. dent. Reinhard Hickel
Tag der mündlichen Prüfung:	08.07.2021

Zusammenfassung

Die chronische Pankreatitis (CP) zeichnet sich durch eine weit verbreitete fibro-inflammatorische Schädigung der Bauchspeicheldrüse aus. Eine Vielzahl von Faktoren wie chronischer Alkoholismus, Tabakkonsum, Autoimmun-erkrankungen, duktale Obstruktion oder genetische Risikofaktoren spielen eine Rolle in der Pathogenese. Die CP ist eine progressive Erkrankung, die zu irreversiblen exo- und endokrinen Funktionsstörungen, chronischen Schmerzen und einem erhöhten Risiko für ein Bauchspeicheldrüsenkarzinom führt. Die Inzidenz und Prävalenz der CP steigt laut aktuellen epidemiologischen Studien kontinuierlich. Das stellt nicht nur eine potentielle Bedrohung der öffentlichen Gesundheit dar, sondern auch eine hohe wirtschaftliche Belastung für unsere Gesellschaft. Histologisch ist die CP, insbesondere in fortgeschrittenen Stadien, durch Atrophie von Azinuszellen, Obstruktion der Ausführungsgänge, starke Immunzellinfiltrate, massive Fibrose und Lipomatose gekennzeichnet. Obwohl die Pathogenese der CP noch nicht vollständig verstanden wird, gehen wir aktuell davon aus, dass die Interaktion von Immunzellen und aktivierten Myofibroblasten, sog. pankreatische Sternzellen (PSCs), die Progression der Erkrankung in Abhängigkeit von intrinsischen und extrinsischen Faktoren entscheidend beeinflusst. Ein besseres mechanistisches Verständnis basierend auf den histopathologischen Veränderungen bei der CP hat daher das Potential, die Entwicklung wirksamer Therapiestrategien zu ermöglichen.

In der vorliegenden Studie haben wir eine Multiplex-Färbetechnik, bestehend aus 28 individuellen Markern, verwendet, um die zelluläre Zusammensetzung des Entzündungs- und Stroma-Kompartiments innerhalb einzelner Gewebe-Mikroarray-Schnitte (TMAs) von 58 operierten Patienten mit CP in Abhängigkeit von der Ätiologie der Erkrankung präzise zu visualisieren. Zusätzlich analysierten wir mithilfe einer automatisierten maschinellen Lernanalyse (AutoML) die Assoziation von zelluläre Komposition mit dem klinischen Schweregrad, um Charakteristika zu identifizieren die mit einer exokrinen

Pankreasinsuffizienz assoziiert sind.

Wir beobachteten ein vermehrtes Auftreten von CD45+-Infiltraten bei Läsionen der autoimmunen Pankreatitis (AIP), im Vergleich zu der alkoholischen CP und anderen Formen der CP. Weitere Analysen von immunzellulären Subtypen zeigten, dass die Häufigkeit von Granulozyten bei der AIP im Vergleich zur alkoholischen CP und anderen CP-Varianten erhöht war. Im Gegensatz dazu war die Dichte zytotoxischer T-Zellen bei der alkoholischen CP und anderen CP Formen im Vergleich zur AIP signifikant erhöht. In ähnlicher Weise war die Häufigkeit aktivierter T-Zellen sowohl bei alkoholischer CP als auch bei anderen CP-Varianten im Vergleich zur AIP deutlich erhöht. Obwohl die zugrundeliegende Ätiologie allein, keinen signifikanten Einfluss auf die Stromaaktivierung bei den Subtypen der CP hat, konnten wir deutliche Unterschiede bei Subgruppenanalyse des Immuninfiltrats, insbesondere bei TH0-Zellen, zytotoxischen T-Zellen und tendenziell auch Granulozyten in Abhängigkeit vom aktivierten Stromaindex und der Ätiologie feststellen, was die Rolle des Aktivierungsmusters des Immuninfiltrats für die Fibrosierung unterstreicht. Darüber hinaus zeigte die AutoML-Berechnung die zehn stärksten Prädiktoren für exokrine Insuffizienz bei Patienten mit CP an. Wir zeigen, dass die Dichte der aktivierten PSCs mit proliferativer Fähigkeit, gefolgt von NK-Zellen und beta-Zellen, am bedeutendsten für die Prädiktion des Beginns einer exokrinen Pankreasdysfunktion ist.

Zusammenfassend haben wir in diesem Projekt eine 12-Plex-Färbetechnik für TMA-Proben von Patienten mit CP etabliert. Darüber hinaus verfeinerten wir ein halbautomatisiertes computergestütztes Analyseverfahren, das effizient zur digitalen Untersuchung histologischen Merkmale der fortgeschrittenen CP eingesetzt werden kann und so quantitative Analysen ermöglicht Weiterhin identifizierten wir die zehn wichtigsten Merkmale, die mit dem Vorliegen einer exokrinen Insuffizienz der Bauchspeicheldrüse assoziiert sind. Diese Arbeit trägt zu einem besseren Verständnis der zugrundeliegenden Pathomechanismen bei Entsteheung und des Fortschreitens der CP bei.

Table of contents

Abbreviations

°C	Grad Celsius
µg	Microgram
µl	Microliter
µM	Micromolar
α-SMA	Alpha-smooth muscle actin
AP	Acute pancreatitis
AIP	Autoimmune pancreatitis
aPSC	activated pancreatic stellate cell
AMCE	3-amino-9-ethylcarbazole
AutoML	Automatic machine learning
AUV	Area under the curve
CLDN2	Claudin 2
CP	Chronic pancreatitis
CTLA	Cytotoxic T lymphocyte antigen
CXCL-1	Chemokine (C-X-C motif) ligand 1
CXC	CXC chemokine
ddH2O	Double-distilled water
DCs	Dendritic cells
DRF	Distributed random forest
ECM	Extracellular matrix
XGBoost	Extreme gradient boosting
XRT	Extremely randomized trees
h	Hour
HCl	Hydrogen chloride
ICAM-1	Intercellular adhesion molecule-1
ID	Identity
IHC	Immunohistochemistry
IFN-γ	Interferon γ

IgG	Immunoglobulin G
IL-1β	Interleukin 1β
IL-4	Interleukin 4
IL-5	Interleukin 5
IL-6	Interleukin 6
IL-9	Interleukin 9
IL-10	Interleukin 10
IL-13	Interleukin 13
IL-18	Interleukin 18
IL-22	Interleukin 22
LFA-1	Lymphocyte function antigen-1
DAB	3, 3 -diaminobenzidine
BSA	Bovine serum albumin
DCs	Dendritic cells
g	Gram
GLM	Generalized linear model
GBM	Gradient boosting machine
H2SO4	Sulfuric acid
KMnO4	Potassium permanganate
M1 Macrophages	Classically activated macrophages
M2 Macrophages	Alternatively activated macrophages
MCP-1	Monocyte chemoattractant protein-1
min	Minutes
MMP7	Matrix metalloprotease 7
MMP9	Matrix metalloproteinase 9
MORC4	MORC Family CW-Type Zinc Finger 4
n	Number
NaOH	Sodium hydroxide
NETs	Neutrophil extracellular traps
NIH	National Institutes of Health

NK cells	Natural killer cells
PBS	Phosphate buffered saline
PBS-T	Phosphate buffered saline with Tween-20
PDAC	Pancreatic ductal adenocarcinoma
PHH3	Phosphohistone H3
PGP9.5	Protein gene product 9.5
PK	Pan-Keratin
PRSS1	Serine protease 2
PRSS2	Serine protease 2
PS	Picrosirius red staining
PSC	Pancreatic stellate cell
PDGF	Platelet-derived growth factors
qPSC	Quiescent pancreatic stellate cell
SAP	Severe acute pancreatitis
SDS	Sodium dodecyl sulfate
SIFT	Scale-invariant feature transform
SPINK1	Serine protease inhibitor Kazal-type 1
TIMP2	Tissue inhibitor metalloproteinase 2
TGFβ	Transforming growth factor β
TMA	Tissue microarray
TNF-α	Tumor necrosis factor-alpha
UK	United Kingdom
US	United States

1. Summary

Chronic pancreatitis (CP) is characterized by a widespread fibroinflammatory injury of the pancreas, which is caused by a variety of factors, such as chronic heavy alcohol consumption, tobacco use, autoimmune disease, ductal obstruction as well as genetic risk factors and rare causative mutations. CP is a progressive disease which ultimately leads to irreversible exocrine and endocrine dysfunction, chronic pain and increased risk of pancreatic cancer. The incidence and prevalence of the disease tend to be continuously increasing according to recent epidemiological studies, which is not simple a potential threat to public health, but brings highly economic burden to society. Histologically, CP, especially at advanced stages, is characterized by severe damage of pancreatic acinar cells, abnormalities of pancreatic ducts, large amounts of immune cell infiltration, massive fibrosis and fatty tissue replacement. Although the fundamental pathogenesis of CP is still not determined, it is well known that immune cellular infiltrates as well as activated pancreatic stellate cells play crucial roles in the development of the disease. Thus, improved understanding of histopathologic changes in CP have the potential to develop efficacious therapeutic regime for the patient involved.

In the present study, we applied multiplex staining technique comprised of 28 individual markers to precisely visualize pancreatic cellular compositions of the inflammatory and stromal compartments within individual tissue microarray (TMA) sections from 58 patients with CP. Additionally, we executed automatic machine learning (AutoML) analytics to the multiplex-stained images coupled with clinical parameters of the patients to identify which features were associated with prediction of exocrine insufficiency.

We observed that CD45+infiltrates are more frequent in lesions from autoimmune pancreatitis (AIP) compared with alcoholic CP and other forms of CP. Further analyses of immune cellular subtypes showed that abundance of granulocytes was statistically enhanced in AIP when compared with alcoholic

CP and other CP. In contrast, density of cytotoxic T cells was significantly amplified in both alcoholic CP and other CP when compared with AIP. Similarly, the frequency of activated T cells was notably enriched in alcoholic CP as well as other CP compared to AIP. Although the etiology alone did not lead to significant changes in stroma activation in the different subtypes, subgroup analysis showed, that TH0 cells, cytotoxic T cells and less pronounced, granulocytes are associated with distinct changes in the activated stroma index (ASI) and relation to the underlying etiology. This further supports that the activation pattern of inflammation plays a role for the progression of fibrosis.

Additionally, AutoML computation robustly indicated the top ten predictors for exocrine insufficiency in patients with CP. We found the density of activated PSCs with proliferative ability, followed by NK cells and islets, are of the greatest importance in predicting the onset of pancreatic exocrine dysfunction.

Overall, in this project, we established a 12-plex staining technique applied to TMA sections from patients with CP and refined a semi-automated computational analysis method which can be efficiently used to analyze digitalized images. Furthermore, we depicted the histological characteristics of advanced CP and compared those features among distinct patient groups. Additionally, we identified top ten features associated with the presence of pancreatic exocrine dysfunction. Our work has the potential to improve the understanding of the underlying mechanisms in developing CP and the progression of the disease.

2. Introduction

Chronic pancreatitis (CP) refers to a fibroinflammatory syndrome of the pancreas, which is induced by a variety of factors including excessive alcohol consumption and smoking, autoimmune disorders as well as genetic risk factors and rare causative mutations [1]. Patho-physiologically, CP is associated with the progressive damage of the pancreatic architectures and ultimately leads to irreversible exocrine and endocrine insufficiency [2].

2.1 Epidemiological features of chronic pancreatitis

The epidemiological features of CP are far from perfectly elucidated. The lack of uniform diagnostic criteria makes it difficult to precisely identify the patients with CP, particularly those who are at early stages. Generally, the acquisition of accurate diagnosis of CP is often based on a comprehensive combination of the potential risk factors, typical clinical manifestations as well as specific imaging features [3]. Thus far, only scarce population-based studies on the prevalence and incidence of CP have been reported in the literature. The incidence of CP in European countries reportedly varies from 4/100,000 in the UK [4] and 6.4/100,000 in Germany [5] to 13.4/100,000 in Finland [6]. A recent population-based investigation conducted by Yadav *et al* identified 106 incident cases of CP in Olmsted county, US, between1977 and 2006, including 89 clinical cases and 17 diagnosed by necropsy [7]. The overall age-adjusted and sex-adjusted incidence rate suggested by the investigation was 4.05/100,000 capita-years and the age-adjusted and sex-adjusted prevalence rate was 41.76 per 100,000 population [7]. There is a significant gender difference in the occurrence of CP in all studies, with men bearing a higher risk of the disease than women. Furthermore, the most recent analyses present an increasing incidence and prevalence of the disease [5]. Data from Yadav and colleagues demonstrate that the incidence rate of CP increased dramatically from 2.49 cases per million inhabitant-years between 1977 and 1986 to 4.35 between 1977 and 2006 [7].

2.2 Risk factors for developing chronic pancreatitis

It is widely accepted that the complicated interaction between genetic (intrinsic) and environmental (extrinsic) factors contributes to the initiation and progression of CP [8]. To date, a number of specific genes, like *PRSS1, SPINK* (see Table 1), that either cause or predispose to the syndrome of CP have been definitely confirmed. Moreover, functional experiments have partly delineated the roles that these genes play in the course of CP, for example, by prematurely activating trypsinogen in the pancreas [9].

Table 1: Summary of common risky gene mutations for developing CP (modified from Beyer *et al* [1])

Risky gene	Common mutation site	Prevalence among patients with CP	Mechanism for developing CP
PRSS1	p.N29I, p.R122C, p.R122H	3–10%	Directly stimulate trypsinogen autoactivation, or indirectly stimulate the activation of cationic trypsinogen via CTRC-related pathways
SPINK1	p.N34S	10%	Unclear
CTRC	p.G60, p.A73T, p.K247_R254del, p.R254W, pV235I	30%	Stimulate autoactivation of cationic trypsinogen, or fail to degrade trypsin
CPA1	p.S282P	3%	Reduce secretion, increase intracellular retention, and cause endoplasmic reticulum stress
CEL-HYB1	hybrid CEL allele	5%	Reduce secretion and increase intracellular retention
CFTR	p.F508del, p.R117H,	7%	Disrupt membrane ion channel activity
CLDN2 and MORC4	rs4409525, rs12008279; rs12688220, rs6622126	3%	Unclear

Researchers have identified mutations in the cationic trypsinogen gene *PRSS1* associated with premature trypsinogen activation, which is directly linked to hereditary pancreatitis, an autosomal-dominant disorder with incomplete

penetrance [10]. A recent large-scale case-control analysis conducted by Derikx *et al* in Europe suggested a conspicuous correlation of the single-nucleotide polymorphisms at the PRSS1–PRSS2 locus and at the CLDN2–MORC4 locus with alcoholic CP [11]. Mutations in *SPINK1*, a serine protease inhibitor gene, are significantly associated with tropical calcific pancreatitis, alongside serving as a disease modifier involved in the progression of recurrent acute pancreatitis (AP) to CP [12, 13]. Accumulating evidences recognize alcohol and smoking as the main environmental risk factors for CP [2]. The association of alcohol intake and tobacco consumption with the incidence of CP tends to follow a dose-dependent pattern, as a recent investigation performed by Di *et al* in Italy suggests smoking more than 5.5 cigarettes per day, and drinking alcohol more than 80 g/d are independent risk factors for the induction of CP [14, 15].

2.3 Etiological classification of chronic pancreatitis

Despite the apparently analogous pathological characteristics, chronic pancreatitis indeed consists of a range of disease entities. Unfortunately, there is still no definitely uniformed and standardized classification of this disorder in the literature, which is partly due to the intricate natural history and the uncertain pathological mechanism of the disease [2, 16]. In the present study, we stratified CP, based on the causative factors, as the following forms: chronic alcoholic pancreatitis, autoimmune pancreatitis (AIP), chronic obstructive pancreatitis, chronic idiopathic pancreatitis, as well as others which are with no clear causes. It is well known that the natural history, clinical manifestation, and treating strategy of CP vary according to the distinct forms and correspondingly causal mechanisms [17]. Improved insights into pathological features of the individual forms of the disease have the potential to bring focused and specific treatments. Previous investigations indicate that excessive alcohol consumption consistently tops the list of major contributors to developing CP [15, 18]. Prolonged alcohol ingestion can sensitize acinar cells to pancreatic stress and may promote intrapancreatic activation of digestive zymogens [19, 20].

Moreover, ethanol metabolites accelerate fibrogenesis through activating pancreatic stellate cells (PSCs) and facilitate chronic inflammatory reactions [21].

AIP is a relatively rare form of pancreatitis and has typically been classified into two subtypes [22]. Type 1 refers to lymphoplasmacytic sclerosing pancreatitis, which is the pancreatic manifestation of IgG4-related disease. Type 2 is known as idiopathic duct-centric pancreatitis with a hallmark of the granulocytic epithelial lesion in the pancreas. These two entities share common morphological characteristics and are sensitive to steroid therapy [23].

Obstructive pancreatitis occurs in the areas upstream from the obstructive sites due to a range of reasons, such as chronic inflammatory strictures which are often secondary to acute pancreatitis, pancreatic trauma, ductal stone, as well as benign or malignant neoplasia [2]. Moreover, ductal occlusion or stricture resulting from the above reasons tends to hamper the normal pancreatic secretory flow and results in ductal hypertension, eventually driving focal inflammatory responses, acinar cell injury, and pre-activation of digestive enzymes [22, 24].

Tropical pancreatitis is a form of idiopathic pancreatitis, with the typical features of early-onset abdominal pain, main pancreatic ductal calcification, and ketosis-resistant diabetes [25]. This type of pancreatitis is more prominent in developing countries, especially in tropical regions, like southern India, where malnutrition and cyanogenic glycosides are relatively common [26].

Still, a large proportion of cases of CP developed without clear evidence of the common causes are labeled as idiopathic.

2.4 Pathogenesis of chronic pancreatitis

The fundamental pathogenesis of CP is still not finely delineated. Over the past decades, several theories have been proposed but few have been validated, partly due to the lack of adequate animal models and the limitation of human tissue access. While compelling evidences show that CP frequently arises from

repetitive bouts of AP [27], other studies suggest that CP can also develop from only one or even on prior episode of AP, especially for idiopathic pancreatitis [1, 16, 18]. The histological characteristics of CP include various degrees of pancreatic edema, parenchymal cell necrosis, ductal structure abnormality, inflammatory responses, and massive fibrosis deposition. [20]. As the disease progresses, pancreatic tissue is replaced by a bulk of extracellular matrix (ECM) and fatty tissue. Moreover, in addition to causing the failure of exocrine and endocrine function, long-standing inflammatory stimuli can put CP patients at risk of developing pancreatic ductal adenocarcinomas [28].

2.4.1 Premature activation of trypsinogen causes acinar cell injury and the following inflammatory responses.

It has been proposed that inappropriately elevated activity of trypsin in the pancreas initiates the onset of pancreatitis and continues to play roles in driving the progression of the disease [29, 30]. This concept was proven by the works from Geisz A and colleagues in a preclinical model where T7D23A knock-in mice rapidly developed spontaneous AP followed by progressive CP manifesting with acinar cell destruction, inflammatory infiltration, fibrosis formation, and fatty tissue replacement [31].

2.4.2 Immune cells play indispensable roles in the progression of pancreatitis

Both innate and adaptive immune systems are involved in the pathophysiological evolution of pancreatitis, including AP and CP. Macrophages play an essential role in innate immune response and are known for their high plasticity. It is widely accepted that classically activated (M1) macrophages, marked by CD68 expression, are mainly implicated in the acute inflammatory response and the early stages of chronic inflammation. Upon the induction of pancreatitis, bone marrow-derived macrophages rapidly travel into the inflamed pancreatic areas and skewed towards M1 phenotype under the control of

chemoattractant factors and inflammatory mediators [32]. In addition to phagocytosing necrotic cellular debris, activated M1 macrophages release a large amount of chemokines and cytokines that are implicated in amplifying inflammatory responses [33, 34]. In contrast to M1, alternatively activated (M2) macrophages, defined by CD206 expression, are more predominant in chronic disease and wound healing, including CP. Animal experiments and clinical trials collectively indicate the remarkable enrichment of M2 macrophages in the lesions of CP [35, 36]. Functional research demonstrates that M2 macrophages are closely linked to the fibrous pathogenesis of CP through complicated crosstalk with activated PSCs [37].

Dendritic cells (DCs), making up a key part of antigen-presenting cell populations, link the innate immune system to the adaptive immune system [38, 39]. The mechanistic role of DCs in the development of CP remains largely undefined. Former investigations depicted dual roles of these cells in the progression of CP. This can be explained, in part, by the fact that DCs indeed include several different subtypes with each of those subtypes exhibiting distinct functions. Previous experiments reveal that DC-Sign+ expressing immature DCs mediate DC migration and adhesion, T cell activities, and immune initiation and escape [40, 41], whereas CD83 expressing mature DCs regulate DC activation and maintain immune homeostasis [42]. Moreover, it is reported that enrichment of DC populations played an important role in the development of pancreatic cancer on the back of CP through inducing pancreatic antigen-restricted TH2 deviated CD4+ T cells via inhibiting MyD88-dependent pathway [43].

It is well studied that during the course of pancreatitis, pathological granulocyte (MPO+) infiltrates, specifically neutrophils, play critical roles in digestive enzymes activation, the severity of acinar cells damage, local and systemic inflammation, as well as complications of severe pancreatitis. Moreover, neutrophil infiltration contributes to the transformation of AP to CP as well as the formation of intrapancreatic stones [44].

In addition to innate immune system, adaptive cell populations are equally critical for the pathogenesis of CP. Undoubtedly, T lymphocytes play a vital role in adaptive immune system. Based on the expression of cell surface antigens, T cells can be split into several subsets, including the cytotoxic T cells (CD8+), the regulatory T cells (FoxP3+), the T helper cells, the memory T cells, and the natural killer (NK) cells (CD56+), with each of them exerting distinct functions [45, 46]. Previous examinations indicate that the proportion of TH1 (Tbet+), TH2 (GATA3+), and TH17 cells (IL17A+) is remarkably enhanced in the peripheral blood of patients with CP compared to the healthy control populations, while the pancreatic lesions are only dominant with TH1 cells and TH17 cells, with the fewer presence of TH2 subpopulations [47]. Further studies demonstrate that the frequency of TH1 and TH2 was enriched in intra-islet regions of CP patients with diabetes compared with healthy controls as well as patients without diabetes, indicating the involvement of these cells in β-cell dysfunction during progression of CP [48]. TH2 cells were described as pro-tumorigenic mediators driving chronic pancreatic fibroinflammatory disease towards malignant transformation [43]. The frequency of cytotoxic T cells was observed significantly expanding in the pancreas of patients with alcoholic CP and tend to be localized closely to pancreatic parenchyma, implying that cytotoxic cells probably lead to tissue disruption [49].

Although accumulating trials indicate the involvement of B cells (CD20+) and NK cells in the pathogenesis of AP [50, 51], investigations on the contribution of these two types of lymphocytes to the development of CP are rare. B cells initiate humoral immunity in the adaptive immune system by producing specific antibodies. B cells initiate humoral immunity in adaptive immune system through producing specific antibodies. Moreover, B cells are frequently involved in the dynamics of T cell proliferation, differentiation, and activation via their antigen-presenting capacity or through producing various cytokines [52]. The immune function of NK cells is analogous to cytotoxic T lymphocytes, with the capacity to kill cancer cells and to produce various inflammatory cytokines, such

as IFN-γ, TNF-α, IL-18 [53]. However, the biological mechanism underlying the role of NK cells in the progress of CP remains to be defined.

2.4.3 PSCs are responsible for fibrous characteristics of CP

During the course of pancreatitis, pancreatic stellate cells (PSCs) experience functional state alternation that switch from quiescent to activated phenotype [54]. So far, it is well documented that activated PSCs play major roles in the development of pancreatic fibrosis. A variety of cytokines, like transforming growth factor β (TGFβ), platelet-derived growth factors (PDGF), and complement component C5a are associated with activation of PSCs and the consequent upregulation of extracellular matrix (ECM) synthesis [54, 55]. It is worth noting that the bi-directional interaction between immune infiltrates and PSCs drives the process of fibrogenesis during CP. Xue *et al.* provided strong evidence that CD4+T cells-derived IL-22 significantly upregulate gene profiles associated with ECM synthesis in PSCs in animal models of CP [56]. Additionally, activated PSCs produce large amounts of IL-4/IL-13, which strongly skew macrophages toward M2 polarization, aggravating pancreatic fibrosis progression [36].

2.5 Aim of this study

While decades of studies from both cell culture systems and animal models have been invented in an attempt to decipher the mechanism underlying the complicated pathogenesis of CP, clinical experts are still facing the huge challenges of translating laboratory findings into clinical practice. This can be partly explained by the fact that animal models fail to entirely mirror the natural course of the development of CP, which highlights the significance of directly analyzing human CP lesions to obtain a pathological fidelity of the disease. Therefore, we sought to collect human specimens from the source of patients resected for CP and evaluated the histopathological signatures, including immune infiltrates, parenchymal cells, and stromal compartments within the lesions using multiplex staining technique together with computational digital

image analysis. The combination of multiplex staining with digital image analysis is not limited to help accurately determine the individual cellular types and perform quantity analysis, but also make it possible to clearly map the spatial distribution characteristics of those cells and their surrounding non-cellular architectures. Animal experiments have consistently provided evidence that immune cells take a key part in pushing the progression of CP. This indicates that deep and extensive understanding of immune signatures within CP lesions has the potential to modify the natural history of the disease and improve the clinical outcomes of the patients. In the present study, we plan to spot the distributional characteristics of immune cells, pancreatic functional cells, and stromal compartments within the lesions from patients with CP. We will further compare those parameters among patients with CP induced by distinct causes, such as alcoholic, autoimmune, obstructive, and idiopathic etiology to stratify patient with histological subtypes of CP. Additionally, we will apply automatic machine learning technique to compute potential features to predict the development of exocrine insufficiency of patients with CP. Our findings have strong potential to explicitly depict the histopathological signatures of CP, which will be helpful to organize future *in vivo* experiments and favor the introduction of efficacious therapeutics.

3 Methods

3.1 Study objective and design

The present study is designed to characterize the histopathological composition of the fibroinflammatory stroma and parenchymal architectures of patients with CP via the application of a comprehensive multiplex-staining technique to a series of tissue microarray sections (TMAs) of CP resection specimens. We will adopt and refine a multiplex staining protocol for analyzing TMAs based on the previous works from Tsuijkawa and colleagues with appropriate modifications [57, 58], which allows us to accomplish a maximum of twelve-consecutive stainings in a single section, starting with hematoxylin staining followed by repeated steps of primary and secondary antibody incubation, AMEC-staining, whole slide digital scanning, and antibody and chromogen removal. To acquire the entire features of stromal compartments together with parenchymal cellular components, three multiplex-staining panels, named lymphoid biomarker panel, myeloid biomarker panel, and pancreatic exocrine-endocrine and stroma biomarker panel, were prepared and stained with corresponding antibodies (Table 2). Hematoxylin staining will complement the histological characterization in terms of morphological changes. Quantification of extracellular matrix composition, immune cell deposition, and pancreatic parenchymal and mesenchymal components was achieved according to the pixel intensity of the staining in tissue cores using an algorithm developed for NIH ImageJ software.

Table 2: Staining panels for multiplex staining assay

Panel / Order	Lymphoid biomarker	Myeloid biomarker	Pancreatic exocrine-endocrine and stroma biomarker	Morphology
1	H*	H*	H*	HE
2	GATA3	DC-Sign	Pan-Keratin	

3	T-bet	CD206	CD45	
4	FoxP3	CD68	PHH3	
5	CD20	MPO	aSMA	
6	CD8	CD20	Insulin	
7	CD4	CD56	PGP9.5	
8	CD3	CD3	Perilipin	
9	CD56	CD45	Amylase	
10	CD45	CD74	Desmin	
11	CTLA4	Tryptase	MMP7	
12	IL17A	CD83	Sirius-Red/Fast-Green	

The lymphoid biomarker panel is designed for comprehensive characterization of lymphocytes, including T cells, B cells, and NK cells, whereas the myeloid biomarker panel focusses on other leukocytes such as macrophages, granulocytes, DCs, and mast cells as well. The so-called pancreatic exocrine-endocrine and stroma biomarker panel concentrates on pancreatic exocrine and endocrine cellular compartments, nerve cells, PSCs, and ECM deposition. The specific marker-combination for each cellular subtype is displayed in Table 3.

Table 3: Cellular lineage and corresponding identification biomarkers

Cellular lineage	Identification biomarkers
Leukocytes	CD45+CK19-Amylase-Insulin-PGP9.5-
Cytotoxic T cells	CD45+CD3+CD8+CD4-
Regulatory T cell	CD45+CD3+CD8-FoxP3+CTLA4+
Activated T cell	CD45+CD3+FoxP3-CTLA4+
TH17	CD45+CD3+CD8-FoxP3-IL17A+
TH1	CD45+CD3+CD4+CD8- IL17A -Tbet+
TH2	CD45+CD3+CD4+CD8- IL17A -GATA3+
T others (TH 0)	CD45+CD3+CD8- IL17A -Tbet-GATA3-
B cell	CD45+CD3-CD56-CD20+
NK cells	CD45+CD3-CD56+CD20-
M1 Macrophages	CD45+CD3-CD20-CD56- MPO -Tryptase-CD68+CD74+CD206-
M2 Macrophages	CD45+CD3-CD20-CD56- MPO -Tryptase-CD68+ CD74+CD206+
DC-Sign+DC	CD45+CD3-CD20-CD56- MPO -Tryptase-CD68- CD74+DC-Sign+CD83-

CD83+ DC	CD45+CD3-CD20-CD56- MPO -Tryptase-CD68- CD74+CD83+
Granulocytes	CD45+CD3-CD20-CD56-MPO+
Mast cells	CD45+ CD3-CD20-CD56- MPO -Tryptase+
PSCs quiescent	CD45-CK19-Amylase-Insulin-PGP9.5-aSMA-Desmin-Perilipin+
PSCs activated	CD45-CK19-Amylase-Insulin-PGP9.5-aSMA+Desmin+Perilipin-
Duct cells	CD45-CK19+Amylase-Insulin-PGP9.5-
Acinar cells	CD45-CK19-Amylase+Insulin-PGP9.5-
Islets	CD45-CK19-Amylase-Insulin+PGP9.5-
Proliferation	CD45-PHH3+
Fibrosis	Picrosirius red-fast green staining
ECM remodeling	MMP7+
Nerves global	CD45-CK19-Amylase-Insulin-PGP9.5+

3.2 Patients

A total of 62 patients identified from the database of Department of Pathology by full text search for diagnosis of “chronic pancreatitis” who underwent surgical pancreatic resection or drainage procedures were found eligible for the present project. Indications for the surgical interventions included pain, biliary obstruction, pseudocysts, severe vascular complications, groove pancreatitis with duodenal obstruction, and suspicion for pancreatic cancer. As for staining controls, a total of 4 adult non-malignant tonsil specimens were included in the TMAs (Figure 1).

3.3 Tissue samples for standardizing antibody concentration

All surgical samples from the patients involved in the present study were provided by Department of Pathology, Hospital of Ludwig-Maximilians-University, Munich, Germany. Two paraformaldehyde-fixed, paraffin-embedded tonsil tissue blocks were sectioned at 2μm and collected on poly-lysine slides for standardizing the concentration of immune cell biomarkers. Chronic pancreatitis tissues were utilized to optimize the concentration of non-immune cell biomarkers. The optimal staining sequence was determined during the course of antibody-concentration standardization based on the staining density of the individual visualized targets.

3.4 Tissue samples for TMAs preparation

Tissues were already embedded in paraffin blocks at the time of TMA development. The paraffin blocks were sectioned at 2μm for the multiplex-staining analysis. With 3 cores per patient, a total of 594 cores made from the 66 patients' CP resection specimens were included. Each panel contains 198 cores. However, after cross-validating the clinical data and pathological outcomes, 4 patients who were initially suspected of suffering CP were ultimately verified with other manifestations and afterward excluded from the study. Thus, a total of 58 patients with confirmed CP were processed for the final image cytometry analysis. The consort diagram about the details of the involved patients for TMAs preparation is delineated in Figure 1.

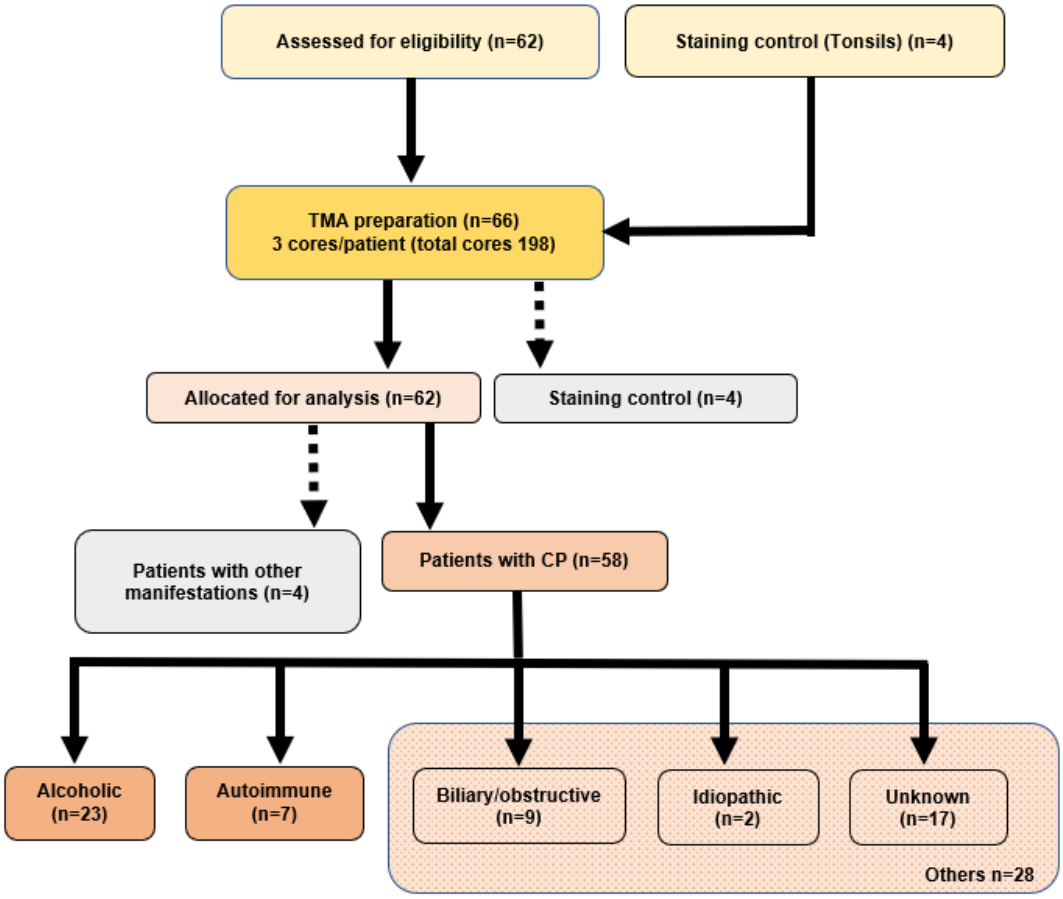

Figure 1. Consort diagram shows the details of the involved patients for TMAs preparation.

3.5 Conventional immunochemical staining for antibody standardization

Paraffin slides were deparaffinized in xylene, for three times with 10 min at each time. After dewaxing, slides were rehydrated through a series of graded alcohols, starting from 100% (2 times) to 95%, 70%, and 50%, for 5 min at each change. Following rehydration, slides were washed with phosphate-buffered saline (PBS) for 5 min. Then, slides were subjected to heat-mediated antigen retrieval for 30 min in a pressure cooker by immersing the slides in 1X antigen retrieval buffer, followed by cooling down the slides in antigen retrieval buffer to room temperature (Table 13). Next, slides were blocked for endogenous peroxidase retrieval though adding 3% hydrogen peroxide on sections for 20min. Slides were then washed with PBS, 3 times with 5min at each time. Afterward, slides were blocked with blocking buffer (1% Aurion BSA in PBS) for 1h at room temperature. Again, slides were washed with PBS, 3 times with 5min at each time. Then, slides were incubated with primary antibody diluted with blocking buffer in the cooling room overnight. The next day, the primary antibody was removed by washing the slides with PBS, 3 times with 5min at each time. Next, slides were incubated with corresponding secondary antibody at room temperature for an hour. The slides were again washed with PBS for 3 times with 5min at each time. The slides were then processed for immunohistochemical staining with DAB peroxidase substrate. After developing staining, slides were washed with running tap water for 2 min. Then, the slides were stained with hematoxylin for 1min and again washed with tap water and followed by 2min ddH_2O washing. The slides were then passed through a series of graded alcohols, starting from 50% to 70%, 95%, and 100%, for the 30s at each change. By the end, sections were coated with permanent mounting medium and fixed with coverslips.

3.6 Multiplex immunochemical staining for digital image cytometry evaluation

To begin with, as the conventional immunochemical staining, TMAs slides were deparaffinized with xylene, followed by rehydrating from a serially graded

alcohol to PBS. After rehydration, TMAs slides were immediately stained with hematoxylin for 45s and followed by immersing the slides in a 0.5% ammonia solution for 2min. Then, TMAs slides were cleaned with 3 times quick dip in ddH_2O. The sections were coated with aqueous mounting media (70% glycine in PBS) and consequently fixed with coverslips, followed by the whole-slide scanning in a Sysmex Panoramic MIDI II slide scanner. After scanning, the coverslips were removed by immersing the slide in ddH_2O for 5min. Slides were then subjected to heat-mediated antigen retrieval for 30 min, a process which is exactly the same as the conventional immunochemical staining, during which the previous hematoxylin staining can also be completely eluted. After cooling down to room temperature, slides were processed for endogenous peroxidase retrieval by adding 3% hydrogen peroxide on sections for 20min. Slides were washed with PBS-T (0.05% Tween® 20 in PBS) for 3 times with 10min at each time. Slides were then blocked with blocking buffer (1% BSA in PBS). After blocking, sections were incubated with the first primary antibody diluted with blocking buffer in the cooling room overnight. The next day, slides were washed with PBS-T for 3 times with 10min at each time. Slides were then incubated with corresponding secondary antibody for an hour at room temperature. Again, slides were washed with PBS-T, three times with 10min at each time. After washing, the slides were processed for immunohistochemical visualization with the alcohol-soluble peroxidase substrate AMEC red. The sections were then coated with aqueous mounting media and covered with coverslips, followed by whole-slide scanning in the Sysmex Panoramic MIDI II slide scanner. Coverslips were removed by immersing slides in ddH_2O for 5min. The sections were then subjected to AMEC red de-staining and antibody stripping (see below). After antibody stripping, slides were washed with PBS for 5 min and proceeded for the next round of staining, starting with from the blocking step as described above (Figure 2).

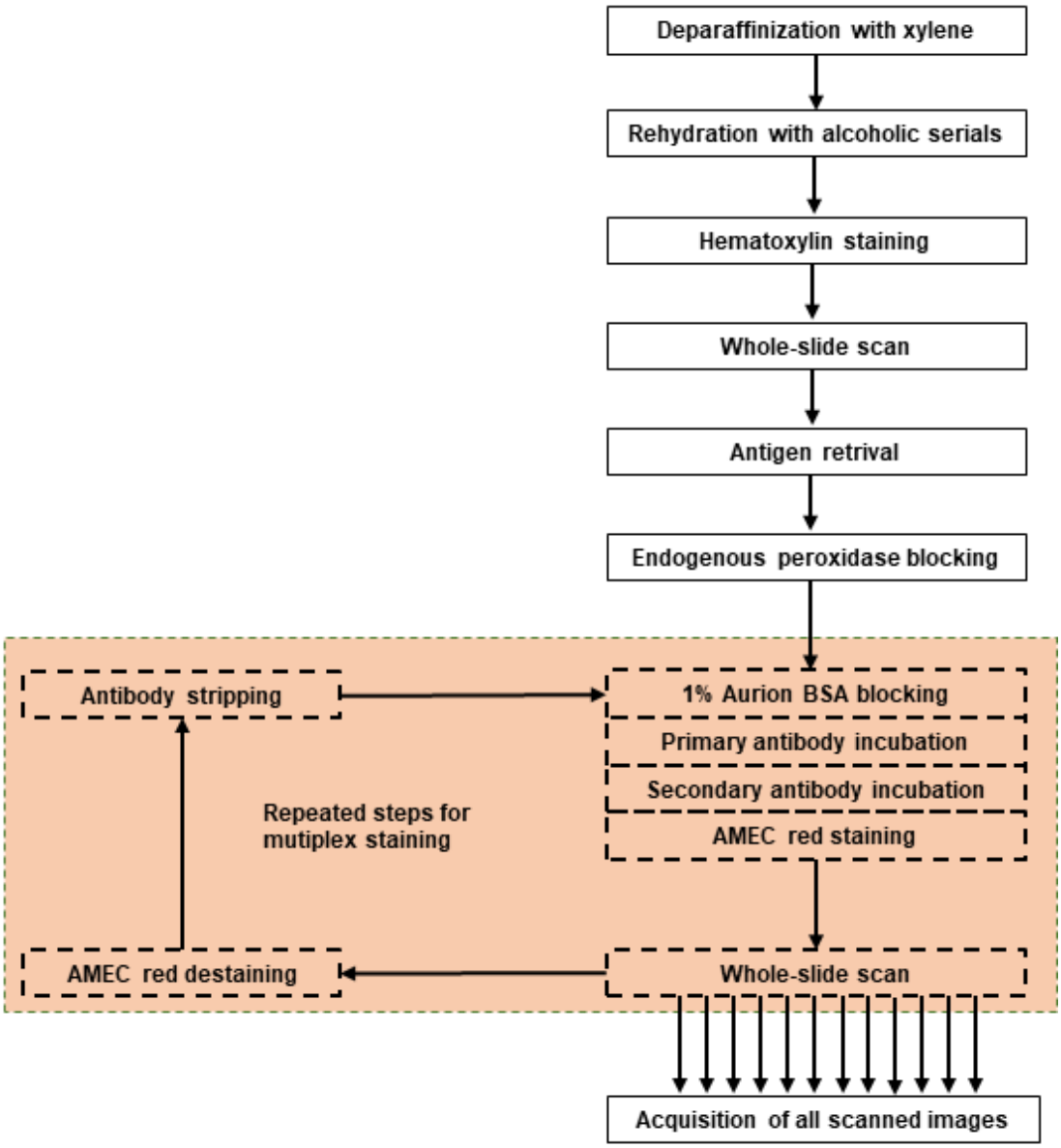

Figure 2. Work-flow chart adopted from Mahajan [58] reflects multiplex immunohistochemical staining. Highlighted Work-flow in brown area denotes multiple antibodies staining cycles.

3.7 Eluting antibody by using glycine-mediated antibody stripping buffer

After scanning the whole slides and removing the coverslips, AMEC red de-staining of the sections was accomplished by dipping the slides in 70% ethanol for 2min, followed by 95% ethanol for 2 min, and backward 70% ethanol for 2min; this process sometimes needs to be repeated until no visible red color has remained. For the lymphoid and myeloid panels in which specific antibodies are applied to label immune cells, antibody stripping is conducted by incubating

the slides in a preheated jar which contains glycine-mediated antibody stripping buffer (Table 13) and then putting the jar in a water bath with the shaking speed of 60 rounds per min at 50°C for 30 min. However, in pancreatic exocrine-endocrine and stroma panel, AMEC staining of non-immune cell biomarkers, like α-SMA, insulin, PGP9.5, amylase, perilipin, and desmin, are relatively strong making it difficult to completely remove the staining color by this stripping approach as described above. Therefore, we attempted to double the concentration of glycine (50mM glycine-HCl, 1%SDS, pH2) along with extending the incubation time to 2 hours, which was proven efficient to entirely elute the staining color developed by those non-immune cell biomarkers.

3.8 Picrosirius Red staining for collagenous protein deposition identification

The last staining in pancreatic exocrine-endocrine and stroma panel is picrosirius red staining (PS), which is performed, immediately following the de-staining of MMP7. After stripped of MMP7 antibody and washing with PBS for 5 min, slides were subjected to specific collagen network visualization, that is picrosirius staining, by utilizing picrosirius red-fast green staining solution to coat individual sections and being kept in a dark box for an hour at room temperature (Table 12). Slides were then proceeded to twice short washing with ddH_2O and passed through a series of alcohol gradients, starting from 50% alcohol to 70%, 95%, and 100% (2 times) alcohol, 30s at each change. Afterward, the sections were cleared with xylene for 3 times, 5 min at each time. Finally, the tissues were coated with permanent mounting medium and covered with coverslips, followed by whole-slide scanning.

3.9 Computational digital image cytometry analysis

All the digital image cytometric analyses were outsourced and performed using automated pipeline consisting of Image J, CellProfiler and FCS express developed in the laboratory

(https://github.com/umahajanlmu/multiplex_image_cytometry). Briefly, it involves the following steps: image registration, deconvolution, feature extraction, and image cytometry. Image registration was achieved by overlapping each of the 12 images per core according to their core identity (ID). Followed by co-registration, all the individual images underwent color deconvolution in order to outline and separate individual cells. These images were then co-localized based on their core ID and cellular features were extracted according to the pixel intensity to define distinct cell phenotypes. The exported images containing all identified cells were then subjected to image cytometric analysis using FCS express software by measuring the pixel intensity of each individual cell within the stacked image. Schematic representation of automated pipeline has been depicted in Figure 3.

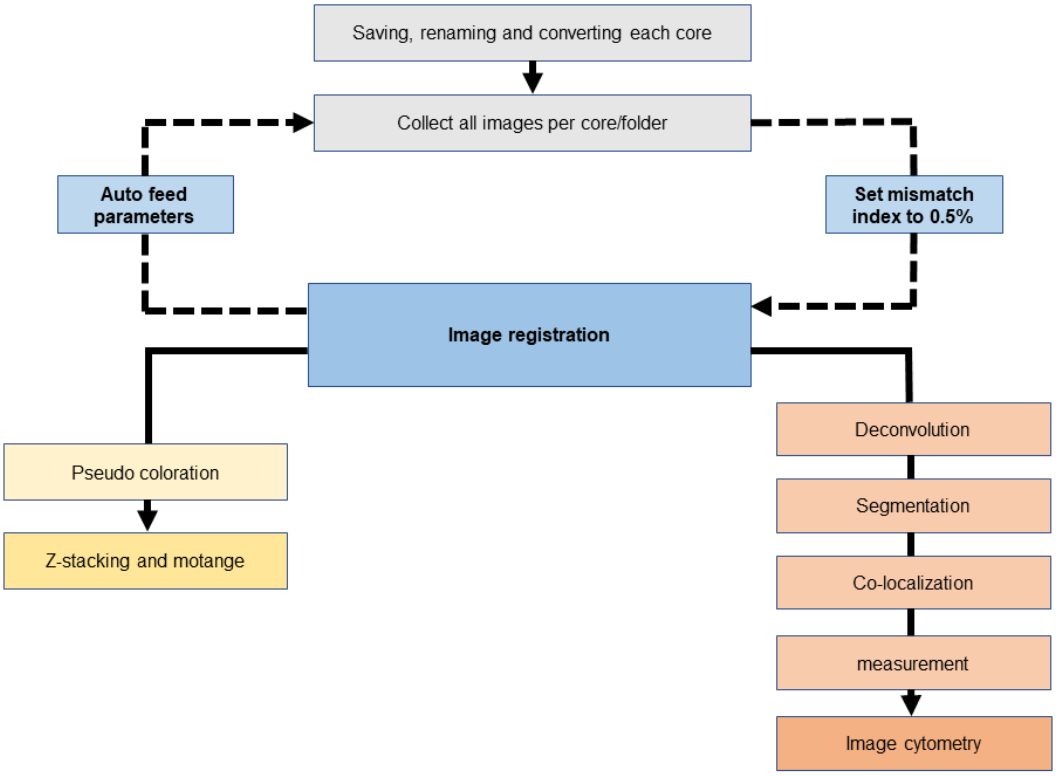

Figure 3. Work-flow chart depicts computational digital image cytometry analysis.

3.10 Statistical analysis

For machine learning, patients were randomly separated into two groups: an endpoint-balanced discovery group (80%) and a test cohort group (20%). We

introduce the binary variables which were defined for all baseline patient data including both clinic and cytometric characteristics (see Table 16). H2O.ai platform (https://www.h2o.ai) was employed for the base predictor to automatically select the optimal machine learning method in the literature. To save computational time, the selection of methods was confined to gradient boosting machine (GBM), generalized linear model (GLM), extreme gradient boosting (XGBoost), distributed random forest (DRF), and extremely randomized trees (XRT). The parameters of each method were optimized using an internal 10-fold cross-validation on the training set, followed by applying the optimal method to the test set to evaluate the final performance. In each loop, the best performing predictor was determined from all obtained predictors employing the performance measure logloss. The selection of predictors was on the basis of the area under the curve (AUC>0.5) and logloss<0.05. We selected variables related to the “base predictor” according to their scaled importance above 0.05 to obtain the “slim predictor” on the basis of a reduced set of variables.

Statistical comparisons in two variables of cell percentages and densities among distinct cell lineages were assessed using Mann-Whitney tests. Statistical analyses of the distribution of CP with distinct causes in different stromal subtypes were conducted using Fisher’s Exact Test. Statistical differences in more than two variables of cell percentages and densities among distinct cell lineages were assessed using Kruskal-Wallis tests. All statistical operations were performed by Graphpad Prism 8. $p < 0.05$ was considered statistically significant for all experiments.

4. Results

4.1 Optimizing sequence of multiplexed biomarkers stained on a single tissue section

Multiplex IHC staining workflow enabling sequential or simultaneous visualization of multiple antigens in a same tissue section using corresponding biomarkers has been proposed and explored by numerous of both pathology experts for diagnostic purpose and laboratory scientists for fundamental research over the last two decades [59-62]. Glass and colleagues initially reported a 5-plex protocol and subsequently expanded to 12-round iteratively labeling strategy realizing reliable evaluation of more than 12 antigens in a single tissue section without losing tissue antigenicity and developing cross-reactivity [57, 63]. Thus, the present study was carried out on the basis of the multiple labeling technique described by Glass and colleagues with some modifications. Briefly, after dewaxing and rehydration, tissue sections were stained with hematoxylin, followed by primary antibody incubation and fragment-specific secondary antibody combination. Antigen visualization were developed by alcohol-soluble peroxidase substrate AMEC, followed by the whole-slide scanning. Repeated signal visualization is accomplished by an iterative procedure composed of de-staining the sections in the gradient ethanol series, dissociating primary antibody in heated citrate buffer, and re-staining the sections with alternative antibodies. To comprehensively explore cellular complexity and architectural alternation of CP lesions, we established three panels of multiple consequential staining with 12 biomarkers in each panel, including 28 distinct epitopes to depict migratory and resident immune cells, pancreatic parenchymal cells, and stromal compartments. Additionally, we performed picrosirius red staining to specifically delineate stromal collagenous protein deposition. Biomarkers used for detecting each of the three panels, along with optimized staining sequence, are displayed in Figure 4. Integrated hierarchical biomarkers utilized for identifying distinct cellular lineages and

subtypes are listed in Table 3.

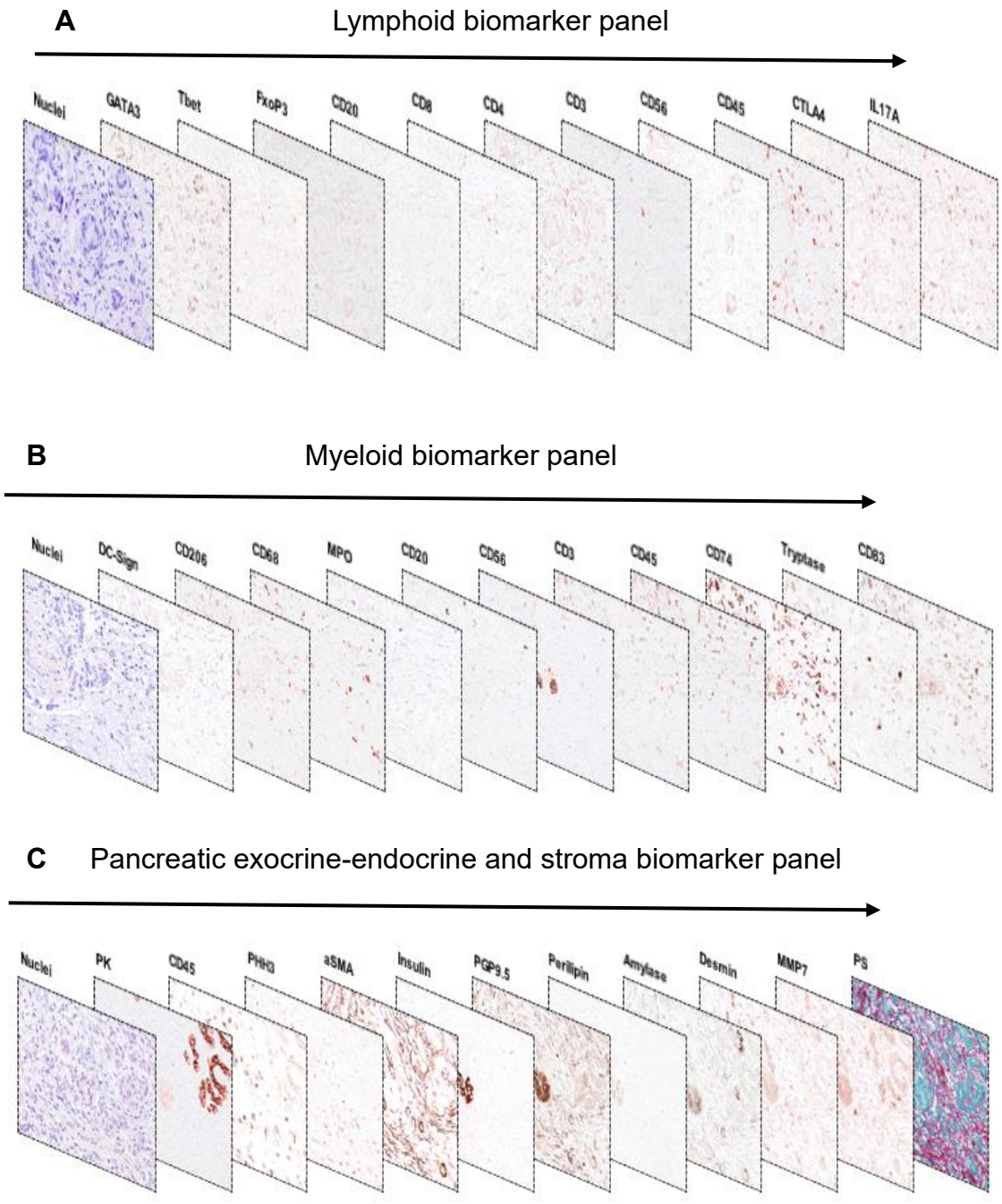

Figure 4: Sequential schematic of 12-color multiplex IHC staining. (A) Representative of digital scanned images from one section of TMAs depicting lymphoid panel biomarkers. **(B)** Representative of digital scanned images from one section of TMAs depicting myeloid panel biomarkers. **(C)** Representative of digital scanned images from one section of TMAs depicting pancreatic exocrine-endocrine and stromal panel biomarkers.

4.2 Establishing serially scanned and digitalized image-processing pipeline

After completing the multiple cycles of IHC staining, each core for a single staining was captured and named in accordance with its slide coordinates. Each of the 12 iteratively digitalized images was sorted according to its core ID and then subjected to the process of co-registration. The precise match of the 12 individual images per core was achieved using a feature detection algorithm of the scale-invariant feature transform (SIFT) [64]. SIFT keypoints of objects within the individual multiple scanned images were first extracted and then stored in a database. The candidate matching features were identified by individually comparing each feature in a new image to this database. The correct matches were determined by the agreement of subsets of keypoints on the object and its location, scale, and orientation from the full set of matches (Figure 5) [65].

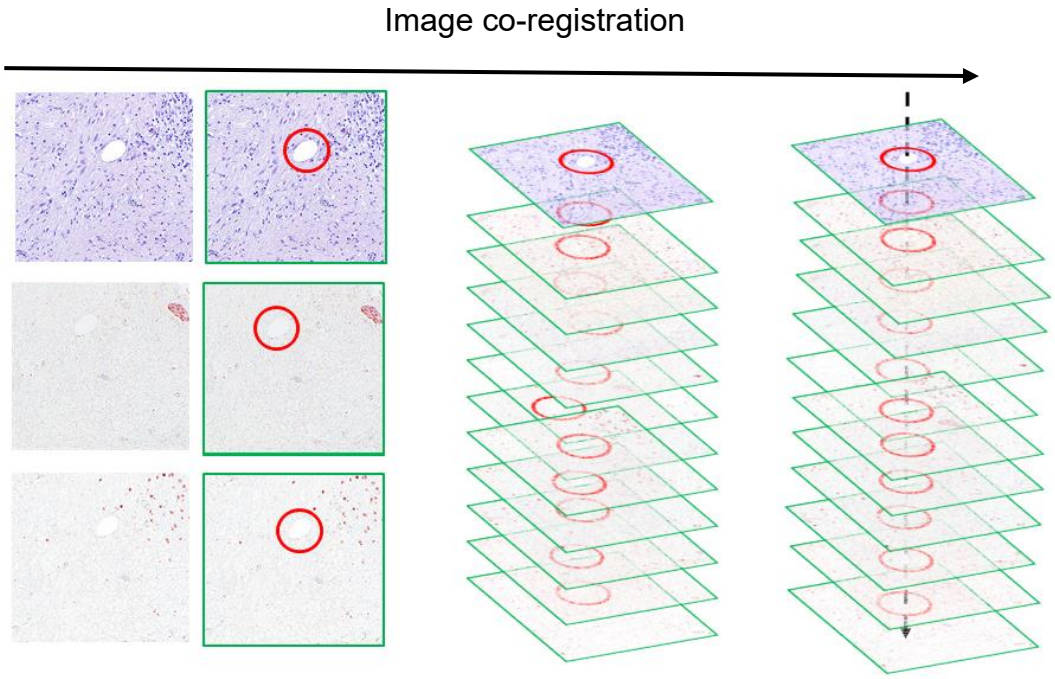

Figure 5: Schematic diagram depicting the process of precise co-registration of iterative scanned images per core. Based on distinct invariant features, iteratively scanned images were automatically adjusted and correctly aligned using CellProfiler pipeline.

The co-registered individual images were then passed to NIH ImageJ software [66], wherein the visualized AMEC and hematoxylin signals were automatically extracted using a color deconvolution algorithm [67], followed by the images converted to grayscale and subsequently assigned with distinct pseudo-color. Z-stacking of the pseudo-colored images was achieved in line with their ID using NIH ImageJ software (Figure 6).

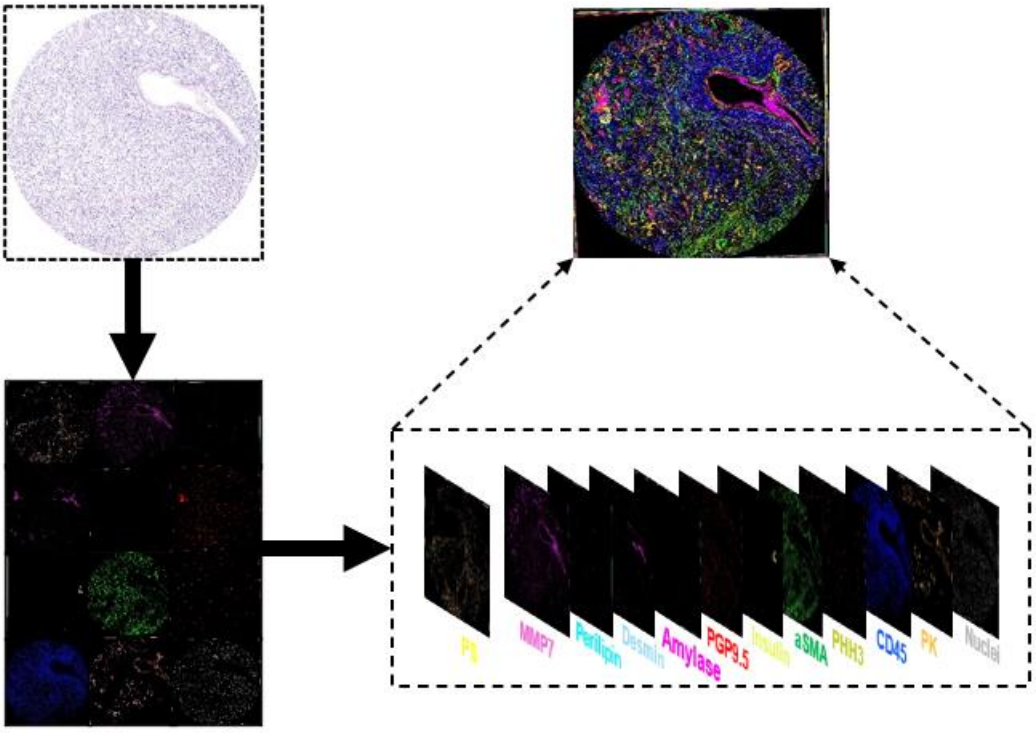

Figure 6: Schematic process pipeline representing pseudo-color assignment and Z-stacking of serial-stained images. Subsequent to co-registration, all biomarkers visualized in consecutive sections were assigned with distinct pseudo-color followed by Z-stacking according to their ID using NIH ImageJ software.

4.3 Stacking the pseudo-colored images depicts geographic distribution of migratory and resident cells and stromal compartments in CP lesions

To specifically determine complexity of infiltrating and resident cellular features and contribution of stromal components in CP lesions, we established three panels of 12-consecutive staining in which spatial distribution of these parameters can be finely preserved and displayed at the tissue level. The lymphoid biomarker panel signals cytotoxic T cells, regulatory T cells, activated

T cells, TH0 cells, TH1 cells, TH2 cells, TH17 cells, B cells, and NK cells (Figure 7A). The myeloid panel visualizes M1 macrophages, M2 macrophages, immature DCs (DC-Sign+), mature DCs ($CD83^{+}$), granulocytes, mast cells (Figure 7B). The pancreatic exocrine-endocrine and stroma panel delineates acinar cells, duct cells, nerve cells, islet cells, fibroblast cells, fibrosis-collagen deposition (Figure 7C).

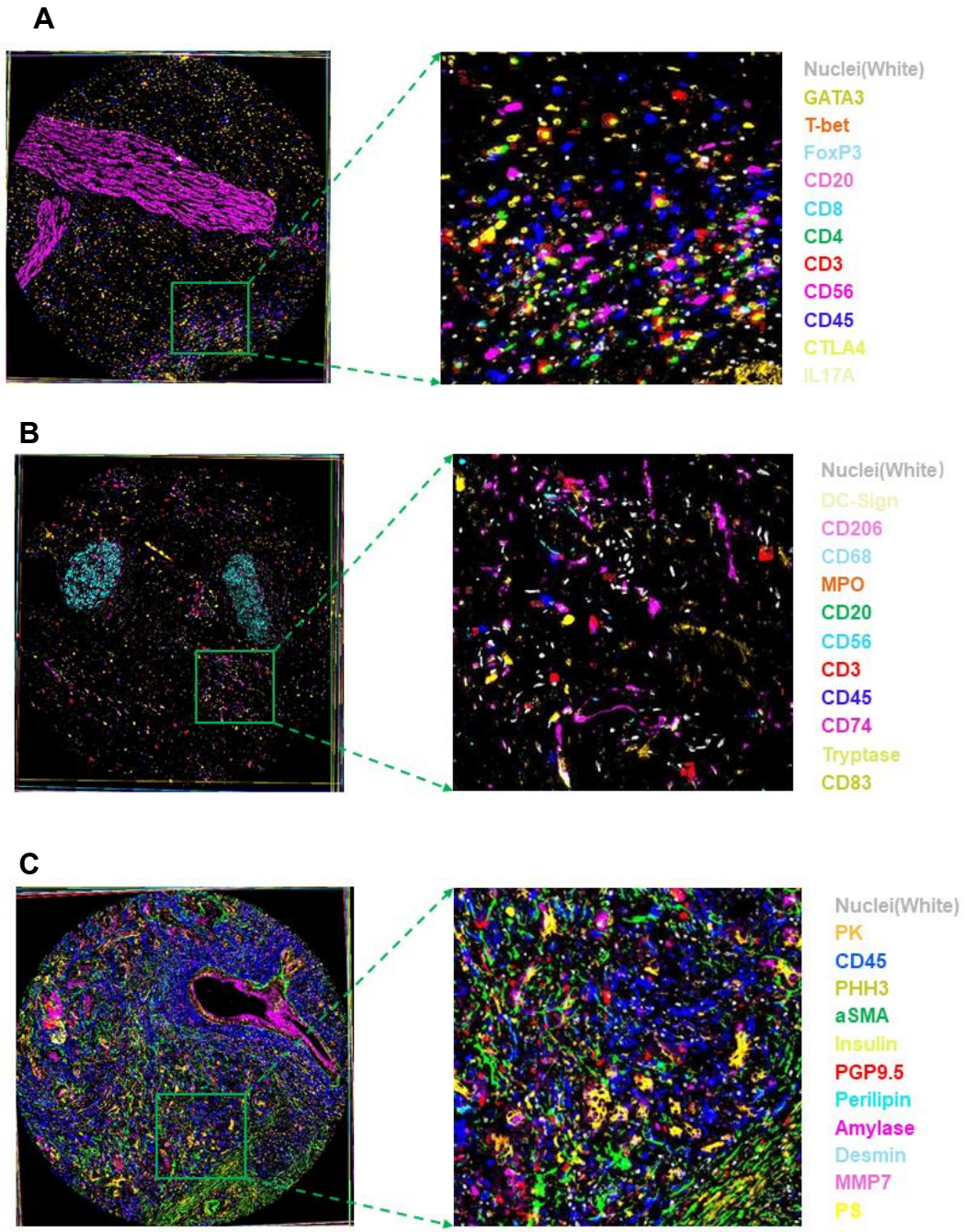

Figure 7: The representative of 12-pseudo-colored aligned images to visualize a single CP section from each of the three panels. (A) Colocalization of 12 biomarkers visualizes with

distinct pseudo-colors enable discernment of lymphoid lineage cells, including cytotoxic T cells, regulatory T cells, activated T cells, TH0 cells, TH1 cells, TH2 cells, TH17 cells, B cells, and NK cells. **(B)** Alignment of pseudo-colored images depicts myeloid lineage cells, such as M1 macrophages, M2 macrophages, immature DCs, mature DCs, granulocytes, and mast cells. **(C)** Colocalization of pseudo-colored images delineates acinar cells, duct cells, nerve cells, islets, and stromal compartments. Biomarkers and corresponding pseudo-colors are displayed in the right.

4.4 Cell image analysis enables reliable identification and quantification of distinct cell phenotypes

To accomplish the identification and quantification of distinct cell types and subtypes in CP lesions, we established an automated digital cytometric image-processing workflow through which single-cell based chromogenic intensities were measured using single-cell segmentation algorithms developed for CellProfiler software (Figure 3, 8) [68]. We utilized hematoxylin-stained images as a basis for single-cell segmentation based on watershed threshold algorithms [67, 69], followed by assigning with pseudo-color for individual signals. The chromogenic intensities in a series of AMEC-stained images were compiled and co-located with the segmented hematoxylin-stained images, generating a merged single-level image that yields multiple informative cellular features, such as cell phenotype, size, shape, and location as well. Single-cell-based information, including pixel intensities, shape-size outcomes, and location, was displayed and precisely analyzed based on the assessment of pixel intensities, a process that is largely analogous to flow cytometric analysis (Figure 8).

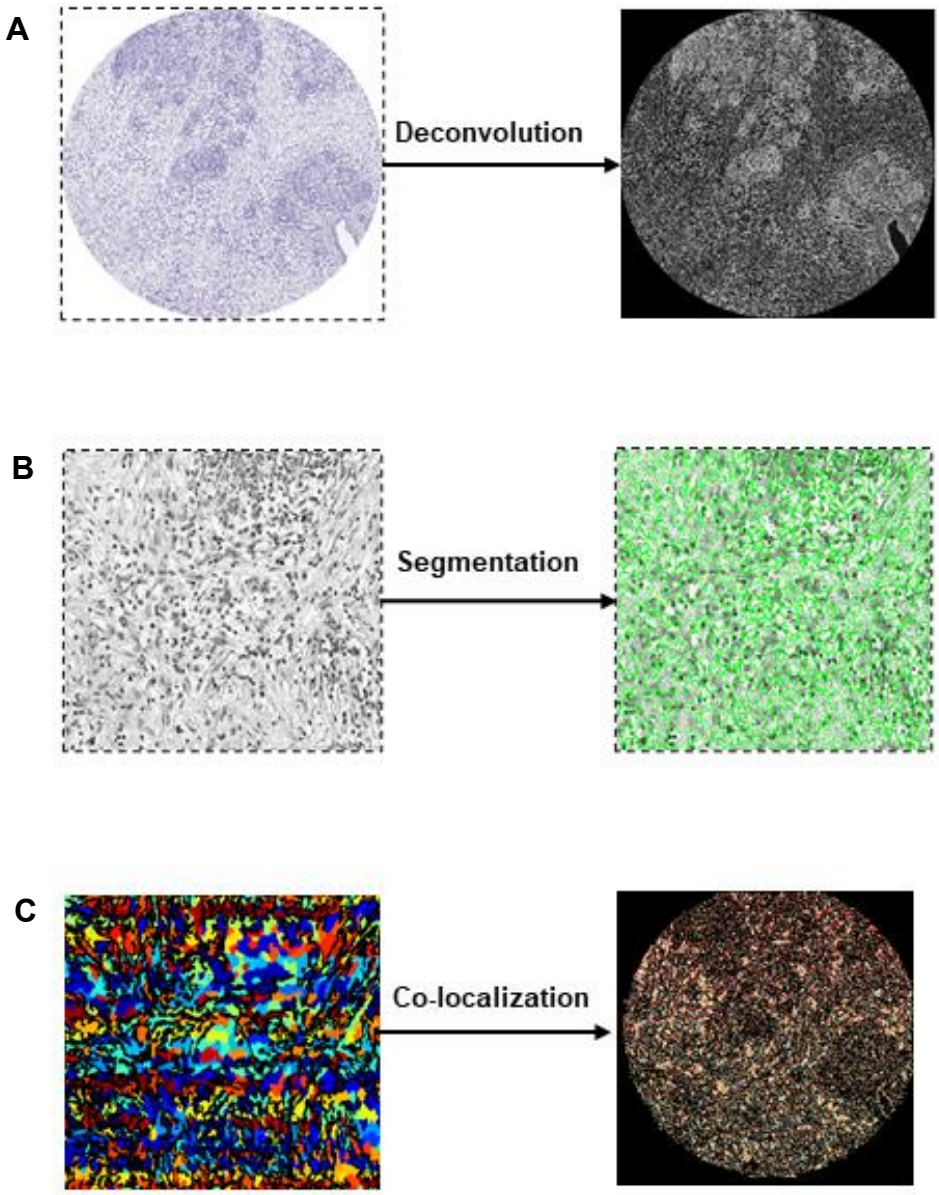

Figure 8 Cytometric image analysis workflow for the quantification of consecutively multiplex-stained images. (A) Hematoxylin-stained images are used as the backbone for deconvolution. **(B)** Following deconvolution, images are automatically separated using SIFT algorithm. **(C)** After segmentation, images are assigned with pseudo-color for individual signals, followed by co-localizing all the corresponding AMEC-stained images using SIFT algorithm. Based on the pixel intensity of chromogenic signals, the read-out of the cytometric image analysis provides multiple cellular information, including cell phenotype, size, shape, and location.

4.5 Qualitative gating strategies used for identifying complex cellular phenotypes and subtypes in the panels

The qualitative gating approaches employed for the image cytometry can

distinguish specific cellular phenotypes and subpopulations in a mixed context, yielding quantitative results largely analogous to polychromatic flow cytometry for dissociated cells [57, 70, 71]. Lymphoid-lineage cellular types and subtypes were identified by a combination of the corresponding lineage-labeling markers, which is depicted in Figure 9. Similarly, gating strategies for determining and quantifying myeloid-lineage cellular contribution in CP lesion were delineated in Figure 10. To explore the characterization of ductal cells, acinar cells, islet cells, and neural cells and alternation of stromal composition in CP tissue, we set the cytometric gating analysis as described in Figure 11.

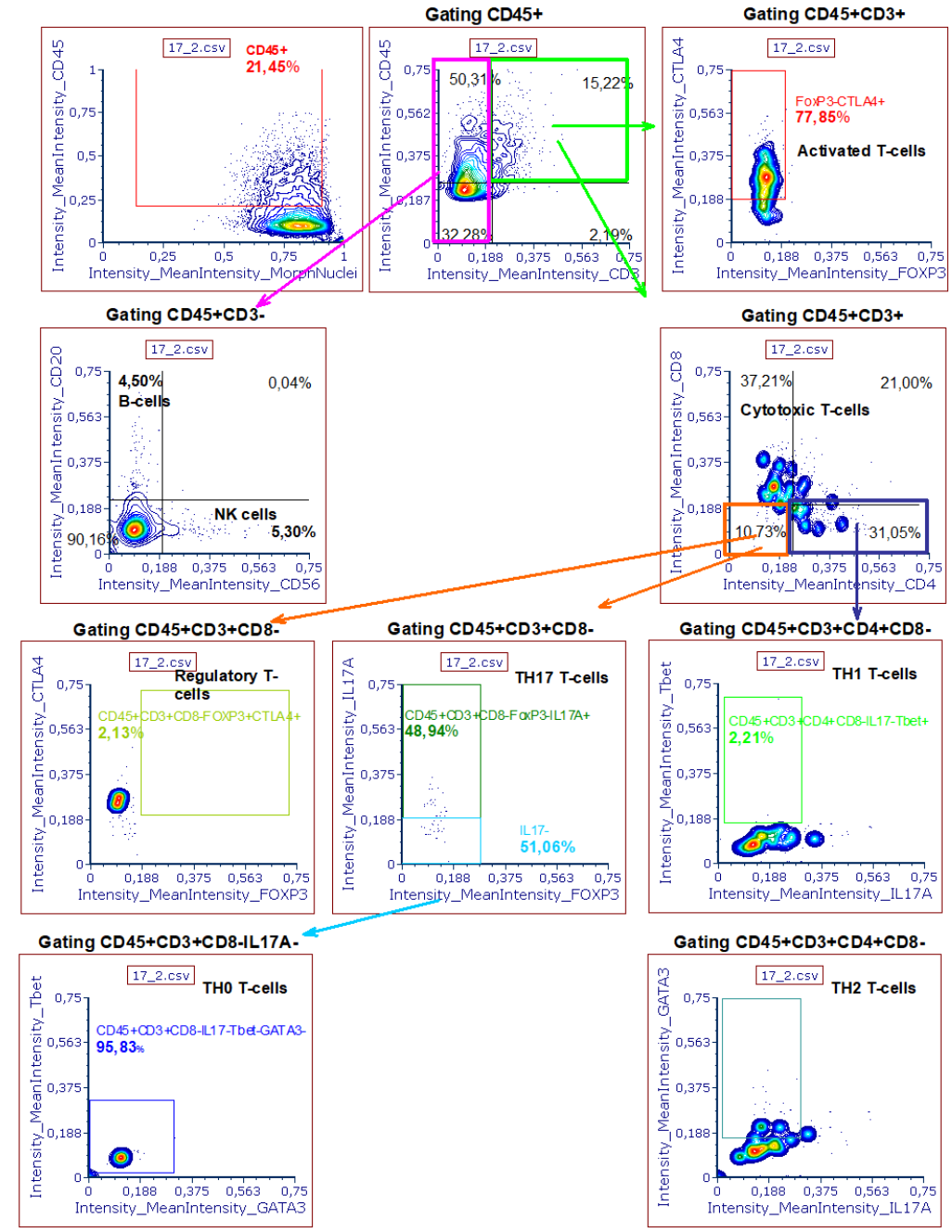

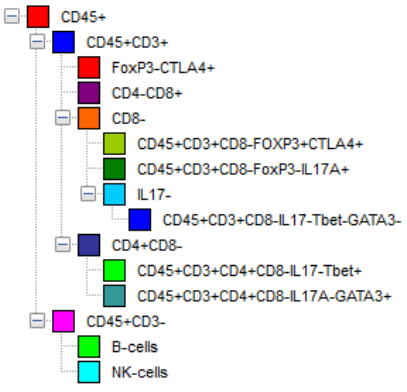

Figure 9 Representative plot of image-based cytometry for lymphoid-lineage cellular analyses from one of the included patients with CP. Image cytometry gating strategies for activated T cells (CTLA4+), cytotoxic T cells (CD8+), regulatory T cells (FoxP3+), TH17 cells (IL17A+), TH1 cells (Tbet+), TH2 cells (GATA3+), TH0 cells and other T subsets (CD45+CD3+CD8-IL17A-Tbet-GATA3-), B cells (CD20+), and NK cells (CD56+) in lymphoid biomarker panel.

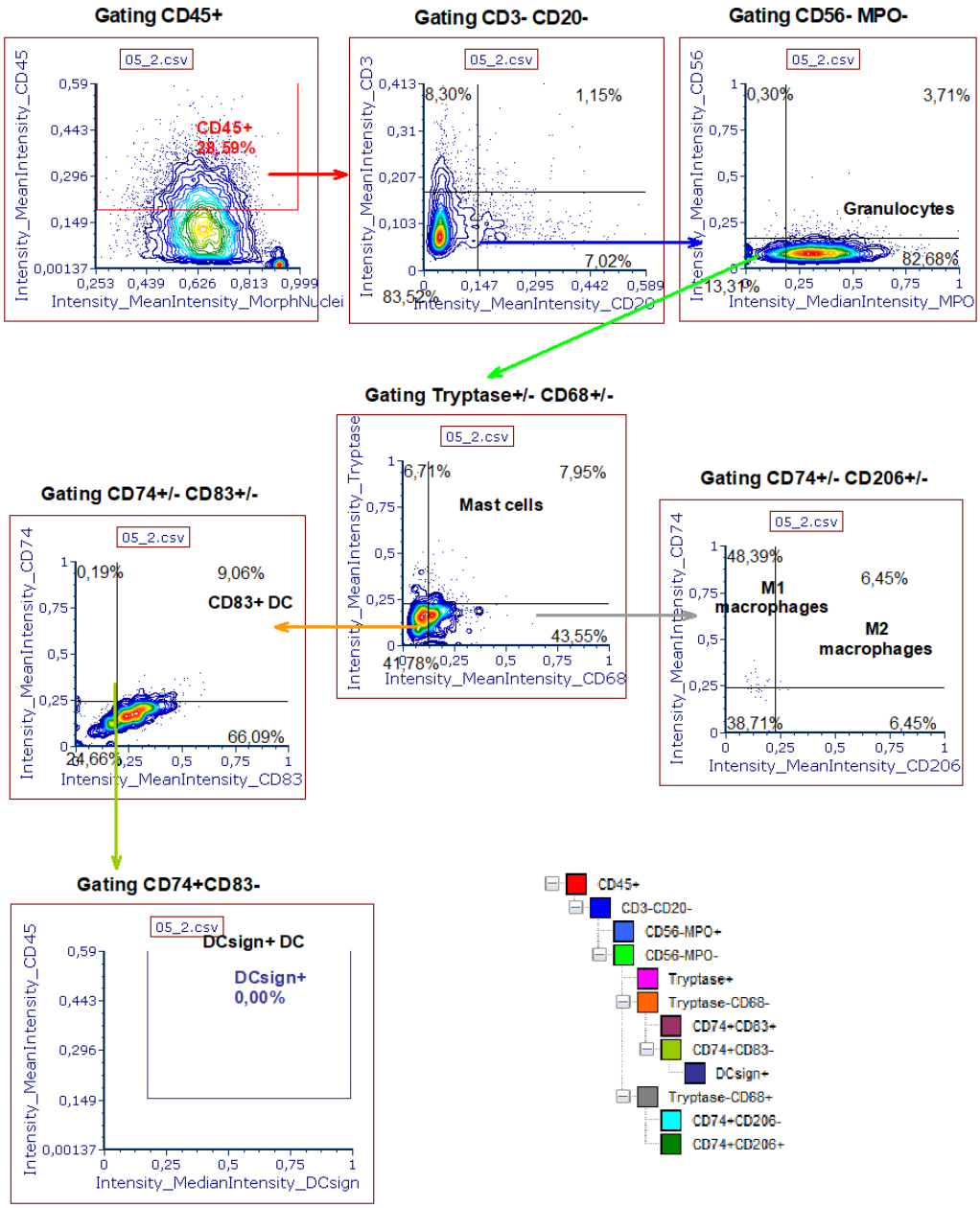

Figure 10 Representative plot of image-based cytometric analyses for the myeloid biomarker panel from one of the involved patients with CP. Image cytometry gating strategies for granulocytes (MPO+), mast cells (Tryptase+), immature dendritic cells (DC-Sign+), mature dendritic cells (CD83+), M1 macrophages (CD68+), and M2 microphages (CD206+) in myeloid biomarker panel.

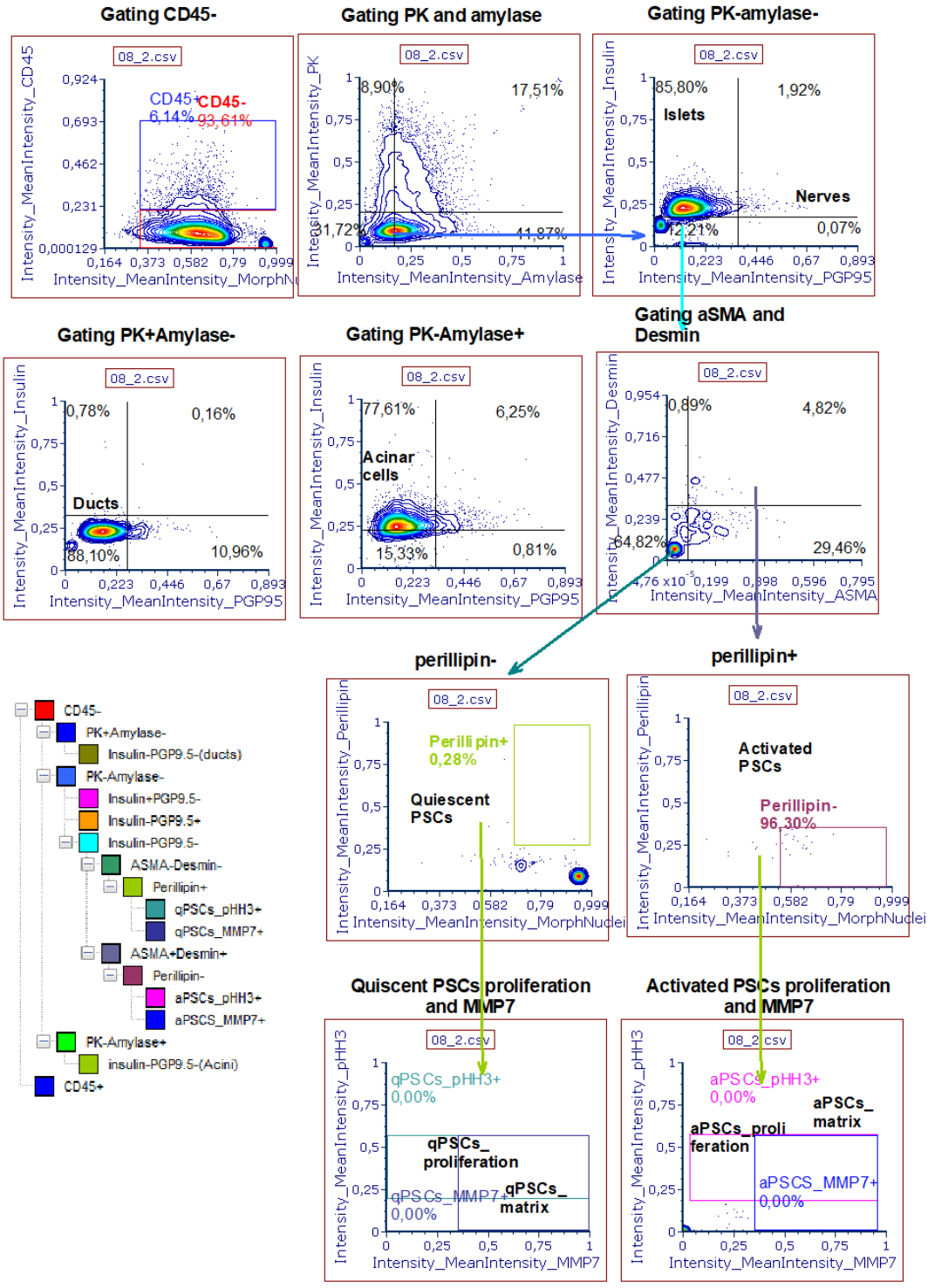

Figure 11 Representative plot of image-based cytometric analyses for the exocrine-endocrine and stroma biomarker panel from one of the included patients with CP. Image cytometry gating strategies for ductal cells (PK+), acinar cells (Amylase+), islet cells (Insulin+), neural cells (PGP9.5+), quiescent PSCs (Perilipin+), activated PSCs (Desmin+aSMA+), and the proliferative and functional status of quiescent and activated PSCs in exocrine-endocrine and stroma biomarker panel.

4.6 General cell distribution in alcoholic CP, AIP, and other CP lesions,

respectively

Based on the etiology of CP, we divided the 58 patients into three subgroups, that are alcoholic CP (n=23), AIP (n=7), and other CP (n=28) which contain biliary or obstructive CP (n=9), idiopathic CP (n=2), and CP without a specific cause identified (n=17).

To explore different cellular contributions to CP lesions, we detected and quantified distinct cell lineages based on the pixel intensity. Then, we classified the extracted cellular data as two categories, including immune cell population (CD45+ cells) and non-immune cell population (CD45- cells), based on a pan-leukocyte biomarker CD45+ staining. As described in table 3, the immune cellular compartments compose of B cells, DCsign+DC (immature phenotype), CD83+DC (mature phenotype), granulocytes, M1 macrophages, M2 macrophages, mast cells, NK cells, as well as T cell subtypes which consist of activated T cells (Act-T cell), cytotoxic T cells (Cyt-T cell), T regulatory cells (Reg-T cells), T others (TH0 cells), TH1, TH2 cells, TH17 cells. The non-immune cellular components involve acinar cells, ductal cells, nerves, islet cells, aPSCs, qPSCs, and collagen deposition. To investigate the contribution of individual cell lineages within CP lesions in the context of distinct etiologies, we compared the relative content of these cells in alcoholic CP, AIP, and other CP, separately. In the part of immune cell population, activated T cells are most predominant, followed by granulocytes, B cells, cytotoxic T cells, TH0 cells, mast cells, NK cells, CD83+DCs, TH2 cells, TH17 cells, T regulatory cells, DCsign+DC, TH1 cells, M1 macrophages, and M2 macrophages.

In alcoholic CP lesions, immune cellular compartments account for 7.67%, far less than non-immune cellular components (92.33%). As for non-immune cellular compartments, acinar cells, duct cells, and islets constitute the top three proportion, followed by quiescent PSCs (qPSCs), nerves, activated PSCs (aPSCs), qPSCs within proliferative state, aPSCs-matrix, aPSCs within proliferative state, and qPSCs-matrix as well (Figure 12).

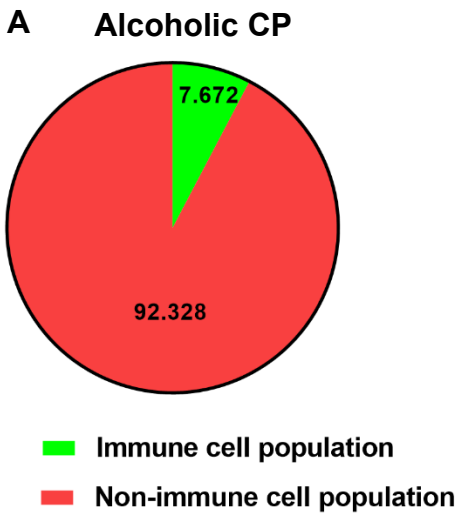

Figure 12 Distribution of immune and non-immune cell population in alcohol-related CP.
A, Pie chart represents the proportion of immune and non-immune cells in alcoholic CP.
B, Bar graph depicts immune cellular distributions in alcoholic CP.
C, Bar graph reflects non-immune cellular contribution to alcoholic CP.

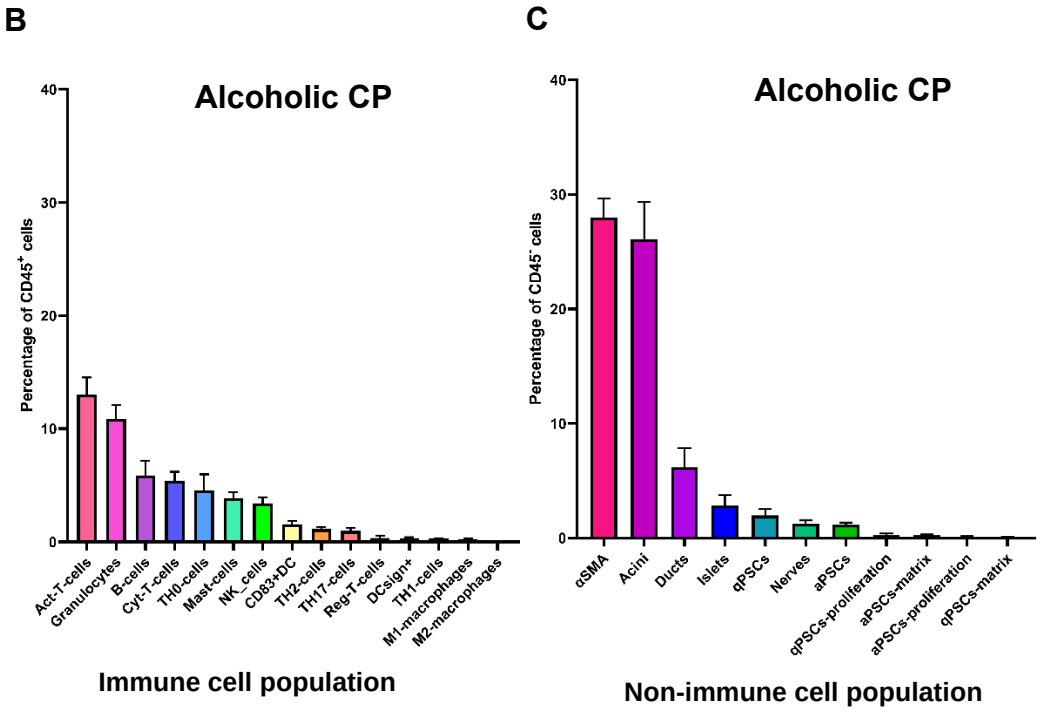

In AIP, immune cell compartments make up 19.39% of the cellular components within the lesions, implying that almost one-fifth of the normal pancreatic architecture was replaced by immune infiltrates (Figure 13A). Further immune cell lineages-tracking analyses demonstrated that granulocyte components are the most abundant in the lesions, largely surpassing other immune infiltrates such as TH0 cells, activated T cells, B cells, MCs, and NK cells. By contrast, the frequency of DCs, macrophages, and other T cell subtypes is relatively less

compared to other immune cells, as shown in Figure 13B. Detection of non-immune cell contents indicated that acinar cells, islet cells, ductal cells still possess the most proportion, followed by aPSCs, qPSCs, aPSCs-matrix, nerves, qPSCs-matrix, proliferative qPSCs, and proliferative aPSCs as well (Figure 13C).

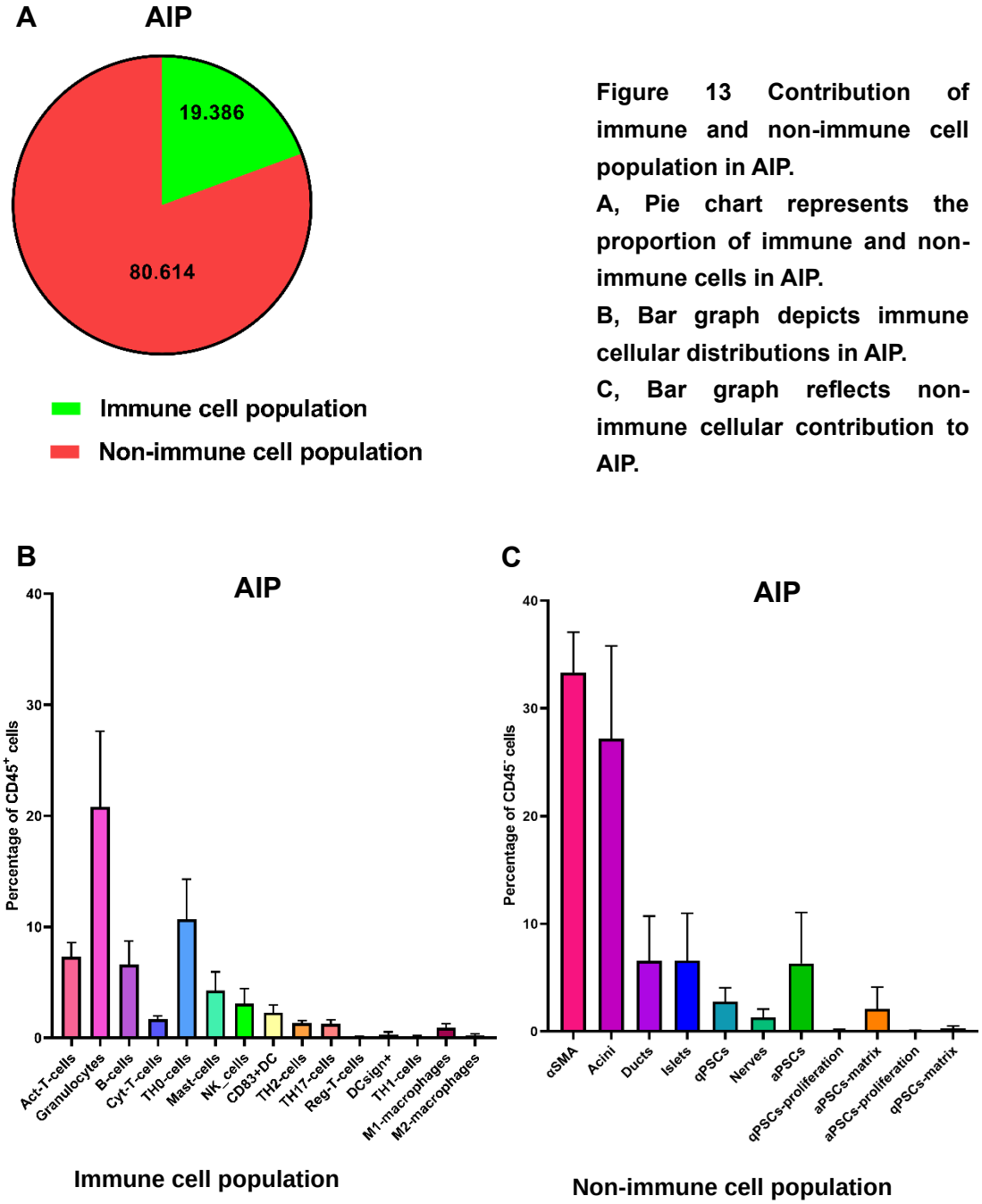

Figure 13 Contribution of immune and non-immune cell population in AIP.
A, Pie chart represents the proportion of immune and non-immune cells in AIP.
B, Bar graph depicts immune cellular distributions in AIP.
C, Bar graph reflects non-immune cellular contribution to AIP.

Our investigation looking at the cellular distribution of other CP subgroup shows that around 7.93% of the components in lesion area are immune compartments,

predominated by activated T cells, granulocytes, cytotoxic T cells, B cells, MCs, TH0 cells, and NK cells (Figure 14A, B). Cellular composition analyses of non-immune compartments demonstrated that the major cellular compartments are acinar cells, followed by islet cells, ductal cells, aPSCs, qPSCs, neural cells, and other PSCs subgroups (Figure 14C).

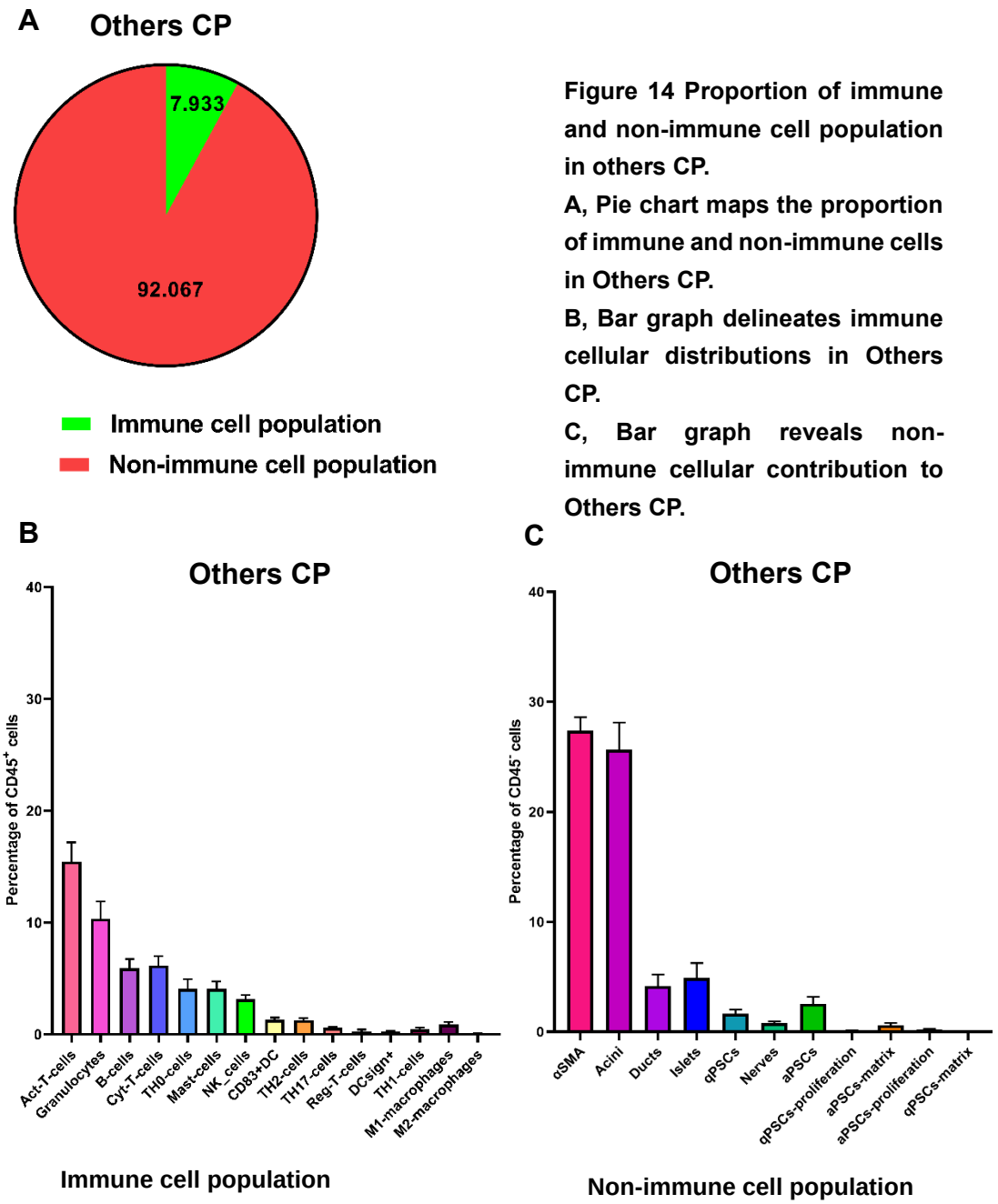

Figure 14 Proportion of immune and non-immune cell population in others CP.
A, Pie chart maps the proportion of immune and non-immune cells in Others CP.
B, Bar graph delineates immune cellular distributions in Others CP.
C, Bar graph reveals non-immune cellular contribution to Others CP.

4.7 CD45+ cell infiltration in AIP lesions is significantly higher than in alcoholic and other CP

Previous animal and human investigations robustly documented that leukocytes are substantially enriched in CP lesions compared with healthy pancreatic samples and play a variety of roles in the advance of CP [21, 35, 49, 72]. However, few studies have focused on the features of infiltrating immune cells in CP based on the distinct etiology. To specifically characterize leukocyte contribution in lesion areas of alcoholic CP, AIP, as well as CP of other causes, CD45+ (pan-leukocyte biomarker) cells were identified. We observed a statistically significant increase in the density of CD45+ leukocytes in autoimmune CP tissues when compared with alcoholic CP and other CP lesions (P=0.047). In contrast, we did not find a marked difference between alcoholic and other CP groups (Figure 15).

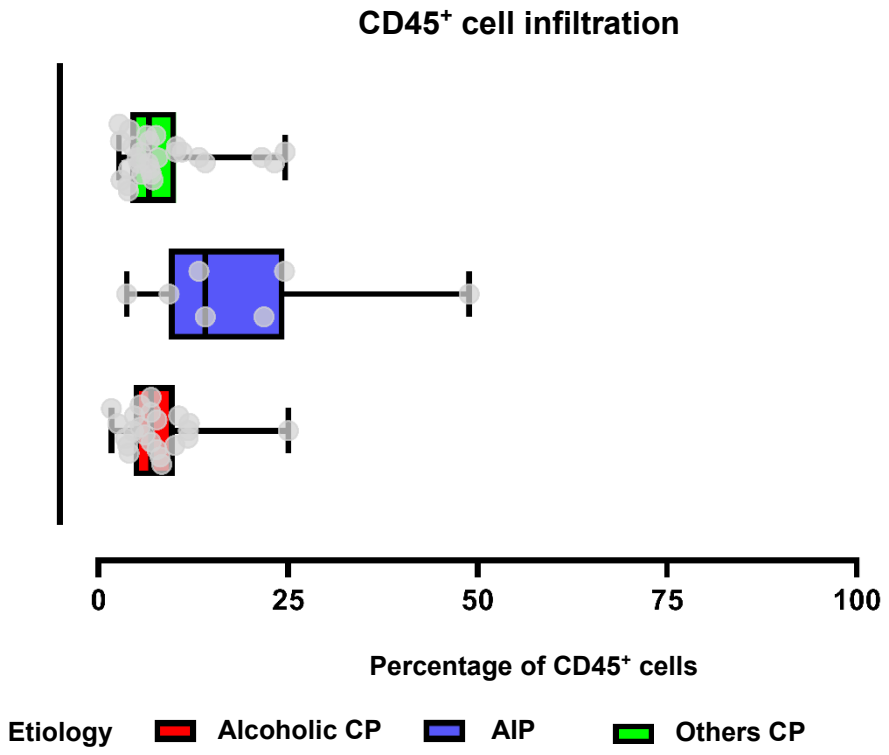

Figure 15 CD45+infiltrates are slightly frequent in AIP compared with alcoholic CP and other CP. The representative graph denotes the mean density of CD45+cells in lesions of the three CP groups based on image cytometry results. Comparable analyses were conducted using Kruskal-Wallis tests.

4.8 Comparison of immune subtypes and stromal compartments among different CP groups indicated a nuanced program driving distinct forms

of the disease

To determine the characterization of immune subsets in different etiological forms of CP, we evaluated the density of individual immune cell subtypes in CP sections signaled by either lymphoid biomarkers or myeloid biomarkers and compared those parameters among the three CP groups. Lymphoid lineage subtype characterization involved the identification of B cells, NK cells, and T cell subsets, including activated T cells, cytotoxic T cells, TH17 cells, TH2 cells, TH1 cells, TH0 cells as well as regulatory T cells. Intriguingly, the density of cytotoxic T cells was significantly amplified in both alcoholic CP and other CP when compared with AIP. A similar tendency was observed in the distribution of activated T cells, although the differences did not reach a statistically significant level between alcoholic CP and AIP. On the contrary, the frequency of TH0 cells was boosted in AIP compared with the other two CP groups. No significant differences of B cells, NK cells, regulatory T cells, TH17 cells, TH1 cells, and TH2 cells were indicated among the three CP subgroups (Figure 16).

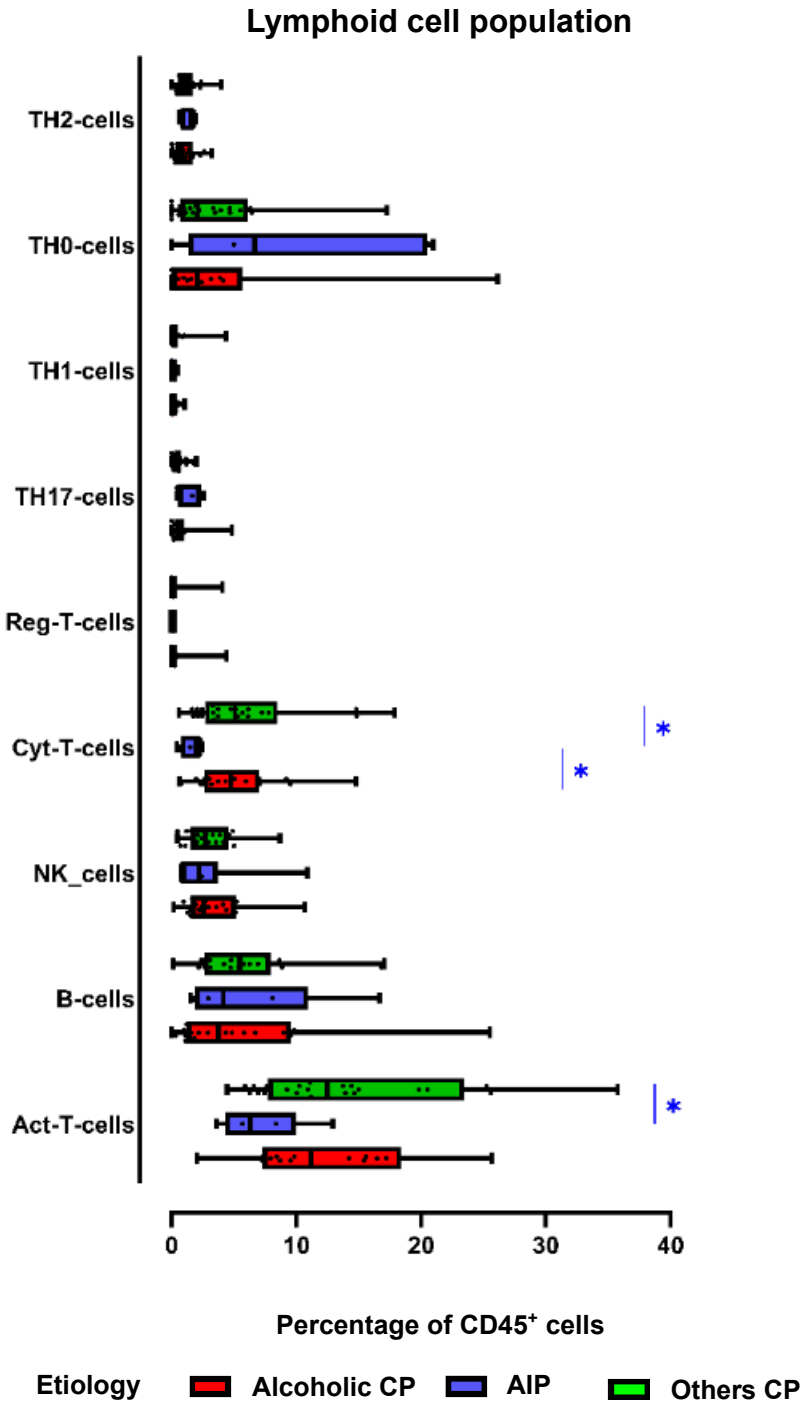

Figure 16 Comparison of the distribution of lymphoid lineage cell subsets, including B cells, NK cells, and T cell subsets in CP lesions among alcoholic CP, AIP and other CP. Comparable analyses were conducted using Kruskal-Wallis tests. Asterisk means significant difference with P <0.05.

Further analyses for myeloid lineage cell subtypes included identification of mast cells, granulocytes, M1 macrophages, M2 macrophages, DCsign+ DCs,

and CD83+DCs. Notably, we found that the abundance of granulocytes was mildly enhanced in AIP when compared with alcoholic CP and other CP. However, no significant differences in the contribution of mast cells, macrophages subsets, and DCs subsets were noticed among the three CP groups (Figure 17).

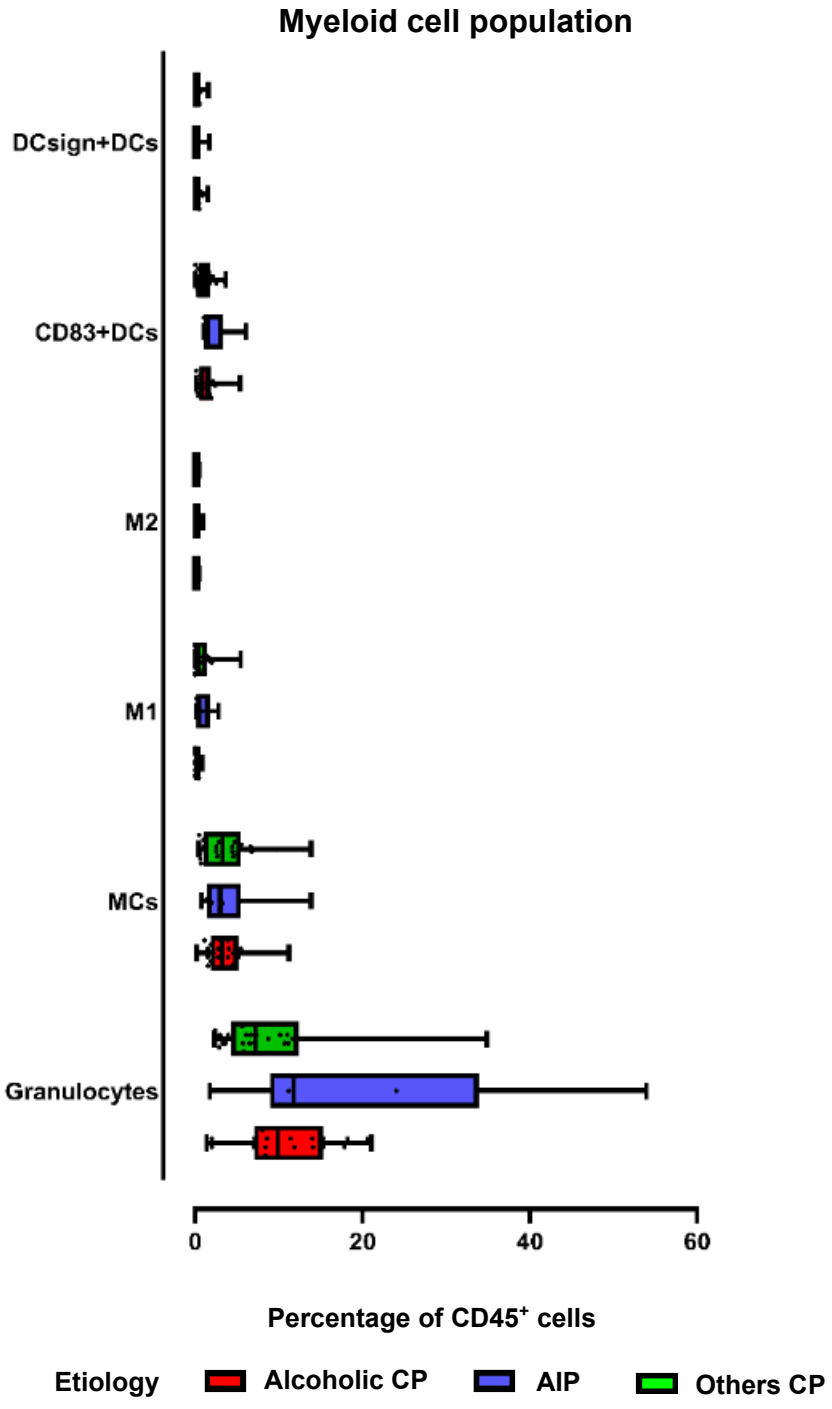

Figure 17 Comparison of the contribution of lymphoid lineage cell subtypes, including mast cells, granulocytes, macrophage subsets, and dendritic cell subsets as well, in CP lesions among alcoholic CP, AIP and other CP. Comparable analyses were conducted using Kruskal-Wallis tests.

We next analyzed the distribution of individual non-immune compartments, including acinar cells, ductal cells, islet cells, nerves, distinct PSCs subsets, and collagen deposition as well, among the three CP groups. We did not find significant divergence in the frequency of acinar cells, ductal cells, and islet cells among alcoholic CP, AIP and other CP. Similarly, no remarkable divarication in the distribution of PSC subtypes including quiescent PSCs, activated PSCs, quiescent PSCs staying at proliferative phases, matrix-producing quiescent PSCs, activated PSCs staying at proliferative phases, and matrix-producing quiescent PSCs among the three CP subgroups. (Figure 18).

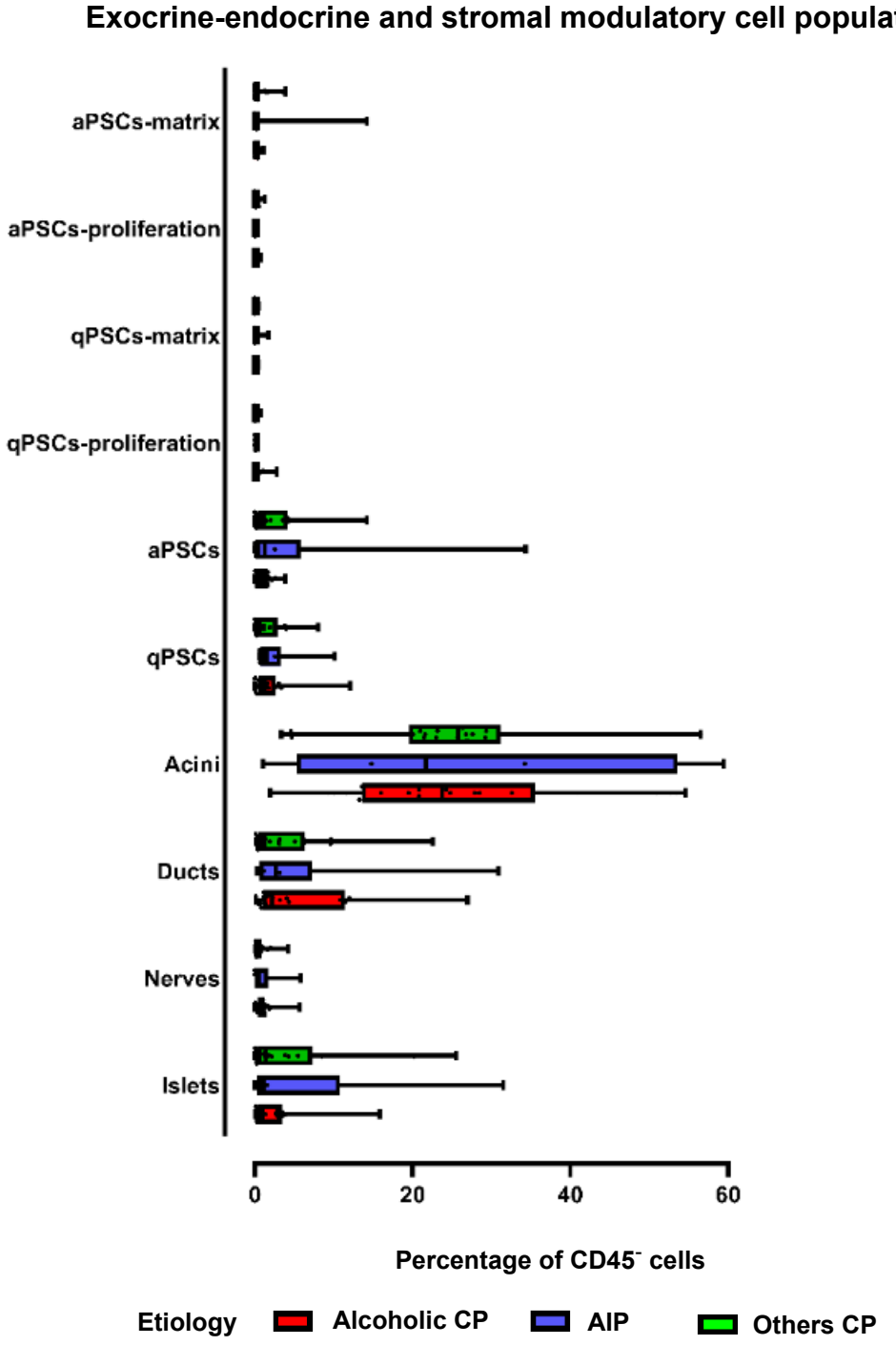

Figure 18 Comparison of the contribution of individual non-immune compartments, including acinar cells, ductal cells, nerves, distinct PSCs subsets, and collagen deposition as well, in CP lesions among alcoholic CP, AIP and other CP. Comparable analyses were conducted using Kruskal-Wallis tests.

4.9 Distinct stromal forms shaped the discrepant pattern of immune infiltration among the three CP groups

Prominent fibrosis formation and extensive collagen deposition represent two major histological features of CP. It is well documented that pathogenic fibrogenesis with the advance of CP is mainly governed by PSCs. Typically, PSCs stay as quiet phenotype and play vital roles in sustaining normal tissue architecture via balancing the synthesis and degradation of ECM components [20, 26]. Upon pancreatic injury, PSCs switch to an activated phenotype, specifically identified by aSMA expression, and produce a bulk of ECM components, particularly collagen. To ascertain whether there were differences in the functional state of PSCs and ECM deposition among the three CP groups, we analyzed the percentage of area occupied by aSMA+ staining and collagen deposition, respectively. We observed the ratio of aPSCs seemed to be higher in AIP compared with alcoholic CP and other CP, but collagen deposition tended to be lower in AIP than the other two groups, despite the differences were not statistically significant (Figure 19).

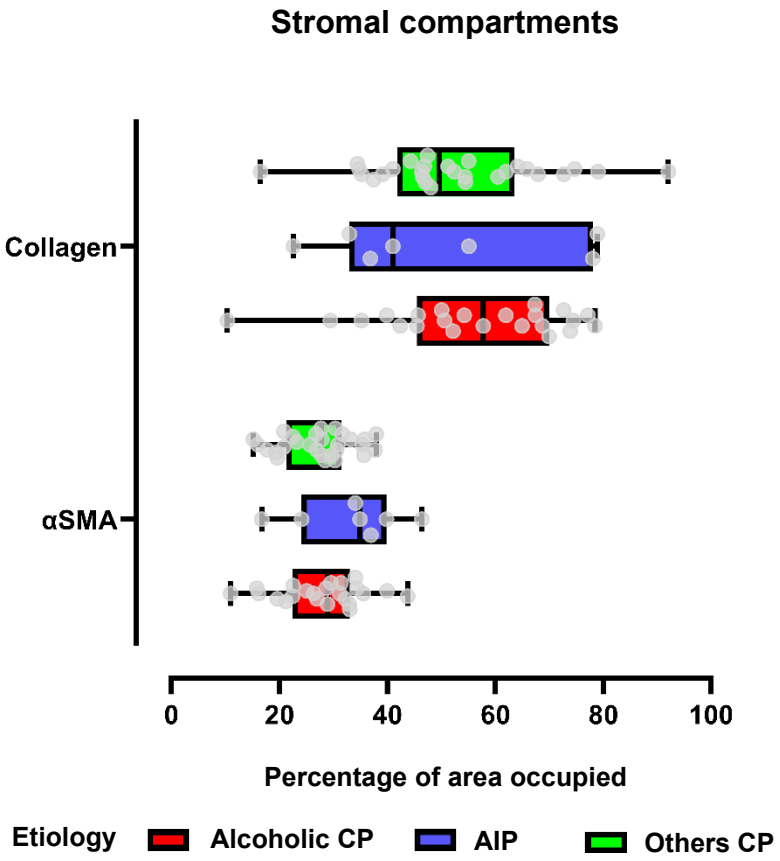

Figure 19 Comparison of percentage of area occupied by aSMA expression and collagen deposition among alcoholic CP, AIP, and other CP. Comparable analyses were conducted using Kruskal-Wallis tests.

One of the common properties between PDAC and CP is the extensive desmoplastic reaction, reflected by PSCs activation and collagen deposition. In the context of PDAC development, four distinct expression patterns of aSMA and collagen were delineated as dormant (low aSMA/high collagen expression), fibrogenic (high aSMA/high collagen expression), fibroytic (high aSMA/low collagen expression), and inert stroma (low aSMA/low collagen expression), which were proven as important prognostic biomarkers for patients with PDAC (Table 4) [73].

Table 4: Definition of different stromal forms based on the expression patterns of aSMA and collagen

	Dormant	Fibrogenic	Fibroytic	Inert
aSMA	low	high	high	low
Collagen	high	high	low	low

Furthermore, previous work from our group found evidence that different stromal subtypes not simply affect the prognostic outcomes of patients with malignant events, but are closely linked to intra-tumoral immune infiltrates [58]. Those results led us to focus on the question of whether the immune infiltrates play roles in shaping distinctive stromal subtypes in the context of CP with different etiology. To figure out the answer, we first analyzed the distribution of the three distinct CP subgroups in different stromal subtypes. We observed that 13.04% (n=3) of alcoholic CP patients were classified into dormant stroma subtype, with 21.73% (n=5) classifying as fibrogenic stroma subtype, 30.43% (n=7) as fibrolytic stroma subtype, and 34.78% (n=8) as inert stroma subtype.
In AIP subgroup, 14.29% (n=1) of patient was defined as fibrogenic stroma, 57.14 % (n=4) of patients as fibrolytic stroma, and 28.57 % (n=2) of patients as inert stroma; however, there is no patient classified into dormant stroma.

Analyses of other CP suggested that 25.00% (n=7) of patients were grouped into dormant stroma subtype, 14.29% (n=4) into fibrogenic stroma subtype, 28.57% (n=8) into fibrolytic CP, and 32.14% (n=9) into inert stroma subtype. Intriguingly, comparison of the distributional characteristics of different CP subgroups in distinct stromal subtypes did not indicated a statistically significant difference.

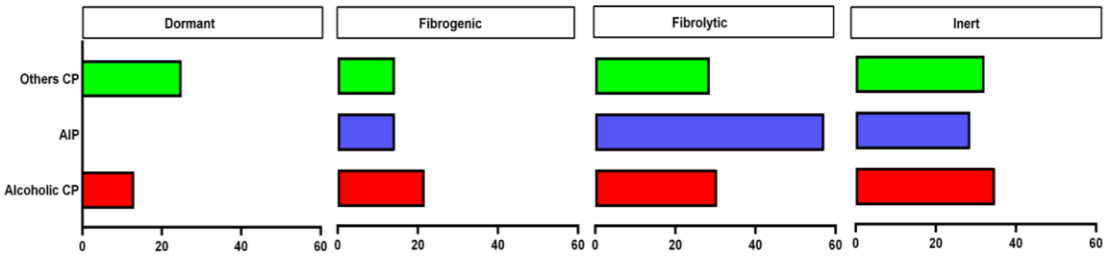

Figure 20 Bar graph annotating the distribution of CP with distinct causes in different stromal subtypes. Comparable analyses were conducted using Fisher's Exact Test. No statistically significant differences were observed among the distribution of etiologically different CP subgroup in individual distinct stromal subtypes.

Furthermore, we compared the contribution of immune infiltrates in different stromal subtypes among the three CP groups. Analyses of lymphoid biomarker panel indicated that fibrolytic stroma in AIP has significantly higher numbers of TH0 cells compared with alcoholic CP and other CP. By contrast, the frequency of both activated T cells and cytotoxic T cells was dramatically reduced in AIP compared with the other two groups in fibrolytic stroma. The density of B cells and NK cells within inert stroma in AIP tend to be higher than in alcoholic CP and other CP, but the percentage of cytotoxic T cells was significantly reduced in AIP compared to other CP group (Figure 20). Additionally, the number of B cells and activated T cells in the context of fibrogenic stroma seem likely to be enriched in alcoholic CP as well as other CP when compared with that of AIP (see Figure 20).

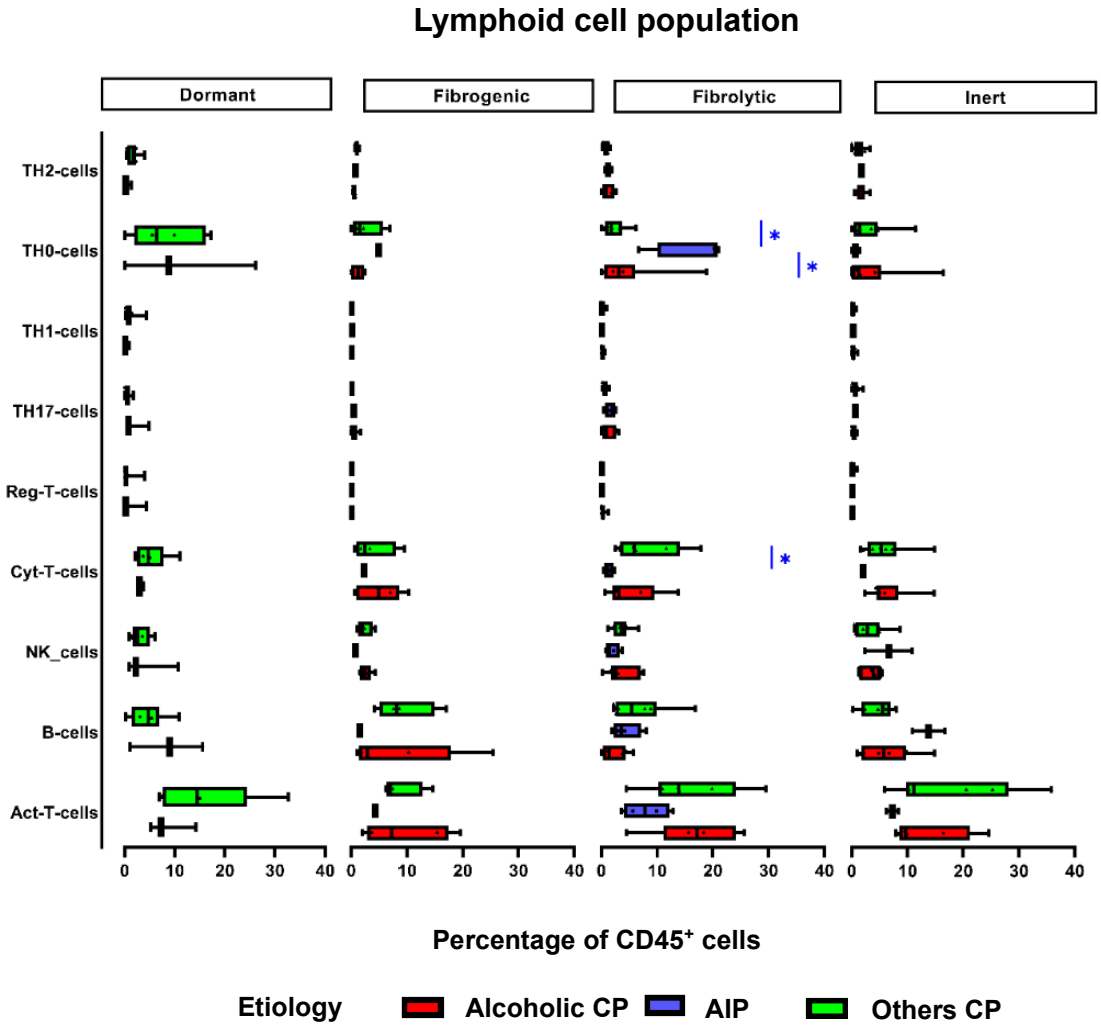

Figure 21 Box and whiskers plot denoting the differential contributions of lymphoid cell subsets in distinct stromal subtype among different CP groups. Comparable analyses were conducted using Mann-Whitney tests and Kruskal-Wallis tests. Asterisk means significant difference with P <0.05.

Data from myeloid biomarker panel analyses suggested that fibrolytic stroma in AIP tends to have more abundance of granulocytes when compared to alcoholic CP and other CP, as demonstrated in Figure 22.

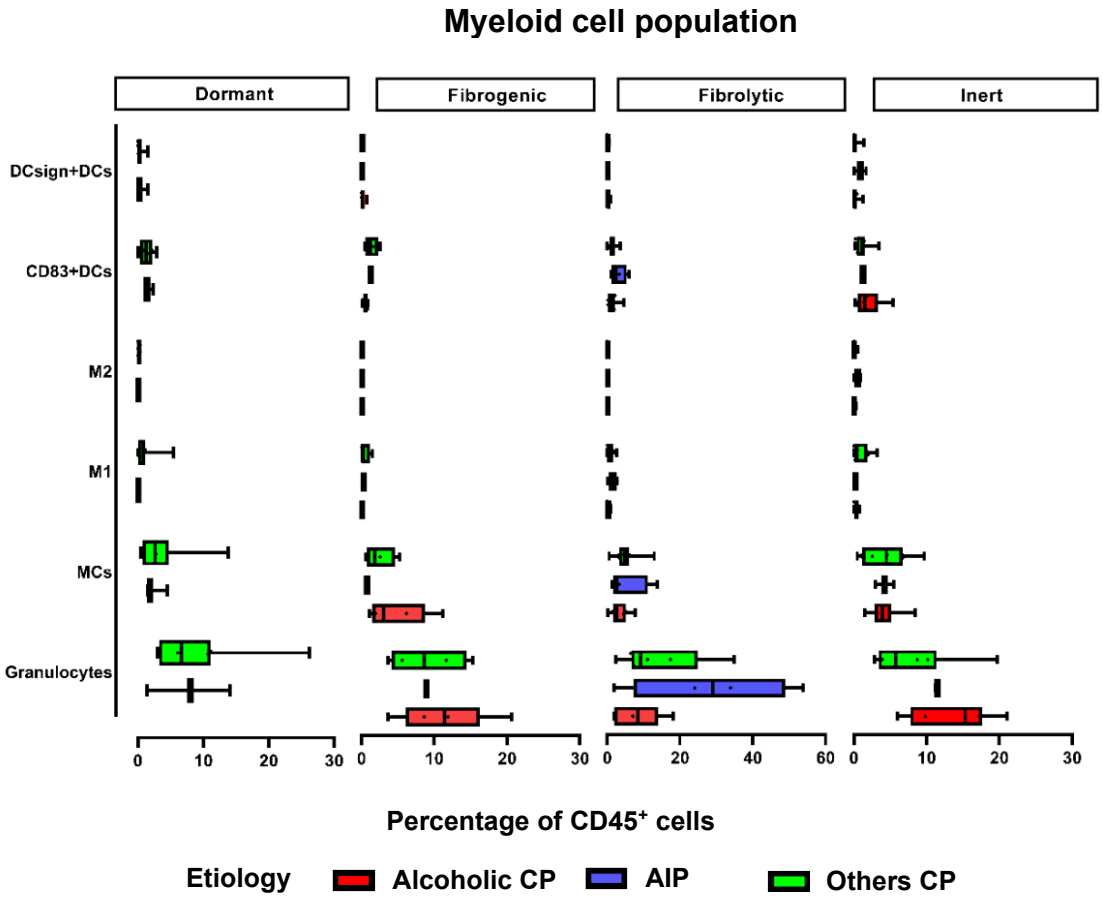

Figure 22 Box and whiskers plot representing the differential contributions of myeloid cell subsets in distinct stromal subtype among different CP groups. Comparable analyses were conducted using Mann-Whitney tests and Kruskal-Wallis tests.

Next, to explore the connection between stromal subtype and the distribution of pancreatic exocrine-endocrine cell populations and stromal compartments in the context of CP of different etiology, comparative correlation analyses among the three CP groups were conducted. It indicated that inert stroma in both alcoholic CP and other CP harbors higher amounts of acinar cells compared with AIP. Similarly, in the context of fibrolytic stroma, higher numbers of acinar cells were revealed in alcoholic CP and other CP when compared with AIP. By contrast, the composition of ductal cells within inert contexture found higher in AIP compared to alcoholic CP and other CP (Figure 23).

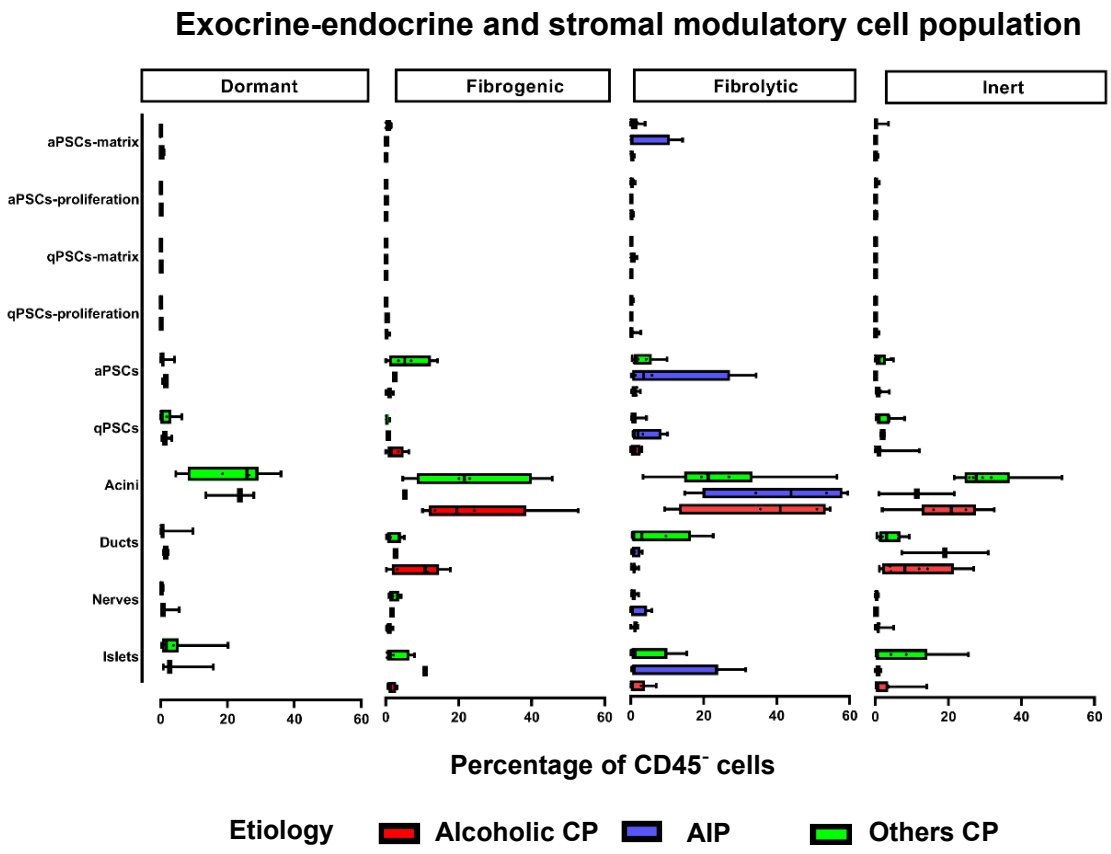

Figure 23 Box and whiskers plot denoting the differential contributions of acinar cells, ductal cells, islet cells, nerve cells, and stromal compartments in distinct stromal subtype among different CP groups. Comparable analyses were conducted using Mann-Whitney tests and Kruskal-Wallis tests.

4.10 AutoML technique predicted top ten features associated with the presence of exocrine insufficiency of patients with CP

One of the most common consequences of CP is the loss of exocrine pancreatic function, due to the destruction of acinar cells, with impact on nutritional status and quality of life. Despite plenty of investigations launched in experimental models and clinical cohorts, the definitive mechanism underlying the development of exocrine insufficiency in patients with CP is still far from completely understood. This is partly because of the hardness to catch the dynamics of acinar cell disruption, especially the kinetics of their interaction with immune infiltrates as well as non-immune cellular compartments during the development of CP. To explore the potential contributors to acinar cell

destruction and the consequent exocrine compromise, we applied computational machine learning techniques together with R programming language statistics to analyze multi-stained TMA image characterization in combination with clinically testing of exocrine function from the matched patients.

To accomplish this combinational analysis, we attempted to collect the clinical data of the 58 included patients with CP. However, 3 patients were excluded from the analysis due to missing clinical exocrine data. Therefore, 55 patients were subjected to the final analysis, with 36 patients not having exocrine insufficiency and 19 patients who had developed exocrine insufficiency at the time of surgery (Figure 24).

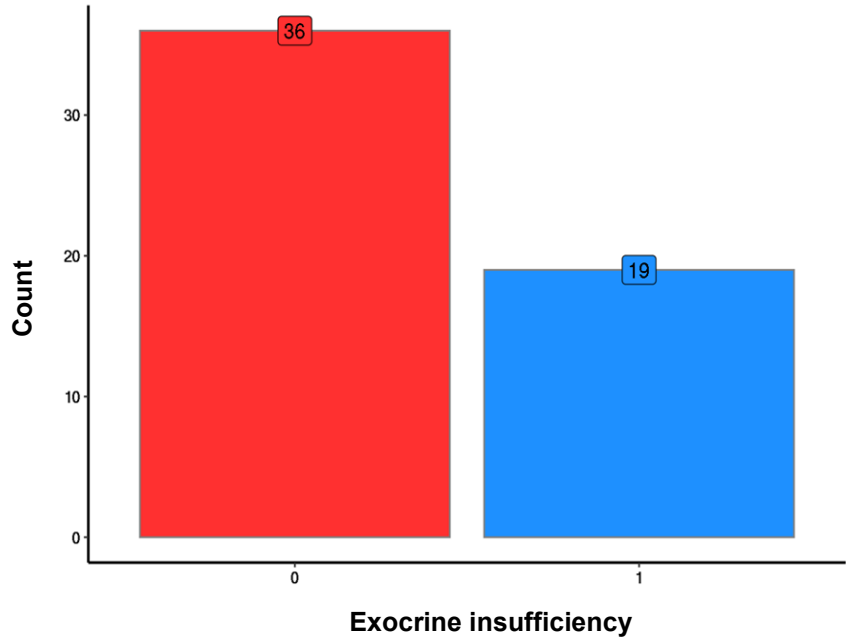

Figure 24 Column chart annotating exocrine function of the 55 analyzed patients with CP, with the red column representing the 36 patients retaining normal exocrine function and the blue column depicting 19 patients evidenced with exocrine insufficiency.

Multiplexed image data from the 55 analyzed patients were randomly split into two subsets, with 80% of those data categorized into training and tuning cohort to create a final model, alongside 20% of those data serving as the testing cohort to assess and optimize the final model performance. To assure a more robust consistency of predicting exocrine insufficiency, we exploited a

combination of a stacked machine learning algorithm implementations provided by the R to generate automatic machine learning models for the present study. As explicitly demonstrated in Figure 25, deep learning dominates the stacked machine learning models, with the assistance of several other models including GBM, GLM, XGBoost, DRF, and XRT)

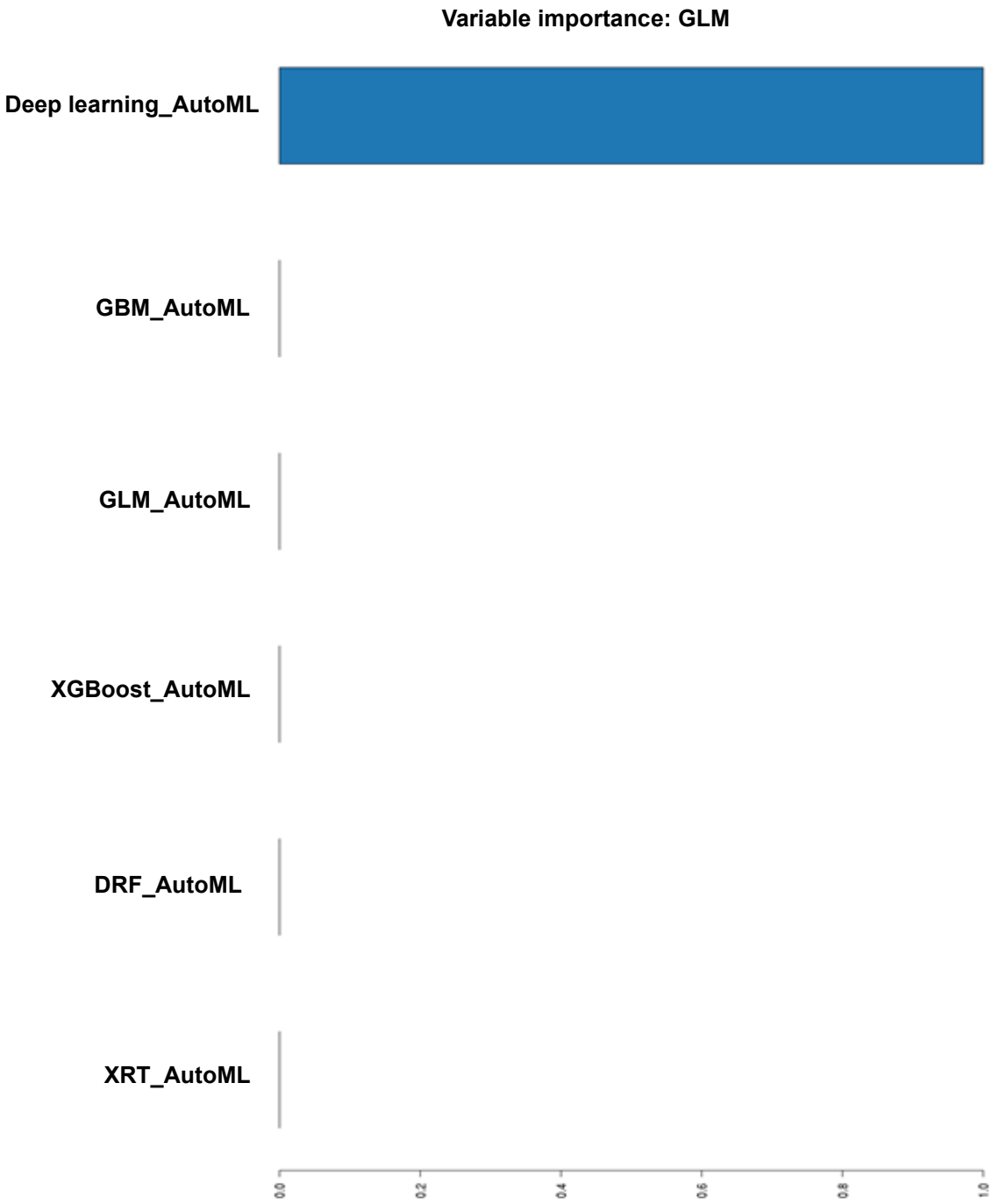

Figure 25 Automatic machine learning models applied to identify potential features to predict exocrine insufficiency. Deep learning model is explicitly prominent in the stacked machine learning model approaches, with the involvement of GBM, GLM, XGBoost, DRF as well as XRT model.

To more accurately find out important potential features on predicting the presence of exocrine insufficiency in patients with CP, we computed the multiplex-stained images using stacked ensemble AutoML models which

incorporated deep learning as well as GBM, GLM, XGBoost, DRF and XRT algorithm. We made use of this methodology based on the fact that the stacked ensembles are proved to be outperforming any of the individual base learner predictions, like GBM and GLM [74]. Stacking the involved base learners was automatically accomplished by the H2O AutoML algorithm implemented in R programming environment. The Partial dependency-based variable importance scores and corresponding partial dependence plots were automatically constructed from the stacked models. As shown in Table 5, we list the top ten features associated with the presence of exocrine dysfunction of patients with CP. We found the number of activated PSCs specifically residing in the proliferative state has the strongest importance in predicting the induction of pancreatic exocrine dysfunction. Following the indicator of proliferative aPSCs, the frequencies of NK cells and islets are the second and third significant predictors of the presence of pancreatic exocrine insufficiency respectively.

Table 5: The top ten predictors for exocrine insufficiency of patients with CP

Variable	Relative importance	Scaled importance	Percentage	Partial dependency plot
aPSCs proliferation	1.000	1.000	0.065	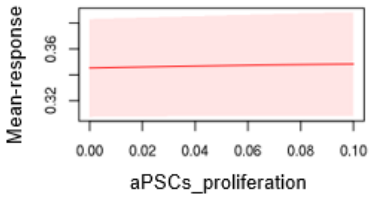
NK cells	0.825	0.825	0.054	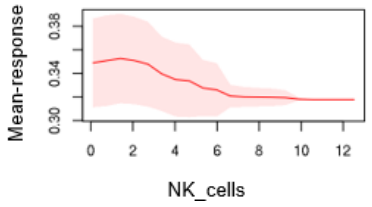
Islets	0.786	0.786	0.051	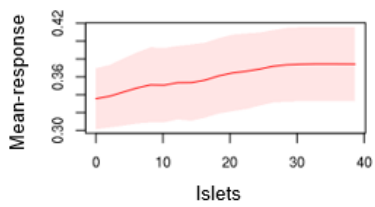

Age at diagnosis	0.754	0.754	0.049	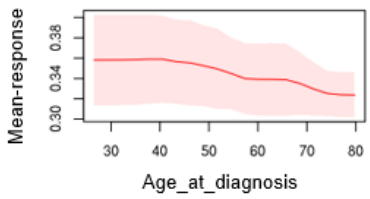
qPSCs	0.705	0.705	0.046	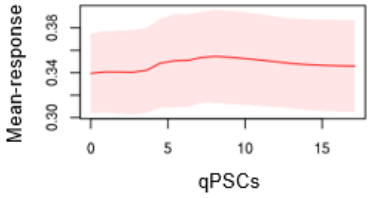
Acini	0.693	0.693	0.045	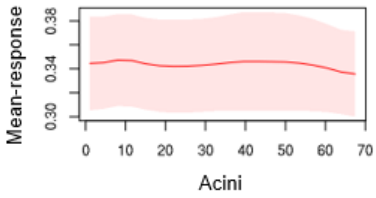
Reg_T_cells	0.676	0.676	0.044	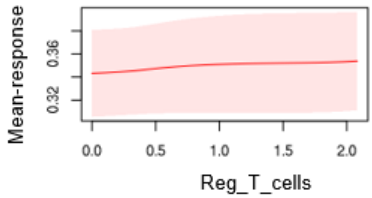
M2	0.670	0.670	0.044	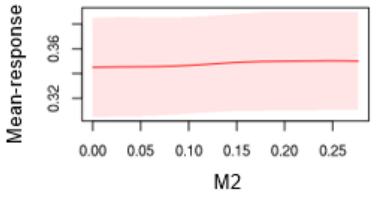
CD83+_DCs	0.665	0.665	0.043	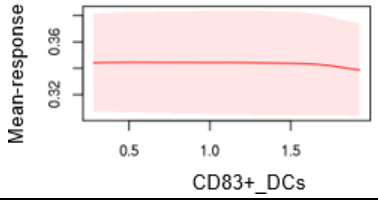
MCs	0.661	0.661	0.043	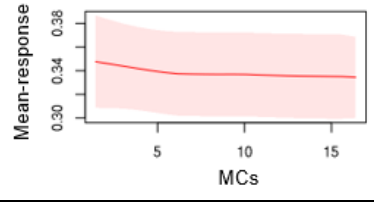

5. Discussion

CP is a fibro-inflammatory disease of the pancreas that causes irreversible destruction of pancreatic parenchyma and extensive extracellular matrix deposition [75]. CP not just links to worsened quality of life and shorter life expectancy due to the consequent disease-related dysfunction and complications but leads to severe socioeconomic burden resulting from an growing incidence and prevalence [7, 76, 77]. Thus far, no causative treatment is available for this disease due to the incomplete understanding of pathogenesis and the lack of druggable targets [78]. It is well documented that inflammation plays an essential role in developing CP, as shown by investigations of inflammatory cell infiltrates in both humans [47, 72, 79] and animal models [36, 56]. While many animal models have been designed to delineate the pathological trajectories of CP, the challenge remains how to accurately translate observations from experimental studies into clinical practice. Additionally, animal models can not entirely mirror the pathogenesis of human CP due to an artificial course of developing the disease and the species barrier. Also, data from animal experiments remain controversial over the question of whether the immune response in CP is uniform or distinct when it comes to the etiology of CP. The same problem needs to be solved in human disease [80]. Nevertheless, human studies are frequently held back by the limitation of pancreatic tissue access. Although investigators turn to scrutinize alternations in peripheral blood inflammatory cells to decipher immune mechanisms involved, observations might not faithfully recapitulate the kinetics of the local immune responses. To overcome these barriers, we utilized CP specimens from patients who underwent surgical intervention to define immune infiltration signatures and pancreatic architecture alternations using a multiplex immunohistochemical staining approach. This staining strategy allows us to repeatedly visualize distinct antigens in a single tissue section, which not simply resolves the difficulty of tissue accessibility, but enables us to precisely discern

distinctive cellular phenotypes. Moreover, the computational image-processing technique serves as a powerful tool for the visualization of multiple antigens within a single multispectral image, clearly displaying the distribution of individual cells and allowing for quantitative assessment of the cellular compartments. However, since the multiplex staining technique cannot provide a direct correlation between protein expression level and signal intensity, we employed thresholding approaches to separate individual cellular compartments according to the corresponding signal intensity [57]. Thus, the process of image cytometric analysis is largely similar to that of flow cytometry with respect to the qualitative gating strategy [81]. Importantly, It is worth noting that image cytometry provides a convenient platform that allows for multiparametric fluorescent analyses of heterogeneous cell lineages, morphological alternations of tissue structure, as well as cell-cell interaction studies [82].

Despite the largely similar histological characteristics, CP refers to a range of disease entities. In the present study, we mainly focus on describing the histological features of chronic alcoholic pancreatitis, AIP, other CP as well as comparing the subtle histological differences among them. While most patients present with the classic abdominal pain [83], the natural history and clinical manifestations vary dramatically depending on different forms of CP, as also found by the range of possible indications for surgery in our cohort [2]. Alcohol has consistently been noted as the most common causative agent for CP, leading to nearly 50% of cases of the disease [7]. The mechanism underlying the induction of alcoholic CP remains largely uncharted. Previous investigations collectively suggest that people harboring specific genetic mutations in certain gene loci, such as *CLDN2, SPINK-1*, have a higher risk of developing alcoholic CP [84, 85]. Moreover, chronic alcohol intake results in the acinar cell susceptible to injury either through increasing levels of digestive and lysosomal enzymes in acinar cells [86] or by intercepting protective mechanisms that

sparing the acinar cell from endoplasmic reticulum stress [87].

AIP is characterized by a rapid response to corticosteroid therapy [88]. Since AIP is frequently along with elevated serum immunoglobulin (Ig) G4 levels and extra-pancreatic organs abundant with IgG4 plasma cell infiltration, clinicians tend to define AIP as a pancreatic manifestation of a multiorgan disease [89]. Chronic obstructive pancreatitis refers to a form of chronic pancreatitis that is caused by physical trauma to the duct or results from partial or complete ductal obstruction. Obstructive pancreatitis appears in the area upstream from the pancreatic duct injury, leaving the downstream pancreas staying intact [90, 91]. It is now well established that pancreatitis starts from acinar cell injury, followed by the infiltration of immune cells and the over-activation of mesenchymal cells. However, whether the pathogenesis of CP resulting from different etiology is uniform or divergent remains to be defined. Additionally, deeply understanding this question has the potential to seek out appropriate therapeutic targets for each type of the disease.

Both innate immunity and adaptive immunity are involved in the pathogenesis of CP. It is now well known that genetic and environmental factors induce initial injury to pancreatic acinar cells, triggering a cascade of events that lead to pre-activated digestive enzymes released into the surrounding tissue and result in local destruction [78]. The injured acinar cells, along with the inflammatory stimulation raised from local damage, incite a series of local and systematic immune responses that involve both innate and adaptive immune response [78, 92, 93]. Moreover, PSCs, which can be activated either by cellular debris from necrotic acinar cells or through interaction with inflammatory infiltrates, play an essential role in fibrosis formation and collagen deposition. Thus, closer examination of histological signatures of pancreatic epithelial cells and non-epithelial cells, particularly immune cell infiltrates and PSCs, in the pancreatitis lesions, have the potential to improve our knowledge of the pathogenesis of the

disease and find out suitable therapeutic targets to intercept disease progression. We, therefore, generated three multiplex staining panels, including myeloid panel, lymphoid panel, and pancreatic exocrine-endocrine and stroma panel, to explore histopathological features of CP using image cytometric analysis. Additionally, we stratified CP into three subgroups on the basis of the distinct etiology and compared the cellular compositions and stromal compartments within CP lesions among different CP subtypes.

In normal pancreatic tissue, acinar and duct cells are the predominant cell populations, whereas the resident immune cells are rarely to be detected [47]. Previous studies from both experimental models and humans are pointing to the fact that the frequency of immune cells is strikingly enriched in the context of CP compared to healthy control [35, 54, 94, 95]. Similarly, our exploration of cellular component analysis of sections from CP tissue shows that around 8% to 20% of cellular composition belongs to the immune cell lineage (Figure 12-14). While it is well established that immune infiltrates serve as key players in developing CP, few studies have confirmed whether there were differences in the contribution of immune cells to the disease progression in the context of distinct etiology. We, therefore, compared the portion of immune cellular compartments among alcoholic CP, AIP, and other CP lesions using CD45+ staining as a pan-leukocyte marker. We observed that the percentage of CD45+ leukocytes significantly increased in AIP, compared to alcoholic CP and other CP.

To further examine whether there are differences in the distribution of the lymphoid cellular subtypes among alcoholic-related CP, AIP, and other CP, we compared B cells and T cell subsets as well. B cells as a subset of lymphocytes differentiate into plasma cells which are well known for their antibody-producing function, initiating humoral immunity in the adaptive immune system. Moreover, B cells play critical roles in the kinetics of T cells proliferation, differentiation,

and activation through their antigen-presentation and polarized cytokine-producing function [52, 96, 97]. Typically, researchers utilize CD20 biomarker to identify B cells, because CD20 is expressed on almost all stages B cell development except early pro-B cells and plasma cells [98]. The role of B cells in the development of pancreatitis is still far from well elucidated. Previous observation demonstrated that B-cell ablation therapy with anti-CD20 antibody is a desirable option for patients with AIP implicating the crucial involvement of B cells in developing the disease [99, 100].Few studies have focused on the contribution of B cells in other subtypes of pancreatitis, like alcoholic pancreatitis and obstructive pancreatitis. In the present study, we did not observe significant discrepancies in the density of B cells among the three CP subgroups. However, whether the density of early stage of B cells as well as plasma cells are also different among the three CP group need to be determined by the ongoing investigations.

NK cells are also considered to be a subset of lymphocytes and are involved in both innate and adaptive immune responses [45]. Functionally, NK cells are particularly similar to cytotoxic T lymphocytes, with the capacity to clear off transformed cells and foreign pathogens and to produce various inflammatory cytokines, like IFN-γ, TNF-α, IL-18 [53]. Previous reports suggest that NK cells are activated in the early stages of AP and also implicated in the pathogenesis of systemic inflammatory response syndrome (SIRS) and infected pancreatitis [101, 102]. However, although the percentage of NK cells in CP lesions is relatively low, the role of NK cells in the progress of the disease needs to be defined by further investigations.

Among T cell subsets, the frequency of cytotoxic T cells and activated T cells was significantly lower in AIP, when compared with alcoholic CP and other CP. In contrast, the frequency of TH0 cells tend to be higher in AIP, compared to alcoholic CP and other CP. However, the density of TH1 cells, TH17 cells, TH2

cells and T regulatory cells are comparative among the three CP groups. It is very clear that cytotoxic T cells play vital roles in immune-related diseases, tumorigenesis, and the elimination of foreign pathogens [103]. Cumulative studies show that the abundance of cytotoxic T cells in the peripheral blood considerably decreases during the course of AP, especially severe acute pancreatitis (SAP) [51, 104]. Moreover, cytotoxic T cells are associated with a secondary hit of infection in the progress of AP [102]. Previous studies looking at the role of cytotoxic T cells in the progress of alcoholic CP suggested that the frequency of cytotoxic cells was significantly enhanced in the pancreatic lesions from patients with alcoholic CP, suggesting the involvement of cell-mediated cytotoxicity. Moreover, the activated cytotoxic cells were frequently identified in the vicinity of areas with parenchyma, indicating that cytotoxic T cells probably lead to tissue disruption in alcoholic CP [49]. Rarer studies have evaluated the potential role of cytotoxic T cells in the pathogenesis of AIP, partially because of their scarce appearance in the disease [89]. This was mirrored by our results that the appearance of cytotoxic T cell subtypes was significantly lower in AIP compared to alcoholic CP and other CP. Altogether, these data suggest that cytotoxic T cells are more active in the progression of alcoholic CP and other CP.

Cytotoxic T lymphocyte antigen-4 (CTLA-4) is a cell surface molecule that is expressed nearly exclusively on T lymphocytes, including both CD4+ and CD8+ T cells [105]. Further investigation on CTLA-4 expression confirmed that CTLA-4 molecule is selectively expressed on the surface of activated T cells, not the resting T cells [105-107]. Functionally, CTLA-4 is a very important molecule in mediating the kinetics of T cell immune activities, such as regulating T cell proliferation, mobility, activation, as well as maintaining of T cell homeostasis [108-111]. Mice with CTLA-4 depletion rapidly develop lymphoproliferative disorder with dramatical lymphocytic infiltration in multiorgan, particularly liver, heart, and pancreas, and widespread tissue destruction [110, 112, 113]. Given

the remarkable role of CTLA-4+ T cells (activated T cells) in mediating T cell immunity, we sought to determine their contribution to the progress of CP. Of note, we found that CTLA-4+ T cells occupied the largest percentage of lymphocytes in the lesions, suggesting the involvement in the development of CP, especially alcoholic CP. Future experiments, therefore, are required to identify the biological function of CTLA-4+ T cell populations in the progress of the disease.

TH17 cells are the main source of IL-17A, which has been confirmed to directly drive various immune-related diseases or indirectly mediate a range of inflammatory responses through enhancing expressions and functions of other cytokines and chemokines, like IL-6, TNF-α, CXCL1, and MCP-1 [114-116]. Clinical investigations show that the serum level of IL-17A is strongly associated with the severity of AP and can predict the clinical outcomes of patients with SAP [117-119]. IL-17A might also drive acinar cell necrosis by upregulating a number of inflammatory mediators, such as IL-1β, and CXC family members [120]. In patients with CP, previous studies suggest that the proportion of TH17 cells markedly increase in both the peripheral blood and the inflamed pancreatic tissues [47]. Furthermore, the increased deviation of TH17 subsets in pancreatic lesions is not just associated with clinical features of advanced CP but contributes to β-cells disruption and fibrosis formation [48, 121, 122]. Our results did not suggest a statistically significant difference of TH17 cell populations among alcoholic CP, AIP, and other CP, implying that these cells probably exert universal function in the progression of CP with regardless of distinct etiology.

TH1 and TH2 subsets exert distinct effector functions during the course of pancreatitis. TH1 cells are characterized by secreting INF-γ that acts as a potential pro-inflammatory cytokine and plays a critical role in immunopathology [123], whereas TH2 cells are known as producing large amounts of IL-4, IL-5,

IL-13, IL-9, and IL-10 that are associated with broad ranges of anti-inflammatory response and mediate type 2 inflammation [124]. The dynamic balance between TH1 cells and TH2 cells is associated with the severity of AP and the progression of CP [89, 125, 126]. In the context of CP, TH1 cells are reportedly associated with pancreatic islet disruption [48], whereas TH2 cells are linked to the transition of the chronic pancreatic fibroinflammatory disease to malignant carcinoma [43]. However, there are contradictory results with regard to the TH1/TH2 balance during the progress of CP [127]. Our previous work indicates that AIP is a T cell-driven disorder in which the subtype of T effect cell is the main responder to disease progression and
pancreatic tissue destruction [128]. Similarly, our present analysis suggests a tendency of a TH2-predominant immune response in the patients with CP at the time of surgery (Figure 16).

The role of naïve CD4+T helper cells (TH0) in developing CP is still not well documented. It is well known that upon activation by corresponding inflammatory cytokines or antigens, TH0 cells can skew into TH1, TH2, and TH17 cells [129]. These effector T cell subsets can induce a cascade of immune response through generating a variety of inflammatory factors, as mentioned above. Our comparative analysis suggested that the frequency of TH0 cells is more dominant in AIP compared to alcoholic CP and other CP. Future experiments are suggested to elucidate the function of TH0 cell subsets in the development of CP, especially AIP.

Treg cells are involved in a broad range of immune responses, such as autoimmunity, inflammation, and tumorigenesis, mainly through regulating the activity of other immune cells, including macrophages, DCs, NK cells, and other T cell subsets as well [130-132]. Previous experiments confirmed that the pancreatitis-specific IL-10 responses were driven by IL-10+INF-γ-FoxP3+ Treg cells, which were amplified not just in bone marrow, peripheral blood, but, most

conspicuously, in CP lesions, and exerted potent function to suppress the proliferation of autologous conventional T cells, suggesting those cells played a crucial role in the control of auto-aggression during the course of CP [72]. Similarly, it is reported that the number of CD4+CD25+ FoxP3+ Treg cells were significantly increased in pancreatic tissues and the peripheral blood of patients with AIP [133, 134]. Additionally, data from animal experiments demonstrate that increasing the number of Treg cells, either by adoptive transfer or by pharmacological approach, significantly attenuate the severity of L-arginine-induced CP by suppressing the overactivation of cytotoxic T cells [135]. Given the potent immune-mediating function of Treg cells, we sought to define whether there were differences in the contribution of Treg cells in the context of CP with different etiology. We compared the density of Treg cells and found that the distribution of Treg cells were comparable among the three CP subgroups.

Neutrophil granulocytes as an essential part of the innate immune system are known for their functions in inflammation resolution. During the course of pancreatitis, intercellular adhesion molecule-1(ICAM-1) is upregulated in acinar cells and plays crucial roles in mediating infiltration of neutrophils into the inflamed pancreas [136]. Moreover, ICAM-1 directly mediates neutrophils adhesion to pancreatic acinar cells, which may further exacerbate inflammatory responses and induce cell death during pancreatitis [137]. In addition to ICAM-1, P-selectin, and lymphocyte function antigen-1 (LFA-1) are evidenced by separate studies in regulating neutrophil recruitment, neutrophil-endothelium interactions, and tissue damage [138, 139]. Infiltrating neutrophils also play critical roles in digestive enzymes activation, further aggravating acinar cell damage [140]. Additionally, neutrophil extracellular traps (NETs) generated by activated neutrophils contribute to the transformation of AP into CP [24]. Few studies have investigated the role of neutrophils in the progression of CP. We, therefore, analyzed the percentage of neutrophils and identified their contribution among different subgroups of CP. Our observations clearly

demonstrated that neutrophils took the largest proportion of myeloid-originated cell populations in CP lesions. Moreover, the density of neutrophils in the lesions of AIP was significantly amplified when compared with that of alcoholic CP and other CP. However, whether the enhanced frequency of neutrophil infiltrates plays more important roles in AIP remains to be defined in animal models and humans.

Macrophages are not just critical to the clearance of necrotic and apoptotic cell debris, but play a vital role in the dynamic of fibrogenesis. Classically, it is thought that M1 macrophages dominate in the context of acute inflammation, whereas M2 macrophages take an essential part in the process of chronic inflammation. During the initial stages of pancreatitis, bone marrow-derived macrophages rapidly migrate into the inflamed pancreatic areas and become the important immune cell populations, mainly M1 macrophages, within the lesions [141]. While it is well known M1 macrophages clear off the injured cell components during pancreatitis, they are also responsive for acinar cell necrosis through producing large amounts of inflammatory mediators and pre-activating digestive enzymes [142-144]. In contrast to M1, M2 macrophages serve as key players in CP, especially during the course of fibrosis formation. During the course of CP, macrophages produce large amounts of tissue inhibitor metalloproteinase 2 (TIMP2) and matrix metalloproteinase 9 (MMP9), meaning they play an immediate role in regulating the metabolism of ECM [36]. Additionally, macrophages are involved in fibrogenesis through a mode of bi-directional interaction with PSCs, which are activated in the inflammatory microenvironment and produce large amounts of ECM [36, 145]. To evaluate the contribution of macrophages in the progress of CP, we quantified the percentage of M1 and M2 macrophages and compared among the AIP, alcoholic CP, and other CP. Our observations revealed that there was no statistically significant discrepancy in the contribution of M1 and M2 macrophages among the three CP subgroups.

DCs, which make up vital parts of antigen-presenting cells, bridging between innate and adaptive immunity. It is well known that DCs play important roles in sustaining immune homeostasis during the course of infection, autoimmune-related disease, and tumorigenesis [41]. Depending on the distinct receptors expressed on the cell surface, the immunomodulatory actions of DCs vary. DC-sign is nearly exclusively expressed on DCs, including both immature and mature DCs [146]. While DC-sign expressing DCs can enhance immune response through activating the resting T cells, promoting T cell proliferation, and skewing T cell bias [147, 148], they can also exert immune inhibitory action by reducing T cell proliferation, and suppressing co-stimulator CD11c, CD83, and CD86 expression [149]. Unlike DC-sign expression, CD83 is only present in fully matured DCs [150]. Similarly, CD83+DC populations show both immune stimulatory and immune inhibitory function through the complex and nuanced interaction with T cells [151]. The impact of DCs, both immature and mature populations, on the evolution of CP is still not well investigated. Our results comparing the distribution of DC-sign+ DCs and CD83+DCs in the lesions among AIP, alcoholic CP, and other CP suggested that the frequency of CD83 expressing CDs appeared to enrich in AIP. Both in vitro and in vivo experiments indicated that CD83 molecules have immunosuppressive roles, such as the inhibition of DC-mediated T cell proliferation and stimulation [152, 153]. Consistently, our findings also revealed a negative correlation between CD83+DC and activated T cells and cytotoxic T cell as well, as clearly illustrated by cellular analyses which AIP appears to have a higher proportion of CD83+DCs but lower proportion of activated T cells and cytotoxic T cell compared to alcoholic CP and other CP. However, the density of DC-sign bearing DCs was on difference among the three CP subgroups. More insights and investigations are required to dissect the more detailed impact of CD83+ DCs population on the pathogenesis of CP.

It is well studied that MCs are involved in both innate and adaptive immune systems and plays crucial roles in allergic reactions and in host-defense immunity. Previous investigations around the impact of MC on the process of AP suggested that activated MC enhances local and systemic inflammation through the degranulation or production of inflammatory mediators [154, 155]. However, the study on the role of MCs in modulating CP is relative rare. It has been reported that MCs is a key contributor to the pathogenesis of pain in patients with CP [156]. Explorations of mechanism underlying MC-associated role in the pain pathology implicate that MC degranulation products, like tryptase and histamine, can directly sensitize nociceptors of the proximal neurons, enhancing nociception neurotransmission [157]. To evaluate the distributional characteristics of MC in CP, we quantified the percentage of MC in the lesions of CP and further compared the findings among alcoholic CP, AIP, and other CP. Surprisingly, we found that MC was the second higher myeloid lineage cell population, perhaps pointing to the high pain intensity in these surgical patients. However, the density of MC was of no difference among the three CP subgroups. These data suggested the remarkable involvement of MC in the pathogenesis of CP, specifically pain development. However, whether the biological role of MC in mediating the evolution of CP with different causes is uniform or divergent remains to be defined in future trials.

It is now very clear that activated PSCs are responsive for the fibrosis formation and collagen deposition, which are two major histological characteristics of CP, especially at later stages of the disease [55, 158]. Strategies designed to impede the activation of PSCs or restrain pathways of ECM deposition have been evidenced as efficacious options for precluding the progression of the disease [54, 159]. Improved knowledge of the phenotype of PSCs and their capabilities of ECM production in the development of CP with distinct etiology provides the great potential of understanding pathological signatures of the disease and formulating corresponding therapeutic regimens. We, therefore,

evaluated the functional and proliferative states of PSCs, fibrosis accumulation, collagen deposition, and compared these parameters among alcoholic CP, AIP, and other CP. We observed that the frequency of ECM-producing activated PSCs was significantly increased in AIP when compared to alcoholic CP and other CP. Similarly, we noticed that the proportion of ECM-producing quiescent subtypes of PSCs was also upregulated in the context of AIP compared to that of the other two subgroups. Additionally, we also found that the density of the quiescent phenotype of PSCs in AIP was the highest of all. The mechanisms underlying the increased abundance of both quiescent and activated PSCs, together with the enhanced proportion of both ECM-producing activated PSCs and quiescent ones, in AIP necessitates further investigations to determine. It has been well investigated that interactions between PSCs and immune infiltrates play critical roles in the progression of CP. For example, previous experiments have pointed out the bidirectional interplay between PSCs and macrophages in the dynamic of inflammatory response and fibrosis formation during CP. Cytokines like IL-4 and IL-13 released by PSCs promote M2 polarization, whereas M2 macrophages produce large amounts of TGFβ and PDGFβ in turn activate PSCs [36, 93]. These observations are in line with our findings that AIP tends to have a higher density of macrophage populations, including both M1 and M2, when compared to alcoholic CP and other CP, partly explaining AIP appearing with higher amounts of activated PSCs and their ECM-producing abilities as well. Moreover, investigations on patients with CP demonstrated that the degrees of MC degranulation were found to rise in parallel with the extents of PSCs activation, hinting the strong involvement of MC in the course of pancreatic fibrogenesis during CP [160]. However, our findings did not show statistically significant differences of MC among alcoholic CP, AIP, and other CP, although AIP found stronger intensity of PSCs activation. This discrepancy perhaps results from the intricate mechanism of the fibrogenesis during the process CP with distinct etiology and the different disease stages. Additionally, experimental models have illustrated that

activated PSCs play as important contributors to drive the impairment of islet endocrine function experienced by some patients with CP as well as the dynamic of islet fibrogenesis associated with certain cases of type 2 diabetes [161]. Our studies showed that patients with AIP have higher chances of developing endocrine dysfunction compared to those with alcoholic CP and other CP, probably because AIP have a higher proportion of activated PSCs.

It has been well studied that the fibro-inflammatory stromal composition has remarkable effects on PDAC initiation, invasion, metastatic dissemination, as well as relapse [162]. Like PDAC, CP is also known for its desmoplastic stroma reaction consisted of activated PSCs, immune cells, and ECM proteins [163]. The complex and subtle interplay between immune infiltrates and PSCs plays a major role in the cascade of desmoplasia. Inflammatory factors generated by immune cells lead to the shift of the quiescent PSCs towards an activated phenotype and the consequent ECM production. Previous studies on PDAC stroma suggest that distinct stromal patterns defined by differential expression of aSMA and collagen robustly predict PFS of patients with the disease [58, 73]. Therefore, to determine the impact of immune migration on modulating stromal composition in the context of CP with distinct etiology, we analyzed the distribution of immune infiltrates in different stromal subtypes and compared those parameters among AIP, alcoholic CP, and other CP. We observed that the frequency of TH0 cells was significantly increased in fibrolytic stroma subtype in AIP when compared with alcoholic CP and other CP. A similar distribution pattern was noted with granulocytes, although the differences did not reach the statistically significant level. In contrast, the density of cytotoxic T cells and activated T cells was apparently decreased in the subtype of fibrolytic stroma of AIP compared to other CP subgroups.

In addition, we compared the distribution of acinar cells, ductal cells, islet cells, and nerve cells among the AIP, alcoholic CP, and other CP. Our results did not

show statistically significant discrepancies in the abundance of those cellular components among the three CP groups. These observations suggest that the degree of impairment in acini, ducts, islets, and neurons among the three CP groups at least at the time of surgery are of no stark differences. However, the underlying pathogenesis contributing to the destruction of those cellular compartments among the three CP groups remains to be determined.

A former trial proved that different patterns of stroma, including dormant, fibrogenic, fibrolytic, and inert stroma, augured strongly for distinct long-term survival of patients with PDAC [73]. These observations were further validated by our recent investigations [58]. Therefore, in attempt to determine whether discrepant stromal subtypes also contribute to distinct outcomes of non-immune cells in the context of CP with different etiology, we evaluated the distributional characteristics of those cells among the three CP groups. Our observations indicated that ductal cells were comparable in the context of dormant stroma between alcoholic CP and other CP. Moreover, in the setting of inert stroma, both alcoholic CP and other CP conserved more ductal structures than that of AIP. In contrast, the number of ductal cells in the context of inert stroma tends to be higher in AIP when compared to alcoholic CP and other CP. However, we did not observe significant difference of immune infiltrates in the context of both dormant stroma and inert stroma between the two CP groups. The underlying mechanism of the discrepant distribution of those non-immune compartments among the three CP groups in the context of inert stroma requires more comprehensive experiments to determine.

Since exocrine dysfunction continues to be a major life-quality threat to most of the patients with CP, particularly those with advanced stages, we attempted to figure out features that are associated with the presence of exocrine insufficiency. We applied the stacked ensemble AutoML models, including deep learning, GBM, GLM, XGBoost, DRF, and XRT model, to compute the multiplex-

stained images together with clinical data of the corresponding patients. Among all the features that are predictively implicated in developing exocrine insufficiency, we listed the top ten predictive factors, including aPSCs proliferation, NK cells, islets, age at diagnosis, qPSCs, acini, T regulatory cells, M2 macrophages, CD83+DCs, and Mast cells (Table 5). We noticed that the number of activated PSCs specifically at proliferative state has the strongest relevance of predicting the presence of pancreatic exocrine insufficiency. The frequency of NK cells was indicated as the second important predictor of the induction of exocrine abnormality, with a negative relationship with maintaining the exocrine function of the pancreas. By contrast, the density of islets is positively correlated with the maintenance of exocrine function during CP, probably pointing towards less severe disease. However, those factors simply belong to computationally predicted findings which are just based on a relatively small size of the database of patients with CP. Whether those predictive factors are virtually critical to precisely augur the appearance of exocrine compromise during CP remains to be answered by a large scale of database and further experimental models. We expect these findings would lay a foundation to reveal the biological process of the development of pancreatic functional abnormality of the patients with CP.

6. Conclusions and Outlook

Our study for the first time indicated that the system of multiplex staining methodology is an efficient tool for comprehensively exploring and defining the pathohistological signatures of CP. The computationally stacked images from multiplex staining not simply take into account of the quantitative information but provide a geographic distribution of visualized features at the tissue level. Our findings revealed that CD45+infiltrates are more abundant within TMA sections from AIP when compared to alcoholic CP and other CP. Immune cellular subtype analyses indicated that granulocytes were statistically enriched in AIP compared with alcoholic CP and other CP. In contrast, the density of cytotoxic T cells was significantly amplified in both alcoholic CP and other CP when compared with AIP. Our investigations looking at stromal compartments did not suggest significant differences among the three CP subgroups. Additionally, AutoML computation robustly indicates the top ten variables, including aPSCs proliferation, NK cells, islets, age at diagnosis, qPSCs, acini, T regulatory cells, M2 macrophages, CD83+DCs, and MCs, which are associated with the prediction of exocrine insufficiency of the patient with CP. Altogether, our work provides detailed information on the histological characteristics of advanced CP. Moreover, we comprehensively compared those features among different patient groups, which will be helpful for designing a specific therapeutic approach for individual patient groups. Additionally, we identified the top ten predictors for pancreatic exocrine insufficiency, providing improved insight into studying the progress of exocrine dysfunction of the patient with CP.

7 References

1. Beyer G, Habtezion A, Werner J et al. Chronic pancreatitis. The Lancet 2020; 396: 499-512.
2. Majumder S, Chari ST. Chronic pancreatitis. The Lancet 2016; 387: 1957-1966.
3. Yamabe A, Irisawa A, Shibukawa G et al. Early diagnosis of chronic pancreatitis: understanding the factors associated with the development of chronic pancreatitis. Fukushima journal of medical science 2017; 2016-2014.
4. Johnson C, Hosking S. National statistics for diet, alcohol consumption, and chronic pancreatitis in England and Wales, 1960-88. Gut 1991; 32: 1401-1405.
5. Levy P, Dominguez-Munoz E, Imrie C et al. Epidemiology of chronic pancreatitis: burden of the disease and consequences. United European Gastroenterol J 2014; 2: 345-354.
6. Jaakkola M, Nordback I. Pancreatitis in Finland between 1970 and 1989. Gut 1993; 34: 1255-1260.
7. Yadav D, Timmons L, Benson JT et al. Incidence, prevalence, and survival of chronic pancreatitis: a population-based study. American Journal of Gastroenterology 2011; 106: 2192-2199.
8. Singh VK, Yadav D, Garg PK. Diagnosis and Management of Chronic Pancreatitis: a review. Jama 2019; 322: 2422-2434.
9. Mayerle J, Sendler M, Hegyi E et al. Genetics, Cell Biology, and Pathophysiology of Pancreatitis. Gastroenterology 2019; 156: 1951-1968 e1951.
10. Whitcomb DC, Gorry MC, Preston RA et al. Hereditary pancreatitis is caused by a mutation in the cationic trypsinogen gene. Nature genetics 1996; 14: 141-145.
11. Derikx MH, Kovacs P, Scholz M et al. Polymorphisms at PRSS1-PRSS2 and CLDN2-MORC4 loci associate with alcoholic and non-alcoholic chronic pancreatitis in a European replication study. Gut 2015; 64: 1426-1433.
12. Bhatia E, Choudhuri G, Sikora SS et al. Tropical calcific pancreatitis: strong association with SPINK1 trypsin inhibitor mutations. Gastroenterology 2002; 123: 1020-1025.
13. Aoun E, Chang CC, Greer JB et al. Pathways to injury in chronic pancreatitis: decoding the role of the high-risk SPINK1 N34S haplotype using meta-analysis. PLoS One 2008; 3: e2003.
14. Di Leo M, Leandro G, Singh SK et al. Low alcohol and cigarette use is associated to the risk of developing chronic pancreatitis. Pancreas 2017; 46: 225-229.
15. Mergener K, Baillie J. Chronic pancreatitis. The Lancet 1997; 350: 1379-1385.
16. Kleeff J, Whitcomb DC, Shimosegawa T et al. Chronic pancreatitis. Nature reviews Disease primers 2017; 3: 1-18.
17. Etemad B, Whitcomb DC. Chronic pancreatitis: diagnosis, classification, and new genetic developments. Gastroenterology 2001; 120: 682-707.
18. Steer ML, Waxman I, Freedman S. Chronic pancreatitis. New England Journal of Medicine 1995; 332: 1482-1490.
19. Pandol SJ, Raraty M. Pathobiology of alcoholic pancreatitis. Pancreatology 2007; 7: 105-114.
20. Witt H, Apte MV, Keim V, Wilson JS. Chronic pancreatitis: challenges and advances in pathogenesis, genetics, diagnosis, and therapy. Gastroenterology 2007; 132: 1557-1573.

21. Deng X, Wang L, Elm MS et al. Chronic Alcohol Consumption Accelerates Fibrosis in Response to Cerulein-Induced Pancreatitis in Rats. The American Journal of Pathology 2005; 166: 93-106.
22. Majumder S, Takahashi N, Chari ST. Autoimmune pancreatitis. Digestive diseases and sciences 2017; 62: 1762-1769.
23. Omiyale AO. Autoimmune pancreatitis. Gland Surg 2016; 5: 318-326.
24. Leppkes M, Maueroder C, Hirth S et al. Externalized decondensed neutrophil chromatin occludes pancreatic ducts and drives pancreatitis. Nat Commun 2016; 7: 10973.
25. Tandon RK. Tropical pancreatitis. J Gastroenterol 2007; 42 Suppl 17: 141-147.
26. Braganza JM, Lee SH, McCloy RF, McMahon MJ. Chronic pancreatitis. The Lancet 2011; 377: 1184-1197.
27. Nøjgaard C, Becker U, Matzen P et al. Progression from acute to chronic pancreatitis: prognostic factors, mortality, and natural course. Pancreas 2011; 40: 1195-1200.
28. Sollie S, Michaud DS, Sarker D et al. Chronic inflammation markers are associated with risk of pancreatic cancer in the Swedish AMORIS cohort study. BMC Cancer 2019; 19: 858.
29. Hegyi E, Sahin-Toth M. Genetic Risk in Chronic Pancreatitis: The Trypsin-Dependent Pathway. Dig Dis Sci 2017; 62: 1692-1701.
30. Sah RP, Saluja AK. Trypsinogen activation in acute and chronic pancreatitis: is it a prerequisite? Gut 2011; 60: 1305-1307.
31. Geisz A, Sahin-Toth M. A preclinical model of chronic pancreatitis driven by trypsinogen autoactivation. Nat Commun 2018; 9: 5033.
32. Makhija R, Kingsnorth AN. Cytokine storm in acute pancreatitis. Journal of hepato-biliary-pancreatic surgery 2002; 9: 401-410.
33. Sakai Y, Masamune A, Satoh A et al. Macrophage migration inhibitory factor is a critical mediator of severe acute pancreatitis. Gastroenterology 2003; 124: 725-736.
34. Saeki K, Kanai T, Nakano M et al. CCL2-induced migration and SOCS3-mediated activation of macrophages are involved in cerulein-induced pancreatitis in mice. Gastroenterology 2012; 142: 1010-1020. e1019.
35. Emmrich J, Weber I, Nausch M et al. Immunohistochemical characterization of the pancreatic cellular infiltrate in normal pancreas, chronic pancreatitis and pancreatic carcinoma. Digestion 1998; 59: 192-198.
36. Xue J, Sharma V, Hsieh MH et al. Alternatively activated macrophages promote pancreatic fibrosis in chronic pancreatitis. Nat Commun 2015; 6: 7158.
37. Detlefsen S, Sipos B, Feyerabend B, Kloppel G. Fibrogenesis in alcoholic chronic pancreatitis: the role of tissue necrosis, macrophages, myofibroblasts and cytokines. Mod Pathol 2006; 19: 1019-1026.
38. del Fresno C, Saz-Leal P, Enamorado M et al. DNGR-1 in dendritic cells limits tissue damage by dampening neutrophil recruitment. Science 2018; 362: 351-356.
39. Sesti-Costa R, Francozo MCS, Silva GK et al. TLR3 is required for survival following Coxsackievirus B3 infection by driving T lymphocyte activation and polarization: The role of dendritic cells. PLoS One 2017; 12: e0185819.
40. Geijtenbeek TB, Torensma R, van Vliet SJ et al. Identification of DC-SIGN, a novel dendritic cell–specific ICAM-3 receptor that supports primary immune responses. Cell 2000; 100: 575-585.

41. Zhou T, Chen Y, Hao L, Zhang Y. DC-SIGN and immunoregulation. 2006.
42. Bates JM, Flanagan K, Mo L et al. Dendritic cell CD83 homotypic interactions regulate inflammation and promote mucosal homeostasis. Mucosal Immunol 2015; 8: 414-428.
43. Ochi A, Nguyen AH, Bedrosian AS et al. MyD88 inhibition amplifies dendritic cell capacity to promote pancreatic carcinogenesis via Th2 cells. J Exp Med 2012; 209: 1671-1687.
44. Jin CX, Hayakawa T, Kitagawa M, Ishiguro H. Lactoferrin in chronic pancreatitis. JOP. J Pancreas (Online) 2009; 10: 237-241.
45. Blom B, Spits H. Development of human lymphoid cells. Annu Rev Immunol 2006; 24: 287-320.
46. Zhou Q, Tao X, Xia S et al. T Lymphocytes: A Promising Immunotherapeutic Target for Pancreatitis and Pancreatic Cancer? Front Oncol 2020; 10: 382.
47. Jupp J, Mansour S, Johnson CD et al. T-cell populations in chronic pancreatitis. Pancreatology 2015; 15: 311-312.
48. Talukdar R, Sasikala M, Kumar PP et al. T-helper cell–mediated islet inflammation contributes to β-cell dysfunction in chronic pancreatitis. Pancreas 2016; 45: 434-442.
49. Hunger RE, Mueller C, Z'graggen K et al. Cytotoxic cells are activated in cellular infiltrates of alcoholic chronic pancreatitis. Gastroenterology 1997; 112: 1656-1663.
50. Wei X, Yao W, Li H et al. B and NK Cells Closely Correlate with the Condition of Patients with Acute Pancreatitis. Gastroenterol Res Pract 2019; 2019: 7568410.
51. Dabrowski A, Osada J, Dabrowska MI, Wereszczynska-Siemiatkowska U. Monocyte subsets and natural killer cells in acute pancreatitis. Pancreatology 2008; 8: 126-134.
52. Hua Z, Hou B. The role of B cell antigen presentation in the initiation of CD4+ T cell response. Immunol Rev 2020.
53. Melaiu O, Lucarini V, Cifaldi L, Fruci D. Influence of the Tumor Microenvironment on NK Cell Function in Solid Tumors. Front Immunol 2019; 10: 3038.
54. Sendler M, Beyer G, Mahajan UM et al. Complement Component 5 Mediates Development of Fibrosis, via Activation of Stellate Cells, in 2 Mouse Models of Chronic Pancreatitis. Gastroenterology 2015; 149: 765-776 e710.
55. Schneider E, Schmid-Kotsas A, Zhao J et al. Identification of mediators stimulating proliferation and matrix synthesis of rat pancreatic stellate cells. American Journal of Physiology-Cell Physiology 2001; 281: C532-C543.
56. Xue J, Zhao Q, Sharma V et al. Aryl Hydrocarbon Receptor Ligands in Cigarette Smoke Induce Production of Interleukin-22 to Promote Pancreatic Fibrosis in Models of Chronic Pancreatitis. Gastroenterology 2016; 151: 1206-1217.
57. Tsujikawa T, Kumar S, Borkar RN et al. Quantitative Multiplex Immunohistochemistry Reveals Myeloid-Inflamed Tumor-Immune Complexity Associated with Poor Prognosis. Cell Rep 2017; 19: 203-217.
58. Mahajan UM, Langhoff E, Goni E et al. Immune Cell and Stromal Signature Associated With Progression-Free Survival of Patients With Resected Pancreatic Ductal Adenocarcinoma. Gastroenterology 2018; 155: 1625-1639 e1622.
59. Lan HY, Mu W, Nikolic-Paterson DJ, Atkins RC. A novel, simple, reliable, and sensitive method for multiple immunoenzyme staining: use of microwave oven heating to block antibody crossreactivity and retrieve antigens. Journal of Histochemistry & Cytochemistry 1995; 43: 97-102.

60. Tornehave D, Hougaard D, Larsson L-I. Microwaving for double indirect immunofluorescence with primary antibodies from the same species and for staining of mouse tissues with mouse monoclonal antibodies. Histochemistry and cell biology 2000; 113: 19-23.
61. Toth ZE, Mezey E. Simultaneous visualization of multiple antigens with tyramide signal amplification using antibodies from the same species. J Histochem Cytochem 2007; 55: 545-554.
62. Pirici D, Mogoanta L, Kumar-Singh S et al. Antibody elution method for multiple immunohistochemistry on primary antibodies raised in the same species and of the same subtype. J Histochem Cytochem 2009; 57: 567-575.
63. Glass G, Papin JA, Mandell JW. SIMPLE: a sequential immunoperoxidase labeling and erasing method. J Histochem Cytochem 2009; 57: 899-905.
64. Lowe DG. Object recognition from local scale-invariant features. In Proceedings of the seventh IEEE international conference on computer vision. Ieee 1999; 1150-1157.
65. Lowe DG. Distinctive image features from scale-invariant keypoints. International journal of computer vision 2004; 60: 91-110.
66. Schneider CA, Rasband WS, Eliceiri KW. NIH Image to ImageJ: 25 years of image analysis. Nat Methods 2012; 9: 671-675.
67. Ruifrok AC, Katz RL, Johnston DA. Comparison of quantification of histochemical staining by hue-saturation-intensity (HSI) transformation and color-deconvolution. Applied Immunohistochemistry & Molecular Morphology 2003; 11: 85-91.
68. Carpenter AE, Jones TR, Lamprecht MR et al. CellProfiler: image analysis software for identifying and quantifying cell phenotypes. Genome Biol 2006; 7: R100.
69. Padmanabhan K, Eddy WF, Crowley JC. A novel algorithm for optimal image thresholding of biological data. Journal of neuroscience methods 2010; 193: 380-384.
70. Gunderson AJ, Kaneda MM, Tsujikawa T et al. Bruton Tyrosine Kinase-Dependent Immune Cell Cross-talk Drives Pancreas Cancer. Cancer Discov 2016; 6: 270-285.
71. Ruffell B, Au A, Rugo HS et al. Leukocyte composition of human breast cancer. Proc Natl Acad Sci U S A 2012; 109: 2796-2801.
72. Schmitz-Winnenthal H, Pietsch DH, Schimmack S et al. Chronic pancreatitis is associated with disease-specific regulatory T-cell responses. Gastroenterology 2010; 138: 1178-1188.
73. Erkan M, Michalski CW, Rieder S et al. The Activated Stroma Index Is a Novel and Independent Prognostic Marker in Pancreatic Ductal Adenocarcinoma. Clinical Gastroenterology and Hepatology 2008; 6: 1155-1161.
74. Van der Laan MJ, Polley EC, Hubbard AE. Super learner. Statistical applications in genetics and molecular biology 2007; 6.
75. Whitcomb DC, Frulloni L, Garg P et al. Chronic pancreatitis: An international draft consensus proposal for a new mechanistic definition. Pancreatology 2016; 16: 218-224.
76. Mullady DK, Yadav D, Amann ST et al. Type of pain, pain-associated complications, quality of life, disability and resource utilisation in chronic pancreatitis: a prospective cohort study. Gut 2011; 60: 77-84.
77. Machicado JD, Amann ST, Anderson MA et al. Quality of Life in Chronic Pancreatitis is Determined by Constant Pain, Disability/Unemployment, Current Smoking, and Associated

Co-Morbidities. Am J Gastroenterol 2017; 112: 633-642.
78. Gukovskaya AS, Gukovsky I, Algul H, Habtezion A. Autophagy, Inflammation, and Immune Dysfunction in the Pathogenesis of Pancreatitis. Gastroenterology 2017; 153: 1212-1226.
79. Grundsten M, Liu G-Z, Permert J et al. Increased central memory T cells in patients with chronic pancreatitis. Pancreatology 2005; 5: 177-182.
80. Layer P, Yamamoto H, Kalthoff L et al. The different courses of early-and late-onset idiopathic and alcoholic chronic pancreatitis. Gastroenterology 1994; 107: 1481-1487.
81. McKinnon KM. Flow Cytometry: An Overview. Curr Protoc Immunol 2018; 120: 5 1 1-5 1 11.
82. Barteneva NS, Fasler-Kan E, Vorobjev IA. Imaging flow cytometry: coping with heterogeneity in biological systems. J Histochem Cytochem 2012; 60: 723-733.
83. Fasanella KE, Davis B, Lyons J et al. Pain in chronic pancreatitis and pancreatic cancer. Gastroenterol Clin North Am 2007; 36: 335-364, ix.
84. Gullo L, Migliori M, Brunetti MA. Alcoholic pancreatitis: new insights into an old disease. Current gastroenterology reports 2005; 7: 96-100.
85. Whitcomb DC, LaRusch J, Krasinskas AM et al. Common genetic variants in the CLDN2 and PRSS1-PRSS2 loci alter risk for alcohol-related and sporadic pancreatitis. Nat Genet 2012; 44: 1349-1354.
86. Apte MV, Pirola RC, Wilson JS. Mechanisms of alcoholic pancreatitis. J Gastroenterol Hepatol 2010; 25: 1816-1826.
87. Pandol SJ, Gorelick FS, Gerloff A, Lugea A. Alcohol abuse, endoplasmic reticulum stress and pancreatitis. Dig Dis 2010; 28: 776-782.
88. Hart PA, Kamisawa T, Brugge WR et al. Long-term outcomes of autoimmune pancreatitis: a multicentre, international analysis. Gut 2013; 62: 1771-1776.
89. Hart PA, Zen Y, Chari ST. Recent Advances in Autoimmune Pancreatitis. Gastroenterology 2015; 149: 39-51.
90. Boerma D, Straatsburg IH, Offerhaus GJ et al. Experimental model of obstructive, chronic pancreatitis in pigs. Dig Surg 2003; 20: 520-526.
91. Klöppel G, Maillet B. Pathology of acute and chronic pancreatitis. Pancreas 1993; 8: 659-670.
92. Zhang H, Neuhofer P, Song L et al. IL-6 trans-signaling promotes pancreatitis-associated lung injury and lethality. J Clin Invest 2013; 123: 1019-1031.
93. Habtezion A. Inflammation in acute and chronic pancreatitis. Curr Opin Gastroenterol 2015; 31: 395-399.
94. Shrikhande S, Martignoni M, Shrikhande M et al. Comparison of histological features and inflammatory cell reaction in alcoholic, idiopathic and tropical chronic pancreatitis. British journal of surgery 2003; 90: 1565-1572.
95. Goecke H, Forssmann U, Uguccioni M et al. Macrophages infiltrating the tissue in chronic pancreatitis express the chemokine receptor CCR5. Surgery 2000; 128: 806-814.
96. Ron Y, De Baetselier P, Gordon J et al. Defective induction of antigen‐reactive proliferating T cells in B cell‐deprived mice. European journal of immunology 1981; 11: 964-968.
97. LeBien TW, Tedder TF. B lymphocytes: how they develop and function. Blood 2008; 112:

1570-1580.
98. Vale AM, Schroeder Jr HW. Clinical consequences of defects in B-cell development. Journal of Allergy and Clinical Immunology 2010; 125: 778-787.
99. Hart PA, Topazian MD, Witzig TE et al. Treatment of relapsing autoimmune pancreatitis with immunomodulators and rituximab: the Mayo Clinic experience. Gut 2013; 62: 1607-1615.
100. Khosroshahi A, Carruthers MN, Deshpande V et al. Rituximab for the treatment of IgG4-related disease: lessons from 10 consecutive patients. Medicine (Baltimore) 2012; 91: 57-66.
101. Mylona V, Koussoulas V, Tzivras D et al. Changes in adaptive and innate immunity in patients with acute pancreatitis and systemic inflammatory response syndrome. Pancreatology 2011; 11: 475-481.
102. Shen Y, Cui NQ. Clinical observation of immunity in patients with secondary infection from severe acute pancreatitis. Inflamm Res 2012; 61: 743-748.
103. Kaech SM, Cui W. Transcriptional control of effector and memory CD8+ T cell differentiation. Nat Rev Immunol 2012; 12: 749-761.
104. Pinhu L, Qin Y, Xiong B et al. Overexpression of Fas and FasL is associated with infectious complications and severity of experimental severe acute pancreatitis by promoting apoptosis of lymphocytes. Inflammation 2014; 37: 1202-1212.
105. Brunet J-F, Denizot F, Luciani M-F et al. A new member of the immunoglobulin superfamily—CTLA-4. Nature 1987; 328: 267-270.
106. Linsley PS, Greene J, Tan P et al. Coexpression and functional cooperation of CTLA-4 and CD28 on activated T lymphocytes. The Journal of experimental medicine 1992; 176: 1595-1604.
107. Freeman G, Lombard D, Gimmi C et al. CTLA-4 and CD28 mRNA are coexpressed in most T cells after activation. Expression of CTLA-4 and CD28 mRNA does not correlate with the pattern of lymphokine production. The Journal of Immunology 1992; 149: 3795-3801.
108. Lu Y, Schneider H, Rudd CE. Murine regulatory T cells differ from conventional T cells in resisting the CTLA-4 reversal of TCR stop-signal. Blood 2012; 120: 4560-4570.
109. Schneider H, Downey J, Smith A et al. Reversal of the TCR stop signal by CTLA-4. science 2006; 313: 1972-1975.
110. Chambers CA, Krummel ME, Boitel B et al. The role of CTLA‐4 in the regulation and initiation of T‐cell responses. Immunological reviews 1996; 153: 27-46.
111. Brunner-Weinzierl MC, Rudd CE. CTLA-4 and PD-1 Control of T-Cell Motility and Migration: Implications for Tumor Immunotherapy. Front Immunol 2018; 9: 2737.
112. Tivol EA, Borriello F, Schweitzer AN et al. Loss of CTLA-4 leads to massive lymphoproliferation and fatal multiorgan tissue destruction, revealing a critical negative regulatory role of CTLA-4. Immunity 1995; 3: 541-547.
113. Waterhouse P, Penninger JM, Timms E et al. Lymphoproliferative disorders with early lethality in mice deficient in Ctla-4. Science 1995; 270: 985-988.
114. Bettelli E, Korn T, Oukka M, Kuchroo VK. Induction and effector functions of T(H)17 cells. Nature 2008; 453: 1051-1057.
115. Hartupee J, Liu C, Novotny M et al. IL-17 enhances chemokine gene expression through mRNA stabilization. J Immunol 2007; 179: 4135-4141.
116. Xu S, Cao X. Interleukin-17 and its expanding biological functions. Cell Mol Immunol 2010; 7: 164-174.

117. Botoi G, Andercou A. Interleukin 17--prognostic marker of severe acute pancreatitis. Chirurgia (Bucharest, Romania: 1990) 2009; 104: 431-438.
118. Jia R, Tang M, Qiu L et al. Increased interleukin-23/17 axis and C-reactive protein are associated with severity of acute pancreatitis in patients. Pancreas 2015; 44: 321-325.
119. Wang D, Tang M, Zong P et al. MiRNA-155 Regulates the Th17/Treg Ratio by Targeting SOCS1 in Severe Acute Pancreatitis. Front Physiol 2018; 9: 686.
120. Ni J, Hu G, Xiong J et al. Involvement of interleukin-17A in pancreatic damage in rat experimental acute necrotizing pancreatitis. Inflammation 2013; 36: 53-65.
121. Zhao Q, Manohar M, Wei Y et al. STING signalling protects against chronic pancreatitis by modulating Th17 response. Gut 2019; 68: 1827-1837.
122. Sasikala M, Ravikanth VV, Murali Manohar K et al. Bach2 repression mediates Th17 cell induced inflammation and associates with clinical features of advanced disease in chronic pancreatitis. United European Gastroenterol J 2018; 6: 272-282.
123. Rahimi K, Ahmadi A, Hassanzadeh K et al. Targeting the balance of T helper cell responses by curcumin in inflammatory and autoimmune states. Autoimmun Rev 2019; 18: 738-748.
124. Pulendran B, Artis D. New paradigms in type 2 immunity. Science 2012; 337: 431-435.
125. Ding L, Yang Y, Li H et al. Circulating Lymphocyte Subsets Induce Secondary Infection in Acute Pancreatitis. Front Cell Infect Microbiol 2020; 10: 128.
126. Li J-P, Yang J, Huang J-R et al. Immunosuppression and the infection caused by gut mucosal barrier dysfunction in patients with early severe acute pancreatitis. Frontiers in bioscience (Landmark edition) 2013; 18: 892-900.
127. Okazaki K, Uchida K, Ohana M et al. Autoimmune-related pancreatitis is associated with autoantibodies and a Th1/Th2-type cellular immune response. Gastroenterology 2000; 118: 573-581.
128. Schwaiger T, van den Brandt C, Fitzner B et al. Autoimmune pancreatitis in MRL/Mp mice is a T cell-mediated disease responsive to cyclosporine A and rapamycin treatment. Gut 2014; 63: 494-505.
129. Liberal R, Longhi MS, Mieli-Vergani G, Vergani D. Pathogenesis of autoimmune hepatitis. Best Practice & Research Clinical Gastroenterology 2011; 25: 653-664.
130. Tiemessen MM, Jagger AL, Evans HG et al. CD4+ CD25+ Foxp3+ regulatory T cells induce alternative activation of human monocytes/macrophages. Proceedings of the national academy of sciences 2007; 104: 19446-19451.
131. Kim JM, Rasmussen JP, Rudensky AY. Regulatory T cells prevent catastrophic autoimmunity throughout the lifespan of mice. Nat Immunol 2007; 8: 191-197.
132. Feuerer M, Shen Y, Littman DR et al. How punctual ablation of regulatory T cells unleashes an autoimmune lesion within the pancreatic islets. Immunity 2009; 31: 654-664.
133. Zen Y, Fujii T, Harada K et al. Th2 and regulatory immune reactions are increased in immunoglobin G4-related sclerosing pancreatitis and cholangitis. Hepatology 2007; 45: 1538-1546.
134. Miyoshi H, Uchida K, Taniguchi T et al. Circulating naïve and CD4+ CD25high regulatory T cells in patients with autoimmune pancreatitis. Pancreas 2008; 36: 133-140.
135. Chen L, Ma C, Bian Y et al. Hydrogen Treatment Protects Mice Against Chronic Pancreatitis by Restoring Regulatory T Cells Loss. Cell Physiol Biochem 2017; 44: 2005-

2016.
136. Xue J, Sharma V, Habtezion A. Immune cells and immune-based therapy in pancreatitis. Immunol Res 2014; 58: 378-386.
137. Zaninovic V, Gukovskaya AS, Gukovsky I et al. Cerulein upregulates ICAM-1 in pancreatic acinar cells, which mediates neutrophil adhesion to these cells. American Journal of Physiology-Gastrointestinal and Liver Physiology 2000; 279: G666-G676.
138. Hartman H, Abdulla A, Awla D et al. P-selectin mediates neutrophil rolling and recruitment in acute pancreatitis. British Journal of Surgery 2012; 99: 246-255.
139. Awla D, Abdulla A, Zhang S et al. Lymphocyte function antigen-1 regulates neutrophil recruitment and tissue damage in acute pancreatitis. Br J Pharmacol 2011; 163: 413-423.
140. Gukovskaya AS, Vaquero E, Zaninovic V et al. Neutrophils and NADPH oxidase mediate intrapancreatic trypsin activation in murine experimental acute pancreatitis. Gastroenterology 2002; 122: 974-984.
141. Saeki K, Kanai T, Nakano M et al. CCL2-induced migration and SOCS3-mediated activation of macrophages are involved in cerulein-induced pancreatitis in mice. Gastroenterology 2012; 142: 1010-1020 e1019.
142. Sendler M, Weiss FU, Golchert J et al. Cathepsin B-Mediated Activation of Trypsinogen in Endocytosing Macrophages Increases Severity of Pancreatitis in Mice. Gastroenterology 2018; 154: 704-718 e710.
143. Sendler M, Dummer A, Weiss FU et al. Tumour necrosis factor α secretion induces protease activation and acinar cell necrosis in acute experimental pancreatitis in mice. Gut 2013; 62: 430-439.
144. Perides G, Weiss ER, Michael ES et al. TNF-alpha-dependent regulation of acute pancreatitis severity by Ly-6C(hi) monocytes in mice. J Biol Chem 2011; 286: 13327-13335.
145. Shi C, Washington MK, Chaturvedi R et al. Fibrogenesis in pancreatic cancer is a dynamic process regulated by macrophage-stellate cell interaction. Lab Invest 2014; 94: 409-421.
146. Bleijs DA, Geijtenbeek TB, Figdor CG, van Kooyk Y. DC-SIGN and LFA-1: a battle for ligand. TRENDS in Immunology 2001; 22: 457-463.
147. van Gisbergen KP, Ludwig IS, Geijtenbeek TB, van Kooyk Y. Interactions of DC-SIGN with Mac-1 and CEACAM1 regulate contact between dendritic cells and neutrophils. FEBS letters 2005; 579: 6159-6168.
148. Engering A, Geijtenbeek TB, van Vliet SJ et al. The dendritic cell-specific adhesion receptor DC-SIGN internalizes antigen for presentation to T cells. The Journal of Immunology 2002; 168: 2118-2126.
149. Zhou T, Sun G-Z, Zhang Y-M et al. The inhibitory effects of anti-P-selectin lectin-EGF monoclonal antibody on maturation and function of human dendritic cells. Chin. J. Cell Biol 2006; 28: 201-205.
150. Prechtel AT, Steinkasserer A. CD83: an update on functions and prospects of the maturation marker of dendritic cells. Arch Dermatol Res 2007; 299: 59-69.
151. Kruse M, Rosorius O, Krätzer F et al. Mature dendritic cells infected with herpes simplex virus type 1 exhibit inhibited T-cell stimulatory capacity. Journal of virology 2000; 74: 7127-7136.
152. Lechmann M, Zinser E, Golka A, Steinkasserer A. Role of CD83 in the

immunomodulation of dendritic cells. International archives of allergy and immunology 2002; 129: 113-118.
153. Fujimoto Y, Tedder TF. CD83: a regulatory molecule of the immune system with great potential for therapeutic application. Journal of medical and dental sciences 2006; 53: 85-91.
154. Yönetçi N, Oruç N, Özütemiz AÖ, Yüce G. Effects of mast-cell stabilization in cerulein-induced acute pancreatitis in rats. International journal of pancreatology 2001; 29: 163-171.
155. Dib M, Zhao X, Wang X, Andersson R. Role of mast cells in the development of pancreatitis‐induced multiple organ dysfunction. British journal of surgery 2002; 89: 172-178.
156. Hoogerwerf WA, Gondesen K, Xiao SY et al. The role of mast cells in the pathogenesis of pain in chronic pancreatitis. BMC Gastroenterol 2005; 5: 8.
157. Aich A, Afrin L, Gupta K. Mast Cell-Mediated Mechanisms of Nociception. International Journal of Molecular Sciences 2015; 16: 29069-29092.
158. Haber PS, Keogh GW, Apte MV et al. Activation of Pancreatic Stellate Cells in Human and Experimental Pancreatic Fibrosis. The American Journal of Pathology 1999; 155: 1087-1095.
159. Apte M, Haber P, Darby S et al. Pancreatic stellate cells are activated by proinflammatory cytokines: implications for pancreatic fibrogenesis. Gut 1999; 44: 534-541.
160. Zimnoch L, Szynaka B, Puchalski Z. Mast cells and pancreatic stellate cells in chronic pancreatitis with differently intensified fibrosis. Hepato-gastroenterology 2002; 49: 1135.
161. Zang G, Sandberg M, Carlsson PO et al. Activated pancreatic stellate cells can impair pancreatic islet function in mice. Ups J Med Sci 2015; 120: 169-180.
162. Sherman MH, Ruth TY, Tseng TW et al. Stromal cues regulate the pancreatic cancer epigenome and metabolome. Proceedings of the National Academy of Sciences 2017; 114: 1129-1134.
163. Rhim AD, Oberstein PE, Thomas DH et al. Stromal elements act to restrain, rather than support, pancreatic ductal adenocarcinoma. Cancer cell 2014; 25: 735-747.

8. Appendix

8.1 Specific chemicals and reagents

Table 6: Specific chemicals and reagents

Reagent	Manufacturer	Catalog#
Albumine fraction V, Bovine serum albumin (BSA)	ROTH, Germany	3737.4
Ammonia solution	ROTH, Germany	CP17.1
Citric acid monohydrate	ROTH, Germany	5110.1
Direct Red 80	Sigma-Aldrich, USA	2610-10-8
Dulbecco´s Phosphate Buffered Saline (PBS)	Biochrom GmbH, Germany	D5652
Ethanol	ROTH, Germany	K928.4
Ethylenediaminetetraacetic acid disodium salt dihydrate (EDTA)	Sigma-Aldrich, USA	E5134-500G
L-ascorbic acid	SERVA, Germany	50-81-7
Glycine	ROTH, Germany	3783.1
Glycine	ROTH, Germany	3908.2
Fast Green FCF	Sigma-Aldrich, USA	2353-45-9
Hematpxylin	ROTH, Germany	3816.1
Hydrochloric acid fuming 37%	ROTH, Germany	4625.1
Hydrogen peroxide 30%	ROTH, Germany	CP26.1
ImmPACT AMEC RED Substrate, Peroxidase (HRP)	Vector, USA	SK-4285
ImmPACT DAB Substrate, Peroxidase	Vector, USA	SK-4105
Goat Serum normal	Dako Denmark; Denmark	
Permanent Mounting medium VectaMount	Vector Laboratories, USA	H-5000-60
Potassium permanganate	Merck, Germany	7722-64-7
Sodium dodecyl sulphate (SDS)	ROTH, Germany	CN30.2
Sodium hydroxide	Merck, Germany	1.06482.1000

Sulfuric acid	Sigma-Aldrich, USA	339741
Tween® 20	ROTH, Germany	9127.1
Xylene	Applichem, Germany	A2476,5000

8.2 Primary antibodies

Table 7: The details of primary antibody used in lymphoid biomarker panel

		Round 1	**Round 2**	**Round 3**	**Round 4**	**Round 5**
Primary Ab	Hematoxylin	GATA3	T-bet	FoxP3	CD20	CD8
Manufacturer		R&D Systems, USA	Cell Marque, Germany	Epitomics, USA	Cell Marque, Germany	Cell Marque, Germany
Catalog#		MAB6330	368R-74	AC-0304RUO	120R-14	108M-94
Concentration		1:50	1:50	1:50	1:100	1:100
Primary reaction		4°C overnight	4°C overnight	4°C overnight	4°C overnight	4°C overnight
Host species		Anti-mouse	Anti-rabbit	Anti-rabbit	Anti-rabbit	Anti-mouse
Secondary reaction		RT 1h	RT 1h	RT 1h	RT 1h	RT 1h
AMEC reaction time		12min	15min	7.4min	1.2min	2.4min
	Round 6	Round 7	**Round 8**	**Round 9**	**Round 10**	**Round 11**
Primary Ab	CD4	CD3	CD56	CD45	CTLA4	IL-17A
Manufacturer	Cell Marque, Germany	Dako, Denmark	Cell Marque, Germany	Dako, Denmark	BioLegend, USA	R&D Systems, USA
Catalog#	104R-14	M7254	156R-94	M0701	369608	MAB317
Concentration	1:100	1:100	1:100	1:100	1:100	1:50
Primary reaction	4°Covernigh t	4°C overnight	4°C overnight	4°C overnight	4°C overnight	4°C overnight
Host species	Anti-rabbit	Anti-mouse	Anti-rabbit	Anti-mouse	Anti-mouse	Anti-mouse
Secondary reaction	RT 1h	RT 1h	RT 1h	RT 1h	RT 1h	RT 1h
AMEC reaction	3.3min	3.4min	2.2min	1.2min	6.1min	6.0min

Table 8: The details of primary antibody used in myeloid biomarker panel

		Round 1	Round 2	Round 3	Round 4	Round 5
Primary Ab	Hematoxylin	DC-sign	CD206	CD68	MPO	CD20
Manufacturer		Santa Cruz, USA	R&D Systems, USA	Dako, Denmark	Sigma Aldrich; Germany	Cell Marque, Germany
Catalog#		SC-74589	MAB25341	M0876	HPA021147	120R-14
Concentration		1:100	1:50	1:100	1:500	1:100
Primary reaction		4°C overnight	4°C overnight	4°C overnight	4°C overnight	4°C overnight
Host species		Anti-mouse	Anti-mouse	Anti-mouse	Anti-rabbit	Anti-rabbit
Secondary reaction		RT 1h	RT 1h	RT 1h	RT 1h	RT 1h
AMEC reaction		10min	3.0min	1.0min	2.3min	2.3min
	Round 6	**Round 7**	**Round 8**	**Round 9**	**Round 10**	**Round 11**
Primary Ab	CD56	CD3	CD45	CD74	Tryptase	CD83
Manufacturer	Cell Marque, Germany	Dako, Denmark	Dako, Denmark	Sigma Aldrich; Germany	Cell Marque, Germany	Sigma Aldrich; Germany
Catalog#	156R-94	M7254	M0701	HPA010592	342R-14	HPA041454
Concentration	1:100	1:100	1:100	1:100	1:100	1:100
Primary reaction	4°C overnight	4°C overnight	4°C overnight	4°C overnight	4°C overnight	4°C overnight
Host species	Anti-rabbit	Anti-mouse	Anti-mouse	Anti-rabbit	Anti-rabbit	Anti-rabbit
Secondary reaction	RT 1h	RT 1h	RT 1h	RT 1h	RT 1h	RT 1h
AMEC reaction	3.2min	6.0min	1.4min	1.0min	1.0min	4.0min

Table 9: The details of primary antibody used in exocrine-endocrine and stroma panel

		Round 1	Round 2	Round 3	Round 4	Round 5
Primary Ab	Hematoxylin	Pan-Keratin	CD45	PHH3	a-SMA	Insulin
Manufacturer		Cell Signaling, USA	Dako, Denmark	Cell Signaling, USA	Dako, Denmark	Abcam, UK
Catalog#		4545	M0701	53348	M0851	AC-0119A
Concentration		1:100	1:100	1:500	1:1000	1:500
Primary reaction		4°C overnight	4°C overnight	4°C overnight	4°C overnight	4°C overnight
Host species		Anti-mouse	Anti-mouse	Anti-rabbit	Anti-mouse	Anti-rabbit
Secondary reaction		RT 1h	RT 1h	RT 1h	RT 1h	RT 1h

AMEC reaction		2.0min	1.3min	3.0min	1.3min	1.4min
	Round 6	**Round 7**	**Round 8**	**Round 9**	**Round 10**	**Round 11**
Primary Ab	PGP9.5	Perilipin	Amylase	Desmin	MMP7	picrosirius red staining
Manufacturer	R&D Systems, USA	Cell Signaling, USA	Santa Cruz, USA	R&D Systems, USA	R&D Systems, USA	
Catalog#	MAB60072	9349S	SC-46657	AF3844	AF2967	
Primary reaction	4°C overnight	4°C overnight	4°C overnight	4°C overnight	4°C overnight	
Host species	Anti-mouse	Anti-rabbit	Anti-mouse	Anti-goat	Anti-goat	
Secondary reaction	RT 1h	RT 1h	RT 1h	RT 1h	RT 1h	
AMEC reaction	2.0min	1.0min	2.0min	3.5min	4.0min	

8.3 Secondary antibodies

Table 10: Secondary antibody

Antibody	**Manufacturer**	**Catalog#**
Anti-Goat IgG	Jackson Immunoresearch, Germany	705-035-003
Anti-Mouse IgG EnVision+System	Dako, Denmark	K4001
Anti-rabbit IgG EnVision+System	Dako, Denmark	K4003

8.4 Equipment

Table 11: Equipment

Equipment	**Manufacturer**
Centrifuge 5702R	Eppendorf, Germany
Cover slips (24 x 24 mm)	Thermo Fisher Scientific, USA
IX50 Phase contrast inverted microscope	Olympus, Japan
Laboratory fume hood ChemFAST TOP 09	ChemFAST, Germany
Mini Plate Spinner Centrifuge-230EU	Corning, USA
Pipettes (0,5 µl - 10 µl, 10 µl - 100 µl, 100 µl - 1000 µl)	Eppendorf, Germany

Reaction tubes (1.5 ml, 2 ml)	Sarstedt, Germany
Reaction tubes (15 ml, 50 ml)	Sarstedt, Germany
Rotary Microtome HM325	Thermo Scientific, USA
Slides Polysine	Thermo Fisher Scientific, USA
Sysmex Panoramic MIDI II slide scanner	Sysmex Deutschland GmbH, Germany
Tissue Cooling Plate COP30	Medite, Germany
Tissue Floatation Bath TFB55	Medite, Germany
Vortex mixer	NeoLab Migge GmbH, Germany
Water bath SW22	Julabo GmbH, Germany

8.5 Computer program

Table 12: Computer program

Program	Producer
Caseviewer (version 2.2)	3DHISTECH, Hungary
CellProfiler	Carpenter Lab
EndNote X9	Thomson Reuters, USA
Microsoft Office	Microsoft, USA
NIH ImageJ	Wayne Rasband, NIH, USA
QuPath (0.1.2)	Bankhead et al.
SIFT	David Lowe et al.

8.6 R programming language and packages

- R version 3.6.3
- alluvial_0.1-2
- arsenal_3.5.0
- caret_6.0-86
- dplyr_1.0.1
- ggplot2_3.3.2
- lattice_0.20-41

- h2o_3.30.0.7
- lime_0.5.1
- janitor_2.0.1
- kableExtra_1.1.0
- knitr_1.29
- tidyr_1.1.1
- RColorBrewer 1.1-2
- rmarkdown_2.3

8.7 Buffer and solution

Table 13: Glycine-mediated antibody stripping buffer

Reagent	Final concentration	Volume	Mass
Glycine	25mM		1.88g
SDS	1%		10g
ddH_2O		1000ml	
HCl		set the pH to 2.0	

Table 14: Antigen retrieval buffer 10X

Reagent	Final concentration	Volume	Mass
Citric Acid	100mM		19.21g
EDTA	20mM		7.4g
Tween	0.5%	5ml	
ddH_2O		1000ml	
NaOH		set the pH to 6.2	

1X working solution was prepared by diluting the 10X original solution with ddH_2O.

Table 15: Picrosirius red-fast green staining solution

Reagent	Amount
L-ascorbic acid	10ml

Fast green FCF	10mg
Direct red 80	10mg
	continuous shaking for 5 to 10 min

8.8 Patient characteristics

Table 16: Patient characteristics

	Alcoholic CP (N=23)	AIP (N=7)	Others CP (N=28)	Total (N=58)	P value
Age_at_Diagnosis					< 0.001
Mean (SD)	45.55 (10.02)	60.44 (14.64)	59.87 (14.79)	54.26 (14.69)	
Range	29.31 - 66.75	41.83 - 75.93	26.52 - 82.47	26.52 - 82.47	
Gender					0.049
f	4 (17.4%)	1 (14.3%)	13 (46.4%)	18 (31.0%)	
m	19 (82.6%)	6 (85.7%)	15 (53.6%)	40 (69.0%)	
Etiology_CP					< 0.001
alcoholic	23 (100.0%)	0 (0.0%)	0 (0.0%)	23 (39.7%)	
autoimmune	0 (0.0%)	7 (100.0%)	0 (0.0%)	7 (12.1%)	
biliary obstructive	0 (0.0%)	0 (0.0%)	9 (32.1%)	9 (15.5%)	
idiopathic	0 (0.0%)	0 (0.0%)	2 (7.1%)	2 (3.4%)	
Other	0 (0.0%)	0 (0.0%)	3 (10.7%)	3 (5.2%)	
unknown	0 (0.0%)	0 (0.0%)	14 (50.0%)	14 (24.1%)	
Previous_surgery					0.134
no	21 (91.3%)	7 (100.0%)	21 (75.0%)	49 (84.5%)	
yes	2 (8.7%)	0 (0.0%)	7 (25.0%)	9 (15.5%)	
Type_of_Previous_surgery					
N-Miss	20	7	21	48	
DPPHR	1 (33.3%)	0	0 (0.0%)	1 (10.0%)	
Frey/Pustow/Drainage	0 (0.0%)	0	1 (14.3%)	1 (10.0%)	
Others	1 (33.3%)	0	3 (42.9%)	4 (40.0%)	
ppWhipple	0 (0.0%)	0	3 (42.9%)	3 (30.0%)	
Whipple	1 (33.3%)	0	0 (0.0%)	1 (10.0%)	
Previous_Endoscopy					0.501
N-Miss	3	1	1	5	
no	4 (20.0%)	1 (16.7%)	9 (33.3%)	14 (26.4%)	
yes	16 (80.0%)	5 (83.3%)	18 (66.7%)	39 (73.6%)	
Repeat_endoscopy					0.226
N-Miss	3	1	2	6	
no	8 (40.0%)	3 (50.0%)	17 (65.4%)	28 (53.8%)	

yes	12 (60.0%)	3 (50.0%)	9 (34.6%)	24 (46.2%)	
Age_at_Surgery					< 0.001
Mean (SD)	46.54 (10.16)	61.99 (14.67)	61.63 (14.03)	55.69 (14.55)	
Range	29.38 - 66.75	41.84 - 75.93	26.52 - 82.53	26.52 - 82.53	
Type_of_surgery					0.042
DPPHR	5 (21.7%)	0 (0.0%)	0 (0.0%)	5 (8.6%)	
Frey/Pustow/Drainage	3 (13.0%)	1 (14.3%)	1 (3.6%)	5 (8.6%)	
Left-resection	3 (13.0%)	1 (14.3%)	4 (14.3%)	8 (13.8%)	
Others	2 (8.7%)	0 (0.0%)	2 (7.1%)	4 (6.9%)	
ppWhipple	8 (34.8%)	2 (28.6%)	15 (53.6%)	25 (43.1%)	
total pancreatectomy	1 (4.3%)	0 (0.0%)	4 (14.3%)	5 (8.6%)	
Whipple	1 (4.3%)	3 (42.9%)	2 (7.1%)	6 (10.3%)	
Current_Smoker					< 0.001
N-Miss	9	1	16	26	
no	1 (7.1%)	6 (100.0%)	9 (75.0%)	16 (50.0%)	
yes	13 (92.9%)	0 (0.0%)	3 (25.0%)	16 (50.0%)	
Previous_Smoker					< 0.001
N-Miss	5	0	14	19	
no	0 (0.0%)	5 (71.4%)	9 (64.3%)	14 (35.9%)	
yes	18 (100.0%)	2 (28.6%)	5 (35.7%)	25 (64.1%)	
Never_Smoker					0.002
N-Miss	5	2	17	24	
no	18 (100.0%)	5 (100.0%)	6 (54.5%)	29 (85.3%)	
yes	0 (0.0%)	0 (0.0%)	5 (45.5%)	5 (14.7%)	
Current_Drinker					0.062
N-Miss	7	1	17	25	
no	10 (62.5%)	5 (83.3%)	11 (100.0%	26 (78.8%)	
yes	6 (37.5%)	1 (16.7%)	0 (0.0%)	7 (21.2%)	
Previous_Drinker					< 0.001
N-Miss	1	1	16	18	
no	1 (4.5%)	5 (83.3%)	10 (83.3%)	16 (40.0%)	
yes	21 (95.5%)	1 (16.7%)	2 (16.7%)	24 (60.0%)	
Never_Drinker					0.001
N-Miss	1	2	19	22	
no	22 (100.0%)	5 (100.0%)	9 (100.0%)	36 (100.0%)	
Height					0.191
N-Miss	9	1	9	19	
Mean (SD)	1.74 (0.07)	1.69 (0.10)	1.68 (0.11)	1.70 (0.10)	
Range	1.61 - 1.87	1.50 - 1.77	1.43 - 1.89	1.43 - 1.89	
Weight					0.461
N-Miss	9	1	9	19	

Mean (SD)	63.86 (15.11)	72.33 (13.59)	67.90 (13.87)	67.13 (14.22)	
Range	40.00 - 95.00	50.00 - 92.00	43.00 - 90.00	40.00 - 95.00	
Exocrine_Insuff					0.800
N-Miss	3	0	0	3	
no	12 (60.0%)	5 (71.4%)	19 (67.9%)	36 (65.5%)	
yes	8 (40.0%)	2 (28.6%)	9 (32.1%)	19 (34.5%)	
Stool_Elastase					
N-Miss	21	7	26	54	
Mean (SD)	69.50 (50.21)	NA	57.50 (37.48)	63.50 (36.83)	
Range	34.00 - 105.00	NA	31.00 - 84.00	31.00 - 105.00	
Endocrine_Insuff					0.280
N-Miss	1	0	0	1	
no	18 (81.8%)	6 (85.7%)	18 (64.3%)	42 (73.7%)	
yes	4 (18.2%)	1 (14.3%)	10 (35.7%)	15 (26.3%)	
Insulin_dependent					0.491
N-Miss	1	0	0	1	
no	20 (90.9%)	6 (85.7%)	22 (78.6%)	48 (84.2%)	
yes	2 (9.1%)	1 (14.3%)	6 (21.4%)	9 (15.8%)	
Analgesics					0.285
Mean (SD)	0.57 (0.95)	0.29 (0.49)	0.25 (0.52)	0.38 (0.72)	
Range	0.00 - 3.00	0.00 - 1.00	0.00 - 2.00	0.00 - 3.00	
BMI					0.031
N-Miss	9	1	9	19	
Mean (SD)	20.98 (4.01)	25.26 (3.27)	24.02 (3.66)	23.12 (4.01)	
Range	13.06 - 27.17	22.22 - 31.10	18.29 - 30.12	13.06 - 31.10	
NRS					0.119
Mean (SD)	4.09 (2.04)	2.86 (3.29)	2.64 (2.61)	3.24 (2.54)	
Range	0.00 - 7.00	0.00 - 8.00	0.00 - 9.00	0.00 - 9.00	
HbA1c					0.245
N-Miss	1	0	1	2	
Mean (SD)	6.06 (0.90)	6.84 (1.05)	6.44 (1.33)	6.34 (1.16)	
Range	5.00 - 8.00	5.70 - 8.40	4.70 - 11.20	4.70 - 11.20	
Platelets					0.893
N-Miss	1	0	0	1	
Mean (SD)	283.14 (94.92)	264.57 (66.05)	270.00 (132.51)	274.40 (111.19)	
CD45+_panel1					0.149
Mean (SD)	8.233 (8.691)	21.566 (19.593)	9.222 (9.249)	10.320 (11.312)	
Range	0.543 – 37.230	2.527 – 59.970	1.007 – 31.400	0.543 – 59.970	
Act-T-cells_CD45+					0.039
Mean (SD)	13.037 (7.157)	7.037 (3.318)	15.444 (9.156)	13.507 (8.203)	
Range	2.040 – 25.680	3.607- 12.917	4.440 – 35.780	2.040 – 35.780	
B-cells_CD45+					0.653
Mean (SD)	5.862 (6.258)	6,601 (5,626)	5,931 (4,301)	5.985 (5.221)	
Range	0.000 - 25.520	1,520 - 16,677	0,137 - 17,050	0.000 – 25.520	

NK-cells_CD45+					0.596
Mean (SD)	3.401 (2.528)	3.075 (3.614)	3.134 (2.010)	3.233 (2.403)	
Range	0.160 – 10.687	0.757 – 10.883	0.473 – 8.690	0.160 – 10.883	
Cyt-T-cells_CD45+					0.004
Mean (SD)	5.377 (3.910)	1.666 (0,805)	6.159 (4.455)	5.307 (4.166)	
Range	0.617 – 14.790	0.427 – 2.437	0.587 – 17.880	0.427 – 17.880	
Reg-T-cells_CD45+					0.921
Mean (SD)	0.342 (0.927)	0.105 (0.076)	0.281 (0.770)	0.284 (0.787)	
Range	0.000 – 4.390	0.000 - 0.237	0.000 – 4.067	0.000 – 4.390	
TH17-cells_CD45+					0.184
Mean (SD)	0.967 (1.200)	1.248 (0.931)	0.603 (0.511)	0.825 (0.908)	
Range	0.000 – 4.827	0.431 – 2.587	0.000 – 2.007	0.000 - 4.827	
TH1-cells_CD45+					0.597
Mean (SD)	0.269 (0.289)	0.162 (0.146)	0.453 (0.839)	0.345 (0.617)	
Range	0.000 – 1.053	0.030 – 0.450	0.000 – 4.347	0.000 - 4.347	
TH0-cells_CD45+					0.173
Mean (SD)	4.535 (6.895)	10.688 (9.525)	4.066 (4.688)	5.051 (6.542)	
Range	0.000 – 26.133	0.000 - 20.987	0.000 – 17.277	0.000 – 26.133	
TH2-cells_CD45+					0.545
Mean (SD)	1.121 (0.906)	1.314 (0.556)	1.272 (0.916)	1.217 (0.868)	
Range	0.037 – 3.223	0.631 – 1.917	0.020 – 4.000	0.020 – 4.000	
CD45+_panel2					< 0.001
Mean (SD)	6.251 (3.610)	21.516 (14.922)	7.089 (7.151)	20.648 (14.860)	
Range	1.100 – 14.260	2.383 – 47.997	1.053 – 30.227	8.498 – 8.747	
Granulocytes_CD45+					0.214
Mean (SD)	10.844 (5.969)	20.804 (18.058)	10.345 (8.197)	11.805 (9.554)	
Range	1.367 – 21.097	1.803 – 53.947	2.360 – 34.900	1.367 - 53.947	
Mast_cells_CD45+					0.968
Mean (SD)	3.861 (2.633)	4.249 (4.496)	4.082 (3.527)	4.015 (3.274)	
Range	0.170 – 11.223	0.773 – 13.840	0.467 – 13.830	0.170 - 13.840	
M1_macrophages_CD45+					0.080
Mean (SD)	0.245 (0.267)	0.909 (0.983)	0.877 (1.250)	0.631 (0.984)	
Range	0.000 - 863	0.137 - 2.757	0.000 – 5,447	0.000 – 5.447	
M2_macrophages_CD45+					0.068
Mean (SD)	0.056 (0.123)	0.211 (0.341)	0.072 (0.135)	0.082 (0.170)	
Range	0.000 - 0.490	0.000 - 0.947	0.000 - 0.530	0.000 - 0.947	
CD83+DC_CD45+					0.0483
Mean (SD)	1.554 (1.402)	2.259 (1.850)	1.316 (0.995)	1.524 (1.294)	
Range	0.127 – 5.377	1.060 – 6.067	0.000 – 3.657	0.000 – 6.607	
DCsign+_CD45+					0.995
Mean (SD)	0.317 (0.459)	0.290 (0.617)	0.238 (0.393)	0.276 (0.443)	
Range	0.000 – 1.540	0.000 – 1.687	0.000 – 1.577	0.000 – 1.687	
CD45+_panel3					0.068
Mean (SD)	8.531 (5.659)	15.007 (12.067)	8.900 (5.549)	9.499 (6.830)	

Range	1.787 – 24.113	5.703 – 38.757	0.670 – 26.937	0.067 – 38.757	
CD45-_panel3					0.113
Mean (SD)	90.640 (6.261)	84.293 (12.363)	89.881 (5.859)	89.507 (7.170)	
Range	72.113 – 97.467	60.340 – 93.957	72.270 – 98.683	60.340 - 98.683	
Islets_CD45-					0.995
Mean (SD)	2.854 (4.200)	6.583 (11.624)	4.886 (7.233)	4.285 (6.890)	
Range	0.070 – 15.830	0.053 – 31.507	0.047 – 25.510	0.047 – 31.507	
Nerve_CD45-					0.164
Mean (SD)	1.277 (1.386)	1.290 (2.069)	0.786 (0.866)	1.042 (1.269)	
Range	0.040 – 5.663	0.003 – 5.800	0.073 – 4.193	0.003 – 5.800	
Ducts_CD45-					0.552
Mean (SD)	6.209 (7.941)	6.564 (10.991)	4.156 (5.633)	5.261 (7.298)	
Range	0.107 – 26.980	0.283 – 30.903	0.120 – 22.580	0.107 – 30.903	
Acini_CD45-					0.968
Mean (SD)	26.108 (15.486)	27.163 (22.867)	25.650 (13.020)	26.014 (15.104)	
Range	1.940 – 54.627	1.047 – 59.460	3.636 – 56.557	1.047 – 59.460	
qPSCs_CD45-					0.365
Mean (SD)	1.971 (2.665)	2.770 (3.404)	1.631 (2.082)	1.903 (2.479)	
Range	0.000 – 12.083	0.573 – 10.113	0.007 – 8.010	0.000 – 12.083	
aPSCs_CD45-					0.906
Mean (SD)	1.157 (0.912)	6.316 (12.536)	2.546 (3.400)	2.450 (4.985)	
Range	0.053 – 3.870	0.000 – 34.350	0.003 – 14.200	0.000 – 34.350	
qPSCs-matrix_CD45-					0.961
Mean (SD)	0.044 (0.090)	0.280 (0.630)	0.057 (0.107)	0.079 (0.237)	
Range	0.000 - 0.403	0.000 - 1.693	0.000 – 0.440	0.000 – 1.693	
qPSCs-proliferation_CD45-					0.511
Mean (SD)	0.277 (0.624)	0.124 (0.167)	0.089 (0.153)	0.168 (0.415)	
Range	0.000 – 2.777	0.000 - 0.373	0.000 – 0.673	0.000 - 2.777	
aPSCs-proliferation_CD45-					0.471
Mean (SD)	0.139 (0.222)	0.062 (0.098)	0.203 (0.332)	0.160 (0.273)	
Range	0.000 - 0.760	0.000 – 0.263	0.000 – 1.260	0.000 – 1.260	
aPSCs-matrix_CD45-					0.391
Mean (SD)	0.253 (0.347)	2.096 (5.342)	0.598 (1.035)	0.642 (1.969)	
Range	0.000 - 1.070	0.000 – 14.207	0.000 – 3.897	0.000 – 14.207	
aSMA					0.202
Mean (SD)	27.975 (7.934)	33.324 (9.916)	27.373 (6.510)	28.330 (7.635)	
Range	10.996 – 43.754	16.755 – 46.453	15.202 – 37.961	10.996 – 46.453	
Collagen					0.532
Mean (SD)	56.138 (17.301)	49.389 (22.142)	52.586 (15.992)	53.608 (17.133)	
Range	10.425 – 78.497	22.625 – 78.945	16.564 – 92.096	10.425 – 92.096	

8.9 List of tables

8.10 List of figures

9. Acknowledgements

I express my sincere gratitude towards those who have been part of my life.

It is my greatest honor to convey my thankfulness to my generous and unselfish mentors, amiable and friendly colleagues, and my dearest friends that I fortunately met them during my three years of medical doctoral study in Ludwig-Maximilians-Universität München, Germany.

My deepest gratitude goes to **Prof. Dr Julia Mayerle** for offering me the opportunity to join the team. She is a brilliant scientist with broad view of innovation and always gave me constructive and valuable suggestions. Whenever I encountered confusion and turned to her for helping during my study, she patiently explained me in detail how the problems happened and how to solve the problems. Her meticulous and enthusiastic attitude towards basic research and clinical works have a profound influence on me with regard to my scientific thinking and my future clinical practice.

I feel very grateful to thank **Dr Georg Beyer** who is my second supervisor. I was immediately attracted by his charming personality when I met him at the first time. Importantly, he not only helped me a lot with regard to my project, but also gave me precious encouragement and advice when I faced frustration throughout my study.

I special thanks are to **PhD. Ujjwal M. Mahajan** for offering me technical assistance so that my project can be carried out, moved on, and completed successfully.

I would like to thank **PhD. Ivonne Regel** for organizing the materials used for my project and providing valuable suggestions that will be of great value to my critical thinking. I also would like to convey my sincere thankfulness to my lab colleagues, Ahmed, Lisa, Svenja, Qi, Quan, Prince, Michal, Simon, Maria, Andrea, Theresa. They not only gave me a lot of assistance during performing experiments, but provided me with comfortable and family-like working atmosphere.

I would like to express my gratitude towards China Scholarship Council (CSC) for giving me fundamental financial support.

Most importantly, I would like to convey my deepest thankfulness to my parents and my sister for their understanding, faith, continuous encouragements and supports, and everything they have done for me.

LMU LUDWIG-MAXIMILIANS-UNIVERSITÄT MÜNCHEN

Dean's Office
Faculty of Medicine

Affidavit

Xue, Yonggan

Surname, first name

Street

Zip code, town

Country

I hereby declare, that the submitted thesis entitled

Identification of distinct histological signatures associated with different causes of chronic pancreatitis using multiplex staining

is my own work. I have only used the sources indicated and have not made unauthorised use of services of a third party. Where the work of others has been quoted or reproduced, the source is always given.

I further declare that the submitted thesis or parts thereof have not been presented as part of an examination degree to any other university.

Beijing, 12.07.2021
Place, date

Yonggan Xue
Signature doctoral candidate